IOM

Leibniz Institute of
Surface Engineering

Biennial Report
2018 / 2019

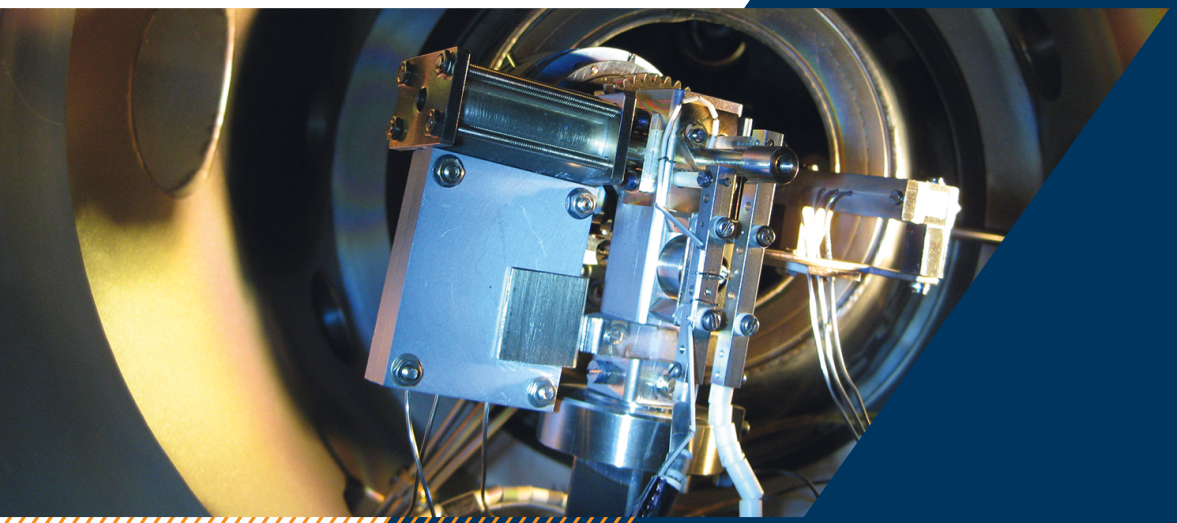

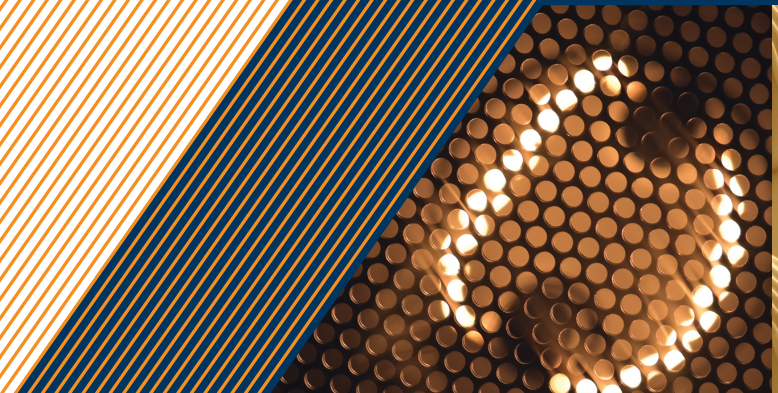

IOM

Leibniz Institute of
Surface Engineering

Tailored Surfaces

Executive Board

Director and CEO
Prof. Dr. André Anders

Phone: +49 (0)341 235 - 2308
Fax: +49 (0)341 235 - 2313

E-Mail: andre.anders@iom-leipzig.de

Members of the Board of Trustees

- **Free State of Saxony, Ministry of State of Science and Art**
  represented by RD'in Cathrin Liebner (chairwoman)
- **Federal Republic of Germany, Federal Ministry of Education and Research**
  represented by MinR Dr.-Ing. Joachim P. Kloock
- **Association of the Leibniz Institute of Surface Engineering (IOM)**
  represented by Dr. Karsten Otte
- **Independend Expert**
  Prof. Jochen M. Schneider, PhD, RWTH Aachen University

Members of the Scientific Advisory Board

- **Prof. Dr. Christina Trautmann (chairwoman)**
  Gesellschaft für Schwerionenforschung GSI Darmstadt
- **Prof. Dr. Karl-Michael Weitzel (deputy chair)**
  Philipps-Universität Marburg
- **Prof. Dr. Katharina AI-Shamery**
  Universität Oldenburg
- **Prof. Dr. Horst Hahn**
  Karlsruher Institut für Technologie
- **PD Dr. Bernd Herzog**
  BASF Grenzach GmbH, Grenzach-Wyhlen
- **Prof. Dr.-Ing. Dr. h. c. Ralf Eckhardt Beyer**
  Fraunhofer-Institut für Werkstoff- und Strahlentechnik und Technische Universität Dresden
- **Prof. Dr. Hans-Gerd Löhmannsröben**
  Universität Potsdam
- **Tino Petsch**
  3D-Micromac, Chemnitz
- **Dr. Helmut Rudigier**
  Chief Technology Officer (CTO) (Oerlikon)
- **Prof. Dr. Andrea A. Robitzki**
  Universität Leipzig

Organisational Structure

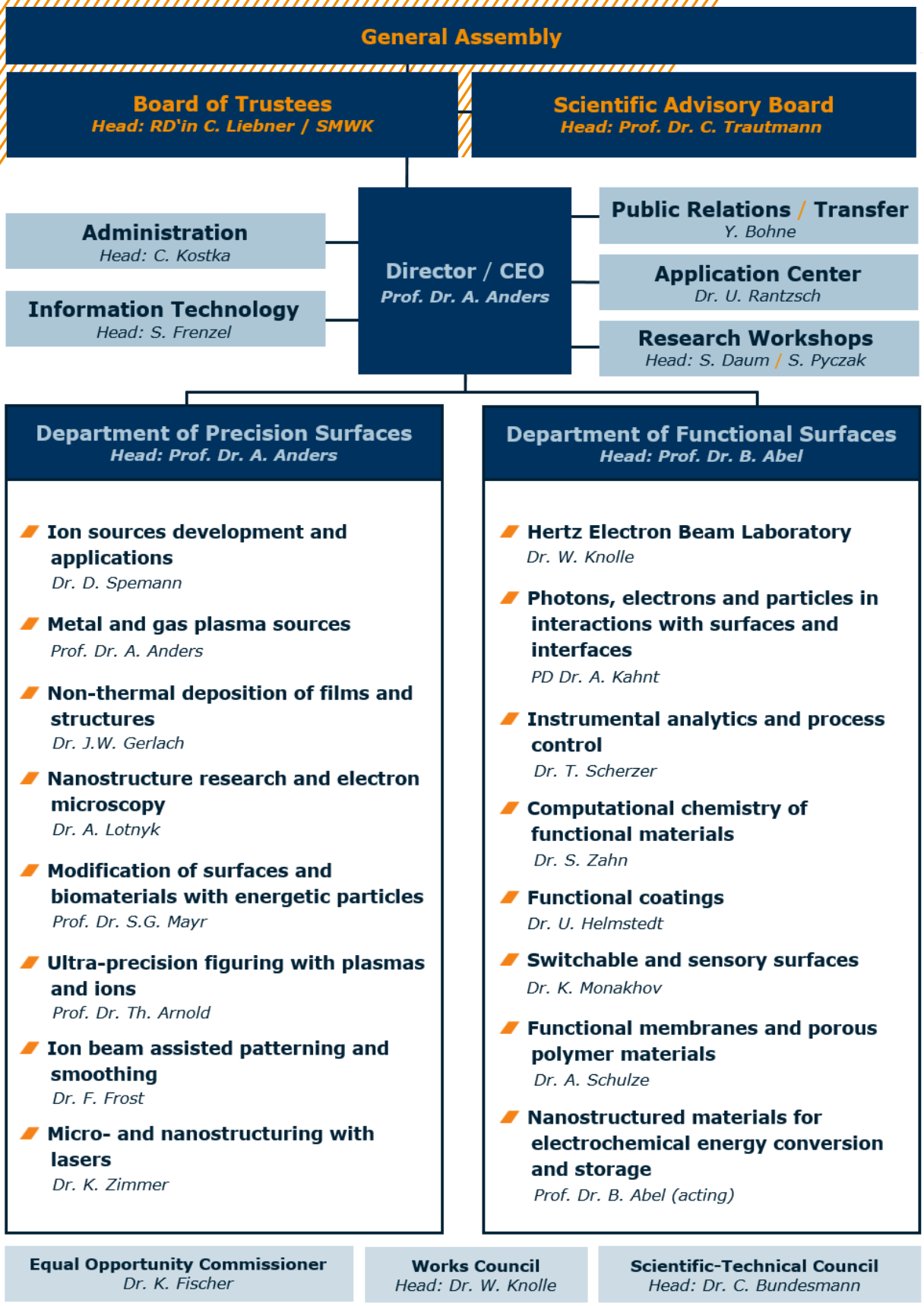

Contents


IOM
Leibniz-Institut für
Oberflächenmodifizierung e.V.

Preface

The Leibniz Institute of Surface Engineering (IOM), a member of the Leibniz Association, was established after German unification based on the recommendation of Germany's Science Council. It evolved from a "Blue List Institute" to a widely recognized research institution. Its research focuses on engineering surfaces and thin films by ion beam, electron, laser and plasma techniques. According to its constitution, the institute performs "application-oriented fundamental research", which allows it to operate at the interesting and rewarding interface of fundamental and applied research with the goal of creating modified surfaces and new materials in economically relevant technology fields.

The main research areas were:

- Tool development: Plasma and ion beam sources
- Thin films with nano and atomic structures
- Beam-based shaping and structuring of surfaces
- Imaging analytics and molecular mechanisms at surface and interfaces
- Functional surfaces and films
- Micro and nanostructured materials and surfaces.

This biennial report 2018/2019 presents selected scientific contributions, a general overview of the scientific life and compilations of published results, talks and patents.

Some particular highlights in 2018 and 2019 were:

- The high resolution scanning transmission electron microscope (HRSTEM) was used to study laser irradiation-induced crystallisation dynamics of epitaxial phase change thin films grown by pulsed laser deposition. Laser-assisted time resolved reflectivity measurements showed the formation of multiple reflectivity states, which may have applications in non-binary memory systems.
- The high potential of high-energy electron crosslinked hydrogels was shown for biomedical applications. New concepts were introduced for the development of biomimetic as well as stimuli-responsive materials and functional surfaces from collagen and gelatin.
- Planarization of single-point diamond turning aluminium surfaces was demonstrated using two subsequent nitrogen ion beam processing steps followed by an oxygen etching step. This resulted in a significantly smoothed aluminium surface over the entire spatial frequency range.
- Photoemission Electron Microscopy (PEEM) was shown to be a tool also applicable to analyze polymer surfaces, allowing us to quantify the average domain size and thus the crystallinity of polymer films.

Besides scientific achievements, IOM made strides in other fields. For example, technology transfer—one of the main objectives of research at IOM—experienced growth and gained steady recognition not the least due to the initiatives of the new Coordinator of the Application Center, Dr. Ulrike Rantzsch.

As a Leibniz Institute, IOM receives its basic funding from the German States and the German Federal Government in equal parts. An important indicator of scientific quality is the amount of additional third party funding, which in 2018 /2019 reached a total of 8,26 Mio EUR.

Within its budget, the institute paid attention to the renewal and upgrade of research equipment. Given the generous investments over the last two decades, the need to renew and improve is significant. For example, among the many improvements, the scanning electron microscope received an EBSD attachment, which allows us to determine the crystalline texture of thin films. To replace the ageing high-resolution XRD equipment, a special funding mechanism (Sondertatbestand) was activated, with the new instrument expected in 2020.

The institute faces a notable gradual generational change. Staff who was with the institute from its inception went to retirement, giving the baton to the next generation. In particular, the institute is indebted to Ms. Viola Zellin, Head of Administration since 1992. We welcomed Ms. Claudia Kostka who took the administrative helm in summer of 2019.

In 2019, IOM founded the IOM Graduate School "Surface Engineering", in order to structure the education of IOM-based young scientists who seek their PhD degree at various universities, and in particular at Leipzig University. Early career scientists are now presenting their results in IOM-open Friday seminars.

Also in 2019, IOM launched "Seed Funding", an internal funding mechanism designed to promote the development and proof-of-principle demonstrations of ideas thereby putting researcher in a better position to apply for future funding.

IOM would like to thank the Leibniz Association and all partners who supported its development. Special thanks go to the Board of Trustees, the Scientific Advisory Board, the Ministry of Science and Arts of the Free State of Saxony, and the Ministry of Education and Research of the Federal Government of Germany. Last but not least, I would like to thank the staff of the institute for their dedicated efforts and excellent contributions in the last two years.

Leipzig, in Spring 2020

Prof. Dr. André Anders
Director

RECTOR OF THE LEIPZIG UNIVERSITY VISITS THE IOM

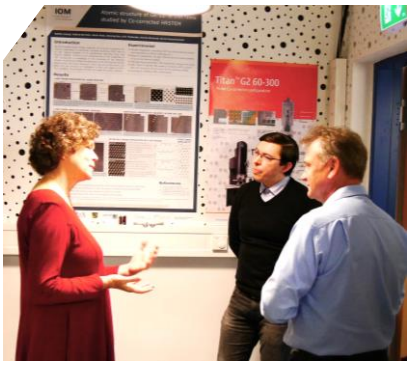


/ Prof. Dr. André Anders received the Rector of the Leipzig University, Prof. Dr. med. Beate A. Schücking at IOM in January 2018. Already since 1998, both institutions have maintained close cooperation relations, which are to be further intensified and sharpened with the visit of the Rector. The cooperation has a high priority for both institutions and is to be further expanded, especially in the areas of transfer, coordination of research activities and graduate training. In addition to the intensification of existing cooperation relations, both the joint development of new cooperation strategies and better networking of locations are of interest, especially with a view to further strengthening Leipzig as a research location and attracting excellent scientists to the region.

AWARD OF THE SOMORJAI-MILLER-PROFESSORSHIP

/ Prof. Dr. Bernd Abel, Deputy Director of IOM and Professor of Technical Chemistry of Polymers at the University of Leipzig received a Somorjai Miller Visiting Professorship at the University of California in Berkeley in the winter semester 2018/19. The Gabor A. and Judith K. Somorjai Visiting Miller Professorship Award is announced annually by the Miller Institute for Basic Research in Science at UC Berkeley and is awarded to 1-2 internationally renowned scientists to initiate or intensify cooperation in the field of chemical sciences.

AWARD OF THE KURT-SCHWABE PRIZE

/ Dr. Agnes Schulze received this prestigious award in 2018 for her outstanding development work on the subject of "Self-cleaning membrane filters for environmentally friendly use in water treatment". The Saxon Academy of Sciences in Leipzig has been awarding the Kurt-Schwabe Prize since 1983 in recognition of outstanding achievements in the natural sciences or technical sciences as well as outstanding personal services to the conservation of nature and its resources.

IQ-INNOVATION AWARD 2018

Photo: Guido Werner

/ Two first prizes went to the IOM spin-off Trionplas Technologies GmbH at the award ceremony by the Central German Metropolitan Region in Gera. The company convinced with an innovative plasma jet process for surface processing of individually shaped optics and thus won the cluster prize Chemistry/ Plastics as well as the local Leipzig Innovation Award. Second place in the cluster went to Dr. Agnes Schulze from IOM, who presented a new innovative refining process for polymer membranes for water purification.

THIRD LEIBNIZ MMS DAYS 2018

/ The third Leibniz MMS Days took place at IOM and were hosted by the Leibniz Network "Mathematical Modeling and Simulation", the Leibniz Institute for Tropospheric Research (TROPOS) and the IOM. The workshop aims to further develop the MMS networking activities in the different Institutes, presenting undergoing work using modern methods of MMS and creating a plattform for discussion on themes of specific and general interest.

FORUM WISSENSCHAFTSMANAGEMENT LEIPZIG (FoWi) 2018



/ At the new series of events "Forum Wissenschaftsmanagement Leipzig", questions and topics relating to administrative science management were addressed and discussed for the first time in a conference. Special focus was placed on the topics of personnel, research infrastructure, purchasing and finance. The aim of the event was to discuss current topics and debates on the management of innovative and successful science institutions and to present action and optimisation concepts. The conference was jointly organized by the Deutsches Biomasseforschungszentrum gemeinnützige GmbH (DBFZ), the Helmholtz Centre for Environmental Research (UFZ), the Leibniz Institute for Tropospheric Research (TROPOS) and the Leibniz Institute of Surface Engineering (IOM).

„LANGE NACHT DER WISSENSCHAFTEN" AND „GIRLS`DAY" AT THE IOM IN APRIL AND JUNE 2018



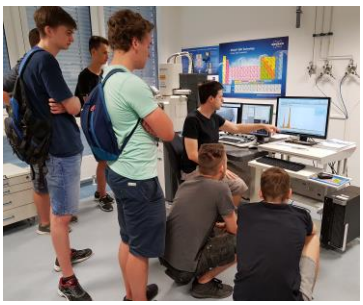


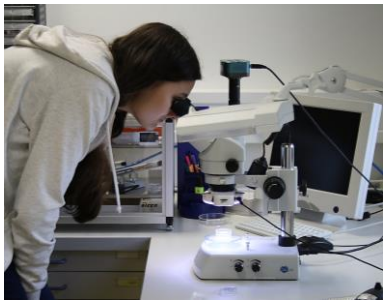

/ The IOM regularly participates in these activities and offers visitors the opportunity to learn more about our research institution. For this purpose, insights into selected high-tech laboratories are given and different research topics of the IOM are presented by staff members.

A NEW START-UP COMPANY FROM THE IOM

qCoat

/ Sustainable and resource-saving water purification by means of membrane refinement: this is one of the goals of the IOM start-up, founded in May 2019. The founders of qCoat GmbH are Dr. Agnes Schulze from IOM as well as the managing directors and former employees of IOM Dr. Alexander Braun and Dr. Karsten Otte. The technological basis of the start-up is a patented process innovation for the stable functionalization of polymer membranes, which has been developed at IOM in recent years. The single-stage immobilization process, integrated in a roll-to-roll pilot plant, allows an environmentally friendly and inexpensive refinement of various membrane types, which are used as membrane filters mainly for filtration and separation processes in water treatment/ waste water treatment, the food industry and medicine/ pharmacy. With this new start-up the IOM continues its series of successful spin-offs since 1998.

STUDENT RESEARCH PROJECT RECEIVES SAXON ENVIRONMENTAL AWARD 2019

Photo: © André Wirsig

Robert Bosch Stiftung

/ In July, Saxony's Environment Minister Thomas Schmidt awarded the Saxon Environmental Prizes 2019. One of the prizes, worth 10,000 euros, went to the student laboratory of the Helmholtz Centre for Environmental Research (UFZ) and the Leibniz Institute of Surface Engineering (IOM) for their environmental education project "Clean Water - a Precious Resource". Pupils from two Leipzig grammar schools (Wilhelm-Ostwald-Gymnasium and the Gustav-Hertz-Gymnasium) spent two years in the UFZ pupils' laboratory researching suitable methods for the disposal and transformation of different substances in ground, drinking and waste water into harmless products. They were supported by scientists from both research institutions (UFZ and IOM) and by the Robert Bosch Foundation, which provided financial support for the project as part of the "Our common future initiative".

COMPETENCE REGION GRAVOMER - KICK-OFF MEETING AT THE IOM



/ The BMBF-funded alliance "GRAVOMER - Competence Region Microstructured Functional Surfaces" started the implementation phase with a kick-off meeting in September 2019. The event brought together players from various Central German companies and from educational and research institutions. The meeting was organized by the initial partners herlac Coswig GmbH, Sächsische Walzengravur GmbH and IOM and took place at IOM in Leipzig. The common goal of the 42 alliance partners is to anchor the competence network for the application-oriented design of surfaces on an industrial scale in the region and to increase its regional and international visibility for the benefit of the partners. GRAVOmer is one of 20 East German alliances that successfully passed the two-stage selection procedure of the programme "WIR! – Wandel durch Innovation in der Region".

IOM JUNIOR SCIENTISTS AT THE LAUNCH CONFERENCE "SCIENCE FOR FUTURE" 2019 IN BEIJING

Photo: Yang Tian Peng

/ As part of the bilateral cooperation between the National Academy of Sciences Leopoldina and the Chinese Academy of Sciences (CAS), the Leopoldina and the Leibniz Association supported the participation of selected young scientists in the German-Chinese conference "Science for Future - All Starts with Basic Research", including Dr. M. Ehrhardt from the IOM. Excellent scientists, among them the two Nobel Prize winners in physics Prof. Dr. Klaus von Klitzing and Prof. Dr. Cheng Ning Yang took part in the conference. A total of 36 young scientists exchanged their latest research results with top scientists.

INTERNATIONAL CONFERENCE ON LASER INTERACTION WITH MATERIAL AND APPLIED LASER 2019 (LIMA)

/ The latest innovations and trends from research and development as well as technological challenges were presented and discussed at the "International Conference on Laser Interaction with Material and Applied Laser 2019 (LIMA)" in Shanghai. Dr. K. Zimmer, head of the working group "Micro- and Nanostructuring with Lasers" at IOM and cooperation partner of the "Joint International Research Laboratory of Laser-based Manufacturing and Materials" in Shanghai was significantly involved in the organization and design of the conference. The creation of a sustainable cooperation network to promote the exchange of information, the cooperative research of new effects and the implementation of concrete scientific projects was the aim of the conference.

AWARDS OF THE INSTITUTE

/ Young Scientist Award 2018

Dr. Stefanie Riedel

For her contribution to the topic
“Elektronenstrahlvernetzte Hydrogel-Systeme”
“Electron beam crosslinked hydrogel systems”

/ Non-scientific Award 2018

Dr. Cornelia Maywald and Nadja Schönherr

For their special commitment in the preparation, support, implementation or organization of Institute's tasks

/ Young Scientist Award 2019

Dr. Christian Laube

For his contribution to the topic
“Surface modification and electron irradiation treatment of nanodiamonds”

/ Non-scientific Award 2019

Ronny Woyciechowski

For his special commitment in the preparation, support, implementation or organization of Institute's tasks

COMPATIBILITY OF CAREER AND PERSONAL LIFE

/ Employees who can successfully balance work and personal life are the most valuable asset for the success of IOM. Flexible working time, a parents child room, the organization of meetings and scientific colloquia within core working hours as well as individualized support in challenging family situations are important measures. Based on these principles, the needs for improvement are regularly assessed and implemented within the certification process “auditberufundfamilie” (“audit work and family”). For example, support of families during working times in other countries has been compiled.

Zertifikat seit 2011
audit berufundfamilie

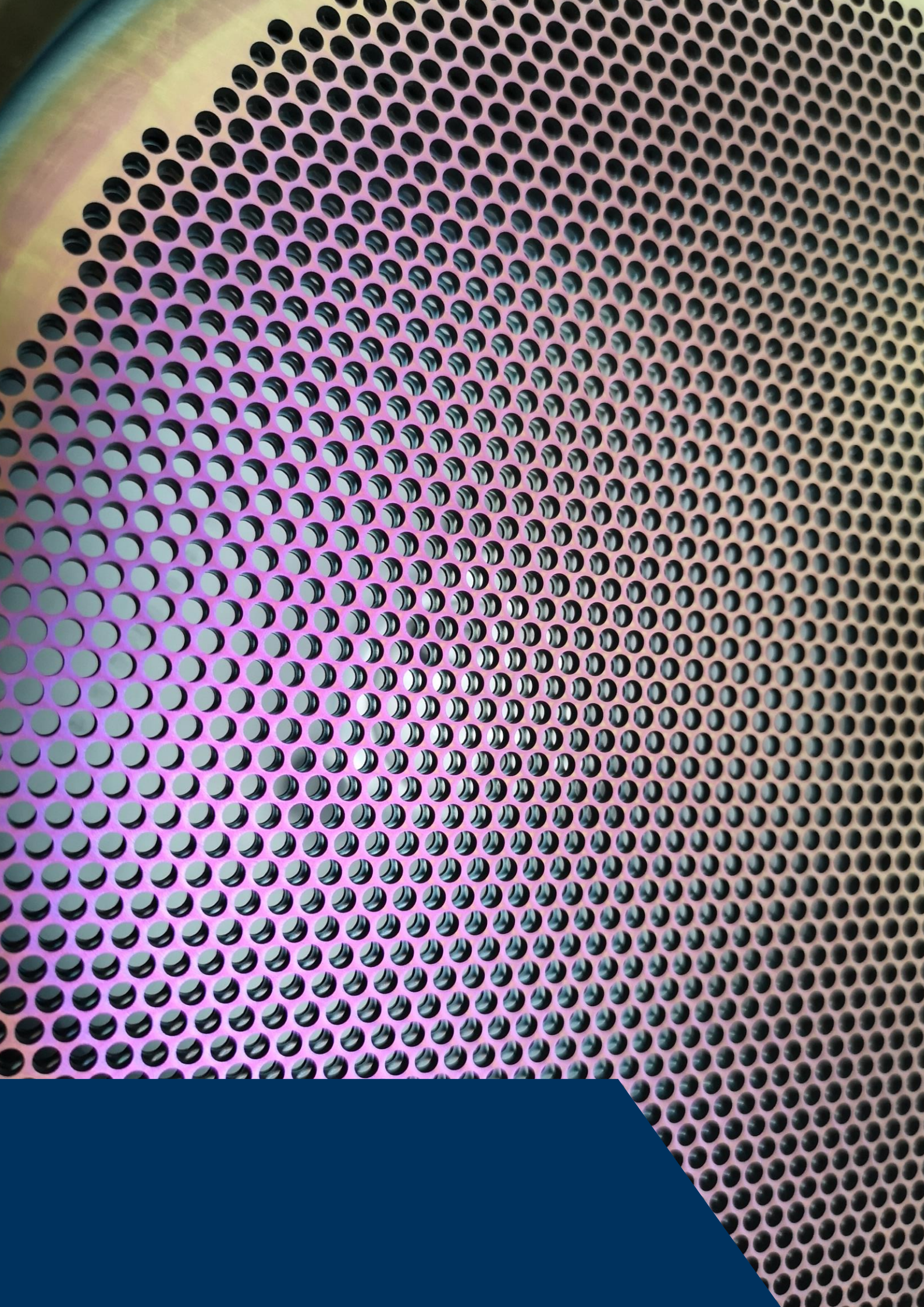

Scientific and Technology Results

Reports

Selected Results

Laser Irradiation-induced Modification and Crystallisation Dynamics of Epitaxial Phase Change Thin Films Grown by Pulsed Laser Deposition

A. Lotnyk, M. Behrens, J.W. Gerlach, M. Ehrhardt, P. Lorenz, B. Rauschenbach

Introduction

The working principle of conventional phase change memory is based on ultrafast reversible phase changes between crystalline and amorphous phases of Ge-Sb-Te (GST) materials. For information storage, a phase change memory device uses a large contrast either in electrical resistance between the amorphous phase (high-resistance state) and crystalline phase (low-resistances state) or in optical reflectivity between the amorphous phase (low reflectivity state) and crystalline phase (high reflectivity phase). Erasing of a GST-based memory cell is achieved by applying a high intensity pulse, either electrical or by a laser beam. These processes lead to the amorphization via melting and subsequent fast quenching of the phase change alloy. However, GST alloys are poor glass formers. Thus, high cooling rates are required to suppress the recrystallization of the alloys during the erase process. On the other hand, the write process is accomplished by applying either electrical or optical pulses with low intensity, resulting in an amorphous-to-crystalline phase transition. Due to intrinsic features of GST alloys, a main challenge in material science is the optimisation of memory writing times, which are limited by the crystallization kinetics of GST alloys. In order to increase the crystallisation rates, several strategies were proposed, including doping of GST materials, pre-crystallization of an amorphous matrix or using GST-based superlattices [1]. Being a nucleation-dominant material, improvements in crystallization speed can be, however, achieved by taking advantage of interface assisted crystal growth along a preferred crystallographic direction using epitaxial thin film systems [2]. This approach will allow to overcome the time-lag originating from the incubation period during nucleation.

This work aims to study structural modifications and crystallisation dynamics of epitaxial $Ge_2Sb_2Te_5$ (GST225) phase change thin films induced by nanosecond single pulse laser irradiation [3-5]. In particular, the epitaxial recrystallization of cubic GST225 (c-GST225) from a transient molten phase during the cool-down process is monitored by time-resolved optical reflectivity measurements and subsequently evaluated by high-resolution scanning transmission electron microscopy (HRSTEM) in detail. The approach to use such epitaxial thin films allowed to develop a method for quantification of ultrafast crystallisation dynamics. The crystallisation process was identified to be purely driven by crystal growth. Thus, direct access to the crystal growth kinetics in an application relevant scenario is shown, excluding any interferences with concomitant nucleation or influence of varying populations of subcritical nuclei in the amorphous phase [5]. Overall, the introduced methodology can be applied to a broad spectrum of similar materials and glasses in order to study solidification characteristics involving crystallization and amorphization on application relevant length and time scales.

Experiment

Epitaxial t-GST225 thin films were deposited on Si(111) substrates by pulsed laser deposition (PLD) [3,4]. The structure of the as-grown thin films was confirmed by X-ray diffraction measurements.

The microstructure of GST225 thin films was studied in a probe Cs-corrected Titan^3 G2 60–300 microscope operating at 300 kV accelerating voltage. High-resolution TEM (HRTEM) micrographs were acquired using a Gatan CCD camera. For HRSTEM, a probe forming annular aperture of 25 mrad was applied and all images were recorded with a HAADF detector using annular ranges of 80-200 mrad. The preparation of specimens for TEM observations were done by a combination of focused high- and low-energy ion beam milling.

To monitor the changes in reflectivity upon laser irradiation, a pump-probe setup was designed with an excimer laser of 248 nm wavelength and 20 ns pulse duration as pump source, whereas a diode laser of 633 nm operating in CW mode was used as probe source. The spot size of the pump laser beam on the surface of the thin films was 0.03 cm². The probe laser beam was detected by a Si photodiode and processed with a digital oscilloscope. The overall time resolution of the setup was 2 ns.

Results and Discussion

The insights into the structural modification of t-GST225 thin films upon ns-laser irradiation was deduced from studies at the nanoscale by using TEM [2]. Figure 1 shows a TEM image of a GST225 thin

film after single ns-pulse laser irradiation at a fluence of 35 mJ/cm^2. The film can be divided into three distinct regions (I, II and III) [2]. According to the image contrast and corresponding nanobeam electron diffraction (NBD) patterns, the region I reveals an amorphous GST phase, whereas regions II and III represent a crystalline structure. The NBD taken from region III revealed the as-grown t-GST255 phase, where the phase did not significantly change upon the laser irradiation. In contrast, the crystal phase in region II is c-GST225. Thus, the results of Figure 1 verify the phase transition from the layered t-GST225 phase to the cubic GST225 phase. The cubic phase forms from a transient molten phase at the melt-crystalline interface upon the cooling process and crystallizes with an epitaxial relationship to the parent phase. These findings are particularly useful for determination of crystallization dynamics of epitaxial GST225 thin films. The combination of TEM (identification of thickness of the cubic phase, d in m) and pump-probe experiments (identification of time needed for the crystallization of cubic phase, t in s) will allow the identification of the crystallization rates (v=d/t) of the c-GST225 phase.

Figure 2 shows the results of pump-probe experiments. The Figure represents the temporal evolution of the reflectivity of epitaxial t-GST225 thin films upon irradiation with a single ns-laser pulse of fluences in the range between 12 and 50 mJ/cm². In general, the reflectivity first decreases after exposing the thin films to the ns-laser pulse. This can be attributed to an initiated melting process of GST225 that fully unfolds at the end of the laser pulse where the maximum temperature is reached [5]. Additionally, high UV light absorption of GST225 results in a strong temperature inhomogeneity along the cross-section

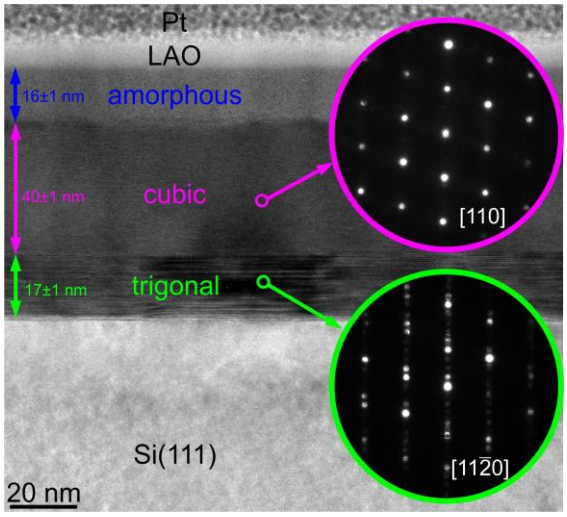

Figure 1: TEM image of a laser irradiated GST225 thin film showing three regions of different crystal structure together with corresponding nanobeam electron diffraction patterns.

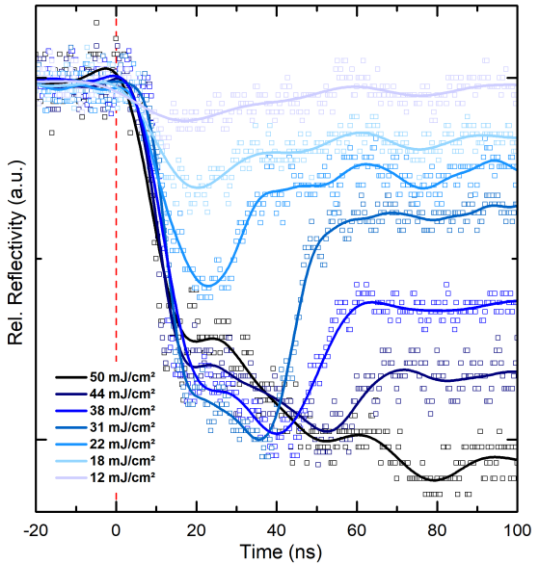

Figure 2: Time dependency of the reflectivity of an epitaxial t-GST thin film during irradiation with a single, 20 ns laser pulse at fluences varying between 12 and 50 mJ/cm². The ns-laser pulse is applied at t = 0 ns.

of the thin film. As a consequence, different cooling rates along the cross-section of the thin film are involved in the subsequent cool-down process of the material causing it to either recrystallize into the cubic phase of GST225 or quench into the amorphous phase (critical cooling rate ~10^9 - 10^{12} K/s). Accordingly, these solidification characteristics become discernible in the further temporal evolution of the reflectivity showing a clear increase in reflectivity. The latter can be ascribed to the recrystallization of c-GST225 from the liquid phase during the cool-down process. However, since c-GST225 exhibits a lower reflectivity than t-GST [3], the initial reflectivity is not fully restored. Moreover, a melt-quenched amorphous layer, which could also form during the cool-down process, might additionally contribute to a reduced reflectivity. Consequently, the final reflectivity is determined by the layer thickness distribution within the evolving three-layer stack consisting of a remaining t-GST225, a recrystallized c-GST225 and a melt-quenched a-GST225 layer (see Figure 1). As a result, by tuning the laser fluence and hence the layer thickness distribution in the GST225 thin film, multiple reflectivity states can be obtained. This paves the way for ultrafast multilevel data storage based on definite repositioning of planar interfaces between distinct layers of single phase GST225, promising enhanced precision and scalability compared to the traditional paradigm of controlling randomly distributed amorphous and polycrystalline fractions of phase-change material. Furthermore, the data encoding process is triggered by only a single ns-laser pulse in each case, whereas most methods rely on the accumulation of multiple pulses in order

to obtain intermediate reflectivity or resistivity levels, which is at the expense of time.

Figure 3(a) shows geometrical phase analysis (GPA) processed TEM images of the GST225 thin films after laser irradiation for two selected fluences of 31 mJ/cm² to 44 mJ/cm². The thickness of the recrystallized c-GST225 layer increases with the increasing fluence, while the thickness of the remaining t-GST225 layer decreases [5]. Remarkably, in the case of a single laser pulse of 44 mJ/cm² applied, a complete transition to the c-GST225 phase occurs, demonstrating an optimized match between the laser fluence and the thin film thickness, whereas for higher fluences amorphization in the upper part of the thin film occurs [5]. Importantly, the measurements reveal an epitaxial relationship between the t-GST225 and c-GST225 layer, which confirms that the recrystallization of the cubic structure is a crystal growth dominated process. The crystallisation starts at the crystalline-melt interface and proceeds in an epitaxial fashion towards the top of the thin film. Nevertheless, as indicated by ab initio molecular dynamics simulations, a supportive element during this recrystallization process could be remaining structural fragments of crystalline GST225 close to the t-GST225 boundary due to incomplete melting, which enables recrystallization with small atomic movements. Interestingly, in the case of 44 mJ/cm², no t-GST225 structure remained at all which shifts the focus to the Si(111) substrate. In this case, the substrate acts as a recrystallization template. However, a corresponding RGB rotation image calculated from GPA (Figure 3), reveals similar tendencies like in Figure 1: an adoption of the orientation of typical t-GST225(111) twins by the recrystallized c-GST225 structure. This might be a sign, that besides the underlying Si(111) substrate also the initial t-GST225 structure dictates the formation of c-GST225 phase. This assumption finds further support by the mostly intact interface between the substrate and the GST225 thin film. A possible scenario could be, that

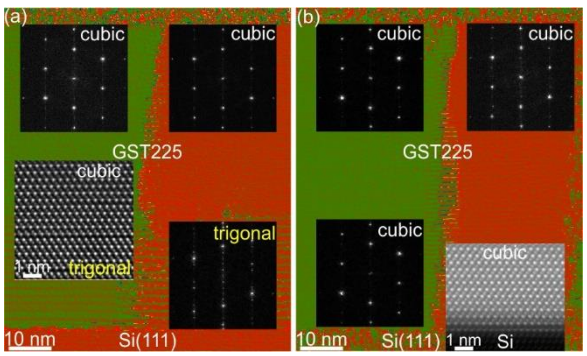

Figure 3: GPA rotation images of t-GST225 thin films irradiated with single ns-laser pulse at fluences of (a) 31 mJ/cm² and (b) 44 mJ/cm². Insets show FFT and HRSTEM images.

at temperatures approaching the melting point the Te sublattice is only weakly fragmented, whereas the mobility of Ge/Sb atoms is strongly increased, leading to an enhanced recrystallization into the cubic structure upon subsequent fast cooling compared to starting from a liquid phase.

By relating the travelled path of the recrystallization front of c-GST225 to the recovery time of the reflectivity extracted from Figure 2, the mean crystal growth velocity of c-GST along the (111) direction can be obtained (Figure 4). However, during the reflectivity measurements a small part of scattered light from the intense UV pump pulse is additionally detected by the photodiode. For higher fluences, this overlap with the probe signal becomes noticeable by a weaker decrease in reflectivity starting at about t = 17 ns due to the impact of the falling edge of the pump pulse. However, the ending point of the recrystallization process is not obscured and can be clearly identified in Figure 2, except for irradiation with 50 mJ/cm², where the 20 nm thick amorphous top layer prevents the detection of the crystallization front by the probe laser due to limited penetration depth of the laser light [5]. The starting point of recrystallization is expected to be at the end of the laser pulse at t = 20 ns where the material immediately starts to cool down and the solid-melt interface being at 900 K starts to move towards the top of the thin film. However, in Figure 2, the minimum in reflectivity for the irradiation fluence of 22 mJ/cm² is at about 24 ns, indicating a delay time of approximately 4 ns for crystallization. This delay time is repeatedly observed during measurements on epitaxial t-GST225 thin films and could be attributed to an instability of forming crystalline nuclei at temperatures still close to the melting point. Obviously, the crystal growth velocity increases with increasing fluence from ~0.4 m/s for 18 mJ/cm² up to ~1.7 m/s for 44 mJ/cm², whereas at higher fluences saturation is observed. This saturation can be expected, considering that for higher fluences an increased part of the thin film is transformed without initiating an amorphization during the cool-down process. In contrast, by further increasing the fluence up to 50 mJ/cm², amorphization due to a comparatively higher cooling rate is found. Accordingly, in the case of 44 mJ/cm², the solidification of GST225 takes place at the highest possible cooling rate. Hence, the highest detectable crystal growth velocity of the employed epitaxial GST225 thin film model system is 1.7 m/s, which is well in line with a recently theoretically predicted value (~1.5 m/s at ~ 700 K). Nevertheless, considering that the obtained crystal growth velocities in the present work represent a mean value covering the entire cross-section of the thin film, peak velocities exceeding 2 m/s are

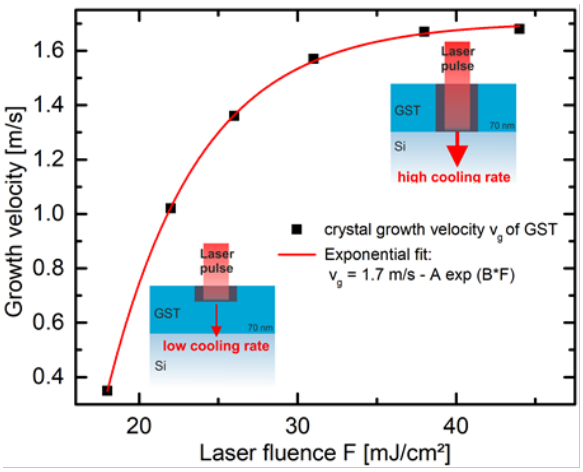

Figure 4: Crystal growth velocities in dependency of applied laser fluences as well as exponential fit to the data with A = 30 m/s and B = -0.17 cm²/mJ..

assumed. Thus, the obtained values also seem plausible with regard to the growth velocities obtained by ultrafast DSC (~2.8 m/s). In contrast, experimental studies capturing crystallization rates of melt-quenched GST in application relevant scenarios mostly report lower maximum growth rates in the range of 1 m/s, while similar values are also reported in earlier theoretical works. In this work, a substantial difference compared to the above-mentioned experimental studies is the use of epitaxial GST225, which allows the directed recrystallization of the c-GST225 structure along its [111] direction, where a planar boundary of either [0001] oriented t-GST225 or [111] oriented Si serves as a recrystallization template. Hence, the slightly increased crystal growth speed found in this work could be due to the improved crystalline quality and the reduced crystal growth activation energy resulting from the epitaxial recrystallization mechanism. It should be also mentioned, that besides different thermal responses of the GST225 thin film to ns-laser heating, the impact of size effects on the viscosity could become crucial during the solidification process, which could lead to reduced crystal growth kinetics in case of only small volumes of GST225 being transformed.

Conclusion

In conclusion, structural modifications and crystal growth dynamics of epitaxial t-GST225 thin films induced by single ns-laser pulse irradiation are studied. By combining laser-assisted time resolved reflectivity measurements with HRSTEM, the ns-laser induced structural transitions are temporally and spatially resolved. It is found, that due to laser heating, the thin films partially melt, followed by epitaxial recrystallization into the cubic phase of GST225 during the subsequent cool down process. This results in the formation of multiple reflectivity states based on the relocation of planar interfaces between single-phase layers of GST225, offering a novel approach to multilevel data storage in phase change memory. By extracting the durations for the growth of the recrystallized c-GST225 layers and the corresponding thicknesses, the obtained crystal growth rates are ranging from 0.4 m/s to 1.7 m/s. The latter represents the upper limit of the employed epitaxial GST225 thin film model system, when amorphization is to be avoided. In essence, the present work sheds light into the crystal growth kinetics of GST225 and beyond that, introduces a method for quantification of crystallization speeds and amorphization processes of a broad variety of similar phase-change systems. Moreover, this work demonstrates amorphization and crystallization of GST225 material by using UV laser with single pulse duration and wavelength only, where in the conventional amorphous-to-crystalline phase transitions lasers with different pulse durations, number and wavelengths are usually applied.

Acknowledgements

The financial support of the Free State of Saxony within the project “Switching with light” (SAB project) is greatly acknowledged. The authors thank Mrs. A. Mill for TEM specimen preparation.

Literature

[1] A. Lotnyk, I. Hilmi, U. Ross, B. Rauschenbach, Nano Research 11 (2018) 1676
[2] M. Behrens, A. Lotnyk, J.W. Gerlach, I. Hilmi, T. Abel, P. Lorenz, B. Rauschenbach, Nanoscale 10 (2018) 22946
[3] M. Behrens, A. Lotnyk, U. Roß, J. Griebel, P. Schumacher, J.W. Gerlach, B. Rauschenbach, CrystEngComm 20 (2018) 3688
[4] A. Lotnyk, M. Behrens, B. Rauschenbach, Nanoscale Adv. 1 (2019) 3836
[5] M. Behrens, A. Lotnyk, J.W. Gerlach, M. Ehrhardt, P. Lorenz, B. Rauschenbach, ACS Appl. Mater. Interfaces 11 (2019) 41544

High-Energy Electron-Treatment of Biological Hydrogels: Biomimetic Hydrogels, Stimuli-Responsive Systems and Functional Surfaces

S. Riedel, P. Hietschold, R. Konieczny, W. Knolle, S. G. Mayr

Introduction

Biological hydrogels such as collagen and gelatin are highly attractive materials for tissue engineering and biomedicine. Due to their excellent biocompatibility and biodegradability, they represent promising candidates in regenerative medicine, cell culture, tissue replacement and wound dressing applications. They are characterized as polymeric networks with the ability to absorb, store and release large amounts of water while maintaining their dimensional stability. Due to this swelling behaviour, hydrogels represent promising materials in biomedical applications where hydration-responsive materials are required. They can be classified into natural and synthetic hydrogels, distinguished by their source.

Natural hydrogels are obtained from biological sources while synthetic hydrogels are artificially produced. While synthetization of hydrogels enables precise control of composition, structure and material properties, natural hydrogels show strong conformity to biological tissue. This conformity is needed in tissue engineering and replacement, as biomedical coatings, culture substrate for cells and tissues or as implants. As the main structural protein in the extracellular matrix, collagen is a highly attractive candidate for biomedical applications due to its biocompatibility and low immunogenicity. As a derivative of collagen, gelatin shows a similar degree of biocompatibility and biodegradability, which makes it extremely interesting as biomaterial. However, in case of gelatin, thermal stability has to be enhanced for many biomedical applications because gelatin undergoes a gel-sol transition at temperatures underneath the human body temperature. Thermal stabilization can be obtained by polymer crosslinking, which further tunes material properties such as network organization, rheological properties, swelling and stimuli-responsiveness.

Electron-beam-induced crosslinking is a reagent-free and efficient technique to crosslink hydrogels [1]. Other methods utilize chemical crosslinkers, dehydrothermal treatment or ionizing radiation. While the use of chemical crosslinkers always introduces additional components into the system and dehydrothermal processing is not applicable to hydrogels in wet state and at room temperature, ionizing radiation promises non-toxic and reagent-free crosslinking under ambient conditions. Compared to radiation techniques utilizing gamma- and UV-irradiation, electron-beam treatment provides higher irradiation rates and higher penetration depths, respectively.

With this, electron-beam-treatment represents a highly favourable and promising technique to crosslink hydrogels for biomedical applications. However, the high potential of electron-beam treated collagen gels and their cytocompatibility is not yet sufficiently investigated. In addition, electron irradiated gelatin shows fascinating features, which can be used to develop stimuli-responsive systems and functional surfaces. These aspects were investigated in more detail in the report period.

Experiment

Collagen gels were prepared from rat-tail collagen (collagen R, 0.4 % solution, Cat. No. 47256.01; SERVA Electrophoresis, Germany) and bovine skin collagen (collagen G, 0.4 % solution, Cat. No. L 7213; Biochrom, Germany) in a ratio of 1:2, respectively. The collagen solution was prepared on ice to avoid polymerization and was gently mixed until homogeneity. A phosphate buffer containing Na_2HPO_4 (Cat. No. 71636; Sigma-Aldrich Chemie GmbH, Germany) and NaH_2PO_4 (Cat. No. 71507; Sigma-Aldrich Chemie GmbH) was added to obtain a pH of 7.5 and a total phosphate molarity of 200 mM in all gels. The collagen samples polymerized at 37 °C and 100 % humidity for 24 h. The samples were rinsed twice and stored in distilled water at room temperature until use.

The gelatin samples are prepared by dispersing gelatin type A from porcine skin (G2500, Sigma-Aldrich Chemie GmbH, Germany) in deionized water with various concentrations up to 10 wt%. After a swelling time of 1 h, the gelatin solution is heated to 60 °C until the gelatin is liquefied and homogenously dispersed. The gelatin solution is poured into moulds or petri dishes to obtain the shapes desired for the experiments. Afterward, they are cooled to 8 °C for at least 2 h to polymerize. Between measurements, the samples are stored at 8 °C.

Irradiation was performed using a 10 MeV linear electron accelerator (MB10-30MP; Mevex Corp.,

Canada). The electron accelerator is equipped with a moving stage with a repetition rate of 180 Hz and a scanning horn with scanning frequency of 3 Hz. The electron pulses have a length of 8 µs. Final doses ranging from 5 to 100 kGy were obtained in steps of 5 kGy. The doses were measured with respect to a graphite dosimeter to an uncertainty of 5 %. During electron beam treatment, the samples were cooled to room temperature by draft to prevent overheating and thereby induced degradation. After irradiation, the samples were stored at 37 °C and 100 % humidity for 48 h and later at RT or 8 °C.

The obtained materials and systems were then analysed via various different techniques depending on the intended application. The biomimetic collagen hydrogels were investigated via FTIR spectroscopy, 3D microscopy, network analysis, rheological measurements and cytocompatibility tests [1]. The developed stimuli-responsive gelatin systems were characterized experimentally via determination of response efficiency [2]. In addition, the system was simulated by molecular dynamics. The functional surfaces were analysed via atomic force microscopy at physiological conditions, 3D microscopy and cytocompatibility as well as long-time degradation tests [3,4].

Results and Discussion

Biomimetic Collagen Gels

The performed experiments were able to demonstrate that electron beam treatment enables precise modification of collagen hydrogels towards controllable ECM model systems [1]. FTIR measurements indicate that electron beam assisted crosslinking induces only minor changes, while the characteristic polymeric structure of collagen is maintained also for doses as high as 100 kGy. Pore size analysis indicates precise tunability of the network pore size. Rheological investigations (see Fig. 1) show network stiffening over one order of magnitude, which correlates with an increase in crosslinking density. Thereby, our cell-experiments (see Fig. 2) revealed an excellent cytocompatibility of electron irradiated collagen gels in terms of cellular viability. With these investigations, high-energy electron irradiation induced crosslinking is shown to be a highly promising technique to tune collagen hydrogels in order to mimic the extracellular matrix and other collagenous tissues by tailoring material characteristics such as structure and mechanics in a physiological relevant range. In addition to excellent cytocompatibility, these defined collagen systems represent 3D tissue models which are highly relevant in cell culture, as coatings or implants and are necessary to study cellular behaviour in biomimetic tissue as in cancer research or to investigate drug delivery and distribution for pharmaceutical applications.

Stimuli-Responsive Gelatin Systems

It was also possible to realize the development of a thermal responsive gelatin system by high-energy electron irradiation for actuatoric applications [2]. This is achieved by introduction of a shape-memory effect (see Figure 3), viz., a temperature-induced transition from a secondary into a primary shape that has been programmed in the first place merely by exposure to energetic electrons without addition of

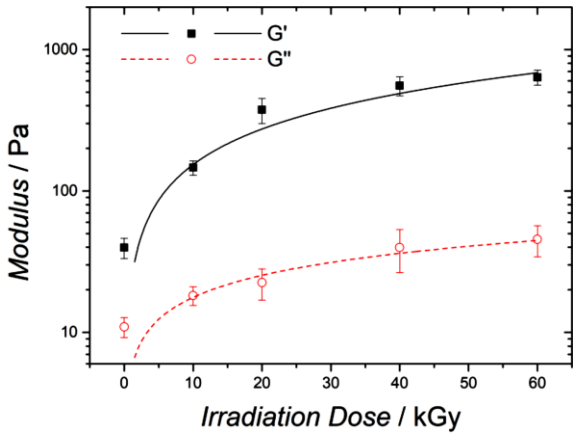

Figure 1: Storage and loss moduli of electron irradiated collagen (2 mg/ml) in dependence on radiation dose, with power law fits. Error bars indicate standard deviation.

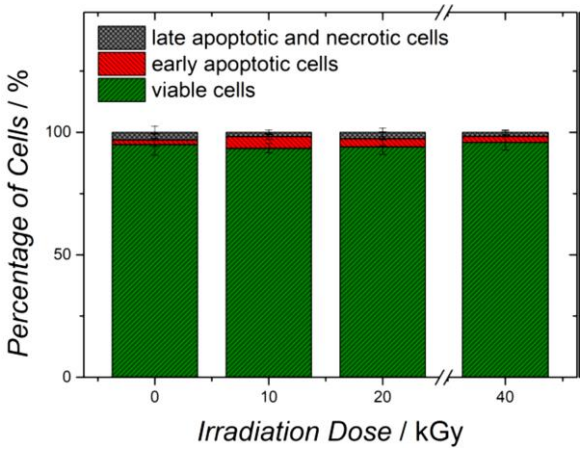

Figure 2: Cellular viability: NIH 3T3 fibroblasts cultured on electron crosslinked collagen gels (2 mg/ml) as function of irradiation dose. Error bars indicate standard deviation.

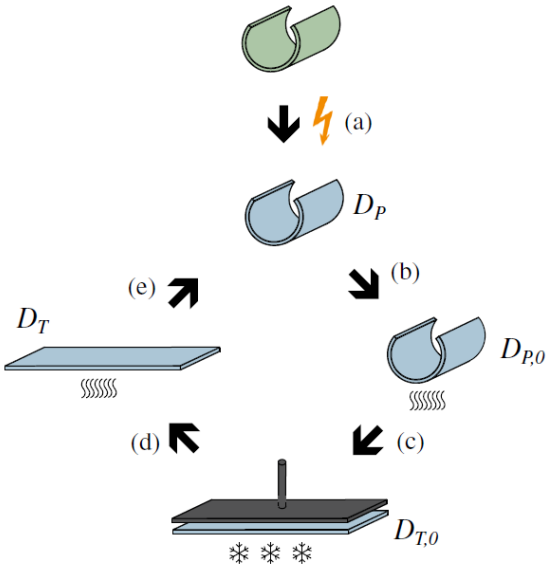

Figure 3: Sketch of the experimental steps of programming and demonstrating the shape-memory effect in electron-beam modified gelatin. Exemplarily, deformation of a bent gelatin layer is shown. (a) Gelatin is irradiated with 10 MeV electrons. (b) Irradiated gelatin is heated to 50 °C. (c) The sample is deformed into a temporary shape and then cooled to 8 °C. (d) The deformed sample is heated again to 50 °C to initiate shape-memory effect resulting in (e) almost complete shape recovery.

potentially hazardous crosslinkers. While this scenario is experimentally quantified for exemplary actuators, a theoretical framework capable of unravelling the molecular foundations and predicting experiments is also presented. It particularly employs molecular dynamics modelling based on force fields that are also derived within this work. Implementing this functionality into a highly accepted material, these findings open an avenue for large-scale application in a broad range of areas.

Functional Gelatin Surfaces

It was further possible to develop mechanically patterned gelatin surfaces (see Figure 4) by a two-step-process involving local as well as global electron irradiation for patterning and thermal stabilization, respectively. Our investigations indicate that focused electron irradiation as used in electron-beam lithography is an effective and precise reagent-free technique to mechanically pattern hydrogels such as gelatin in order to obtain functional biomaterials and -surfaces. We were able to show that gelatin layers have a precise topographical and mechanical pattern with excellent periodicity after local irradiation in the dry state and following rehydration. Irradiation using highly focused electron beams further enables creation of various different patterns in the µm-range and even lower. Global electron irradiation in wet conditions induces thermal

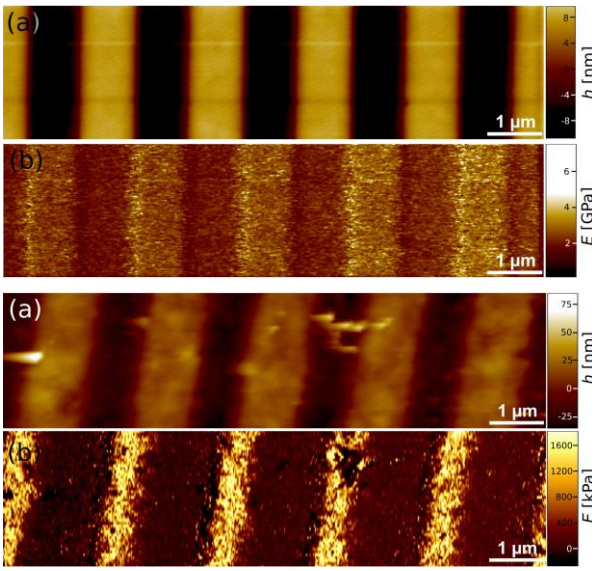

Figure 4: AFM images of mechanically patterned gelatin layers. Top: Dry state before global irradiation. Bottom: Wet state after global irradiation. (a) Topographical image showing height information of the layer. (b) Mechanical image showing local E-modulus.

stability of the functionalized layers for possible biomedical applications. By varying the hydrogel, irradiation conditions, as well as gel concentration, customization of the reagent free mechanically patterned polymer substrate is possible.

Next to mechanically patterned gelatin surfaces, topographically patterned gelatin hydrogels are of high interest for example to develop customized culture substrates for tissue regeneration. Therefore, we described a patterning method utilizing moulding wherein a silicon template was used to transfer customized stripe patterns onto gelatin hydrogels. The patterned hydrogels were then stabilized against gel−sol transition by high-energy electron beam treatment, inducing network crosslinking. Pattern transfer was then investigated in dependence on gelatin concentration and irradiation dose. In addition, cytocompatibility experiments of HUVECs and NHDFs on the patterned hydrogels were performed. The study showed gelatin concentration dependencies of the pattern transfer. It was able to determine a pattern transfer optimum at gel concentrations around 12−14 wt %. In addition, the effect of irradiation dose on pattern transfer was investigated, showing strong dependencies on dose, which enables precise adaption of the pattern. Long-time experiments (see Figure 5) at physiological conditions demonstrated stability of the pattern up to 40 days, which enables long-time applications. The cytocompatibility tests demonstrated good biocompatibility and low toxicity to HUVECs and even better biocompatibility and extremely low toxicity to NHDFs in pres-

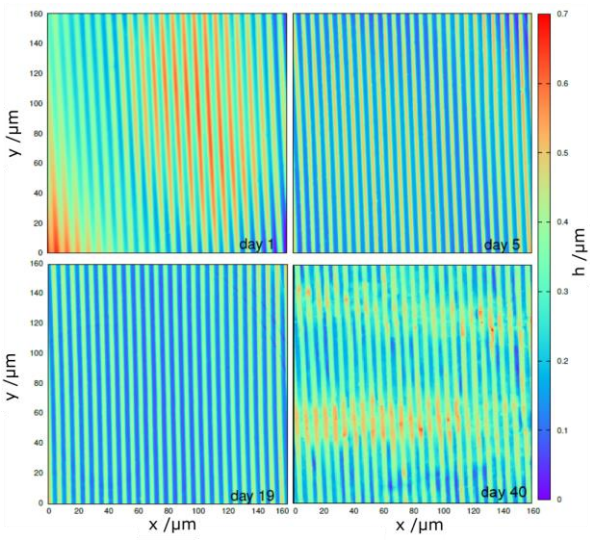

Figure 5: Representative surface topography of a 10 wt % 40 kGy gelatin sample stored in PBS at 37 °C, 5 % CO_2, and 100 % humidity. Top left: day 1. Top right: day 5. Bottom left: day 19. Bottom right: day 40.

ence of patterned gelatine hydrogels. Significant differences between cells grown on plain gelatin hydrogels compared to cells grown on patterned hydrogels were found. This indicates excellent contact guidance potential and improved cellular growth support of patterned hydrogel substrates, pointing out their potential usage for regenerative medicine applications. Future genetic analysis of cells cultured on cross-linked patterned and unpatterned gelatin in comparison with in vivo grown fibroblasts will unravel the differences of the 3D model and the in vivo condition.

Conclusion

In conclusion, we were able to demonstrate the high potential of high-energy electron crosslinked hydrogels for biomedical applications. We introduced new concepts for the development of biomimetic as well as stimuli-responsive materials and functional surfaces from collagen and gelatin. High-energy electron-crosslinking was shown to be a highly advantageous technique to tune various material properties such as mechanical and structural properties or stimuli-response while excellently maintaining cytocompatibility and chemical integrity. These investigations and concepts might be the basis for optimized synthetization of highly functional, customizable and smart biocompatible hydrogel materials for specific applications such as in regenerative medicine, implant development or tissue engineering.

Literature

[1] S. Riedel*, P. Hietschold*, C. Krömmelbein, T. Kunschmann, R. Konieczny, W. Knolle, C. Mierke, M. Zink, S. G. Mayr, Materials & Design 168 (2019) 107606; *contributed equally
[2] S. Riedel, S. G. Mayr, Physical Review Applied 9 (2018) 024011
[3] S. Riedel, K. Bela, E. I. Wisotzki, C. Suckfüll, J. Zajadacz, S. G. Mayr, Materials & Design 153 (2018) 80
[4] M. Tadsen*, R. P. Friedrich*, S. Riedel*, C. Alexiou, S.G. Mayr, Applied Materials & Interfaces 11 (2019) 7450; *contributed equally

Ion Beam Planarization of Optical Aluminium Surfaces

M. Ulitschka, J. Bauer, T. Arnold

Introduction

For many years aluminium has been used as construction material for optical mirrors, e.g. in laser systems, spectrometers, or telescopes, as it is cheap, lightweight, and can be easily machined employing ultra-precision single point diamond turning or milling technologies. Furthermore, aluminium has a high reflection coefficient which ranges from the infrared to the shortwave visible (VIS) and ultraviolet (UV) spectral range with values well above 90%. The surface error topography after manufacturing by single-point diamond turning (SPDT) is applicable in the infrared spectral range. The optical surface has roughness values of typically below 10 nm root mean square (RMS) and at best 2 – 3 nm. The machined surface after SPDT exhibits a periodic groove pattern microstructures left by the cutting tool. Those so-called turning marks have a pitch of some microns and an amplitude ranging between 10 – 30 nm. Therefore, these periodic patterns have similar effects as a diffraction grating in optical applications in visible and ultraviolet spectral range. Thus, for increasing demands on the optical surface quality in the shortwave VIS and UV spectral range further improvement of the surface form and roughness is required. Standard optical surfacing techniques comprise a processing chain where preshaped aluminium surfaces are coated by amorphous NiP for further diamond turning, followed by mechanical polishing or ion beam planarization (IPB) and form error correction steps employing e.g. magnetorheological finishing (MRF) or ion beam finishing (IBF). NiP has an isotropic amorphous matrix which is suitable for the combination of SPDT and polishing processes, as well as ion beam techniques. Diamond-turned NiP reveals even smoother surfaces than pure aluminium and can be further improved by one or multiple sequential ion beam planarization processes where turning marks are successfully reduced. Hence, micro roughness values of <1 nm RMS are achievable, resulting in sufficiently smooth optical surfaces. Finally, an additional metallization layer on top of the NiP coating is necessary to realize the desired reflective properties for the specific application. However, the mismatch of thermal expansion coefficients between aluminium and NiP coating can cause mechanical stress formation under thermal load conditions resulting in bending and distortion of the optical surface. Hence, it is desirable to perform form correction and smoothing of the optical surface on the pure aluminium surface with no further coating by means of ion beam techniques directly after the premachining by SPDT. However, the microstructure of aluminium leads to severe roughening when bombarded with inert gas ions such as argon. In contrast, it has been shown that reactive ion beam etching (RIBE) using reactive process gases such as oxygen and nitrogen allows the original surface topography to be maintained during ion beam processing. Thus, this technology allows figure error correction of aluminium mirrors without degradation of the surface quality, as it was shown in [1]. The IBP process represents another promising technology also for the treatment of pure aluminium surfaces. In IBP the rough substrate surface is covered with a planarizing layer of a specific thickness, so that the high-spatial frequency surface roughness features are fully embedded and surface waviness is levelled to a considerable extend. As a result, a smooth and planar surface is revealed. Depending on the initial surface quality, the thickness of the planarizing film typically ranges between some 100 nm and a few microns. Then, the plane surface is transferred to the underlying substrate by ion beam etching. To ensure an optimum surface transfer, the etch rates of planarizing film and aluminium substrate should be equal.

In most cases the planarizing layer consists of a photoresist applied by spin coating to the surface. In the present work the preparation of the photoresist layer was investigated aiming at maximum stability and roughness preservation during ion beam etching using nitrogen as process gas. The optimum preparation steps were explored based on roughness evaluation, analysis of chemical modifications, and etch resistance of the photoresist during ion beam irradiation. Furthermore, a process route for smoothing of aluminium surfaces was evaluated to attain the required surface quality. Reactive ion beam etching-based planarization was conducted on single-point diamond turned aluminium alloys (RSA Al905 and RSA Al6061). Such alloys are standard materials in optical mirror fabrication. The optimum process route and the roughness evaluation was explored by topographic analysis applying a combination of white light interferometry and atomic force microscopy measurements. It has turned out that a 2-step process (comprising the nitrogen ion beam planarization step followed by an ion beam irradiation using oxygen as process gas) results in a significant improvement of

aluminium surface roughness over a broad spatial frequency range.

Experiment

For the experiments diamond turned aluminium disc samples of 50 mm in diameter were used as test substrates. The negative working photoresist ma-N 2405 (micro resist technology) was employed as the planarization layer. The substrates were cleaned with acetone prior to photoresist spin coating performed at 30 seconds at 3000 rotations per minute. The substrates were prebaked at 90°C to evaporate the solvents. In accordance to the thickness of the substrate materials, the baking times for silicon wafer and aluminium substrate were adapted. Conventional DUV exposure in a photolithography system was then applied to provide a homogeneous and well crosslinked polymer matrix. An optional postbaking step was applied at 150°C on a hotplate for 2 minutes on silicon wafer and 10 minutes on aluminium. After all application steps the photoresist layer thickness was approximately 500 nm.

Ion beam machining experiments were performed in a high vacuum chamber with a base pressure of $2x10^{-5}$ Pa. The ion beam was generated by a 13.56 MHz radio frequency (RF) ion source with a focusing triple grid extraction system allowing a constriction of the free-beam without use of an aperture. The water-cooled sample holder was mounted on a five-axis motion system. The water cooling ensures efficient heat dissipation from the sample reducing thermal effects during the process. The ion beam parameters were chosen to result in a Gaussian shaped ion current density distribution function exhibiting a full-width at half maximum (FWHM) of 4-15 mm. Nitrogen and oxygen process gas was used for the generation of low-energy ion beams at ≤1.5 kV beam voltage. The machining experiments were performed at normal ion beam incidence angle with respect to the substrate surface.

In order to investigate the effects in resist etching, preliminary experiments were performed on spin coated silicon wafers with a diameter of 2 inch. An aluminium mask with an opening diameter of 13 mm defined the machining area for ion beam test etching experiments to determine the etch rates of planarization layer and aluminium. The ion beam was scanned applying a raster path over the surface with a constant velocity of 4 mm/s and a line pitch of 1 mm in order to ensure a homogeneous material removal.

Ion beam planarization experiments on RSA Al6061 and RSA Al905 were performed in a two-step process. In the first planarization process step the entire aluminium mirror surface, coated with the photoresist layer, without an additional mask was etched with N_2. During this process step 8 – 10 scan repetitions were necessary to remove the whole photoresist layer. In a subsequent second process step the aluminium surface was etched directly with O_2 within 1 scan repetition. For the second RIBE finishing step no photoresist layer was used.

The sample topography was analyzed by white light interferometry (WLI; Bruker NPFLEXTM 3D Surface Metrology System) and atomic force microscopy (AFM; Bruker Dimension ICON). For WLI an objective with 5fold magnification was used with a 1x field of view multiplier in phase-shift interferometry mode. The image size was 1230 µm x 925 µm with a pixel resolution of 640 x 480. AFM was operated in tapping mode in a xy -closed loop configuration. Scanning areas of 10 µm x 10 µm and 50 µm x 50 µm were measured with a pixel resolution of 1024 x 1024. The raw data were subjected to a plane correction consisting of a global plane fit and a line-wise correction subtracting a fitted polynomial function of the 3rd order from each scan line via SPIP™ software. Surface roughness analysis was performed via calculating the power spectral density (PSD) function using a self-written MATLAB® script. By calculating the square root of the integrated PSD, root mean square (RMS) roughness values were evaluated. The spatial frequency ranges for waviness/roughness and microroughness were defined as 0.0024 μm^{-1}–1.7 μm^{-1} and 1.7 μm^{-1}–20 μm^{-1}, respectively. Consequently, the full range RMS roughness was calculated in the spatial frequency range of 0.0024 μm^{-1} – 20 μm^{-1}.

Results and Discussion

The initial aim of the work was to determine the optimum postbaking temperature of the photoresist in order to obtain maximum long term stability of the resist layer. GC-MS measurements indicate that remaining amounts of organic solvent are almost completely removed during postbaking at 150°C. AFM measurements reveal that the initial surface roughness of approximately 0.35 nm RMS is preserved. Postbaking at elevated temperatures above 200°C shows thermo-oxidative degradations. This result is of high importance since the degradation mechanism can also be expected to appear during ion beam treatments, if the heat dissipation is not sufficient. Indeed, a strong resist degradation was observed at either high ion current densities, which are accompanied by a strong thermal impact into the resist layer, or for insufficient sample cooling.

In a next step, the capability of the photoresist to embed the roughness features of a SPDT aluminium surface was investigated.

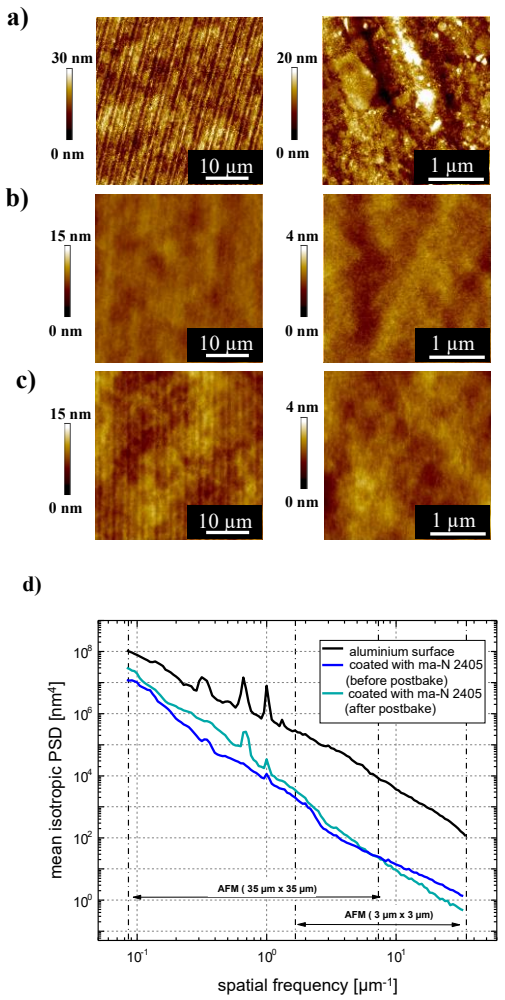

Figure 1: AFM measurements a) bare Al905 surface, b) spin-coated, prebaked and DUV exposed, c) after postbaking and d) PSD function.

From Fig. 1 it can be seen that the initial surface of Al905 is dominated by 3 µm spaced turning marks corresponding to the PSD deviation at 0.3 μm^{-1} with several superstructures (Fig. 1(a/d)). After photoresist coating the turning structures were almost fully embedded and a smooth surface is revealed (Fig. 1(b)). As a consequence, the PSD curve is strongly decreased in the spatial frequency range of 0.086 μm^{-1}-34.7 μm^{-1} and the PSD deviations corresponding to the turning marks are almost completely removed (Fig. 1d). However, these structures become more apparent if postbaking is applied (Fig. 1c). Due to a shrinkage of the layer during temperature treatment the turning marks are transferred into the negative photoresist. On the other hand, the granular structure after exposure is smoothed during heating (see Fig. 1b/c). That may be attributed to flowing of the polymer due to structural reorganization

Roughness evolution of the resist surface during RIBE was determined performing stepwise material removal. It could be shown that for removal up to 450 nm the RMS value of approx. 0.26 nm is mainly preserved. It was also shown, that the etch rate remains constant, if postbaking is applied. Omitting this preparation step results in initially higher rates that decrease with increasing etching depth or etching time, respectively. This behavior may be due to remaining organic solvent in the thin photoresist layer. With increasing material removal, the remaining organic solvent evaporates resulting in the same steady state etching conditions as the postbaked layer, and an etching rate of 1.1 mm³/h is achieved.

Direct RIBE machining was performed on both aluminium alloys to investigate etching rate and roughness evolution. Etch rates have been determined to be 0.54 mm³/h and 0.68 mm³/h for RSA Al6061 and RSA Al905, respectively, which results in etch selectivities of 0.53 and 0.61. Fig. 2 shows PSD functions for both tested alloys before and after ion etching. The distinct peaks located between 0.3 μm^{-1} and 1 μm^{-1} correspond to the evenly spaced turning marks. After the etching process the waviness and roughness is mainly preserved. However, in the high frequency range, the microroughness increases. From AFM measurements (not shown here) it can be concluded that small particles and granules with diameters of several hundreds of nanometers are formed on the Al905 surface, whereas on the Al6061 surface small etch pits with sizes in the sub-micrometer range are observed. TOF-SIMS experiments performed in positive mode reveal several alloying constituents in Al905 such as Ti, Ni, Cu, Ga, Fe, Mn, and Mg and Zr. The particles formed on the surface after RIBE machining are mainly due to Cu and Ni

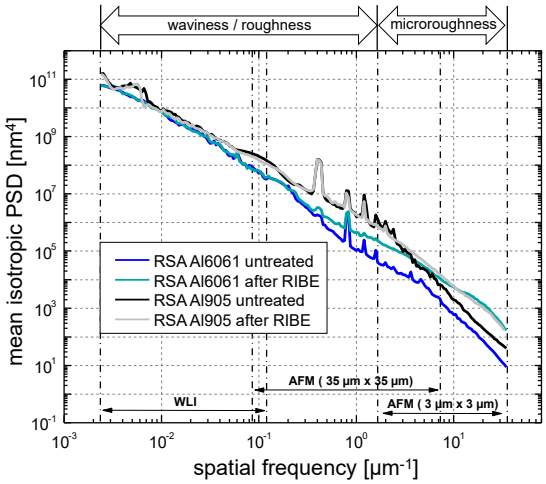

Figure 2: PSD functions of RSA Al6061 and Al905 surfaces before and after direct RIBE processing with no resist layer.

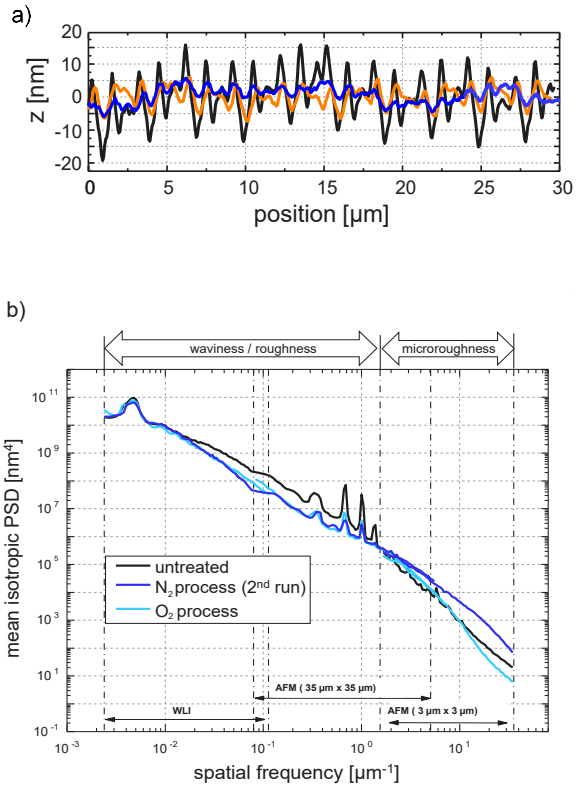

Figure 3: a) Surface indicating the turning marks at black: initial, orange: 1st IBP run, blue: 2nd IBP run; b) PSD functions of RSA Al905 after planarization and O2 step.

precipitates that are unevenly distributed over the surface. Significant Si and Mg fractions are found together within the etch pits on the Al6061 surface [2].

After having clarified the individual processes taking place during nitrogen irradiation, the planarization of aluminium surfaces has been investigated. Results for Al905 are shown in Fig. 3. The initial surface roughness was 9.7 ± 1.6 nm RMS, while the turning mark height was 23.6 ± 0.8 nm. As shown in Fig. 3(a), during the first run, the turning marks are reduced in height by about 66.5 % with smoothed edges. Due to a selectivity of 0.52 of the first planarization run, the height reduction is larger than expected. The reduction of the turning mark height may additionally be enhanced by the ion incidence angle dependent sputter yield as a function of the local surface error slope. Consequently, the roughness features with high slope border areas may be gradually smoothed. During the second run a further reduction of 44.5 % in turning mark height is observed correlated to a selectivity of 0.55. Hence, after two subsequent planarization steps the final roughness could be decreased down to 5.9 ± 1.1 nm RMS and the turning marks height shrinked to 4.3 ± 0.5 nm, which is an overall decrease by 82%. However, an increase of the microroughness during the process is observed, as shown in Fig. 3(b). As a result, the surface exhibits a diffusive shine. For applications in the VIS and UV spectral range a further reduction of the increased microroughness is prerequisite. Additionally, the formed nitride layer has to be removed. Thus, a subsequent ion beam machining with 1.5 keV oxygen ions was applied. Here, the material removal was chosen to be below 10 nm to avoid inhomogeneous matrix structure effects [3]. After RIBE machining with oxygen process gas the turning marks remain almost unchanged, while the microroughness determined in the range is remarkably reduced.

AFM and TOF-SIMS measurements revealed that particles were reduced and an oxynitride layer of approx. 16 nm thickness is formed on top of the surface. Above 10 µm^{-1} spatial frequency the PSD curve runs even below PSD curve of the untreated surface indicating a smooting in this region [4].

Conclusion

A processing route for planarization of SPDT aluminium surfaces was investigated and the underlying mechanisms were elucidated. It could be shown that the application of two subsequent IBP steps using nitrogen followed by an oxygen etching step results in a significantly smoothed aluminium surface over the entire measured spatial frequency range. In addition to the RIBE-based surface figuring technique, this promising technology enables the smoothing of high-spatial frequency errors of single-point diamond turned aluminium alloys while preserving or even improving the initial microroughness.

Literature

[1] J. Bauer, F. Frost, T. Arnold, J. Phys. D Appl. Phys. 50 (2017) 085101
[2] M. Ulitschka, J. Bauer, F. Frost, T. Arnold, Proc. SPIE 11032, EUV and X-ray Optics: Synergy between Laboratory and Space VI (2019)
[3] J. Bauer, F. Frost, A. Lehmann, M. Ulitschka, Y. Li, T. Arnold, Opt. Eng. 58 (2019) 092612
[4] M. Ulitschka, J. Bauer, F. Frost, T. Arnold, J. Astron. Telesc. Instrum. Syst. 6 (2020) 014001

Surface Modification and Electron Irradiation of Nanodiamonds

C. Laube, W. Knolle, A. Kahnt, J. Griebel, A. Lotnyk, J. Zhou, A. Prager, B. Abel
in collaboration with
Y.L. Mindarava, F. Jelezko, Institute for Quantum Optics, Ulm University,Germany
J. Wrachtrup, T. Oeckinghaus, A. Denisenko, Institute of Physics, University of Stuttgart, Germany
C. Jentgens, Microdiamant AG, Lengwil, Switzerland

Introduction

Nanodiamonds (NDs) are a rather new member of nanocarbons, and have attracted considerable attention in life sciences since the early investigations on NDs in the late 1990s. The still increasing interest in NDs derives from several superior properties of this carbon nanomaterial, such as the high mechanical robustness, the high content of organic functionalities on the particle surface, or a good biocompatibility. Color centers , in particular the NV^- center, inside the NDs are known to exhibit excellent optical properties for sensory and histological application, such as a low photobleaching, light emission in the long wavelength (up to 850 nm) and long fluorescence lifetimes. Due to the special electronic structure of the NV- center even optical detected magnetic resonance, hyperpolarization at room temperature, and magnetic resonance imaging applications were demonstrated in the literature. Even if the large band gap (5.5 eV) of diamond materials suggest it to be inadequate for semiconductor applications, other superior properties, such as the high charge carrier mobility and heat conductivity still make diamond a promising future material regarding electronic applications, in particular regarding high frequency and voltage devices. Furthermore, NDs derived material like nanoonions have been demonstrated to be promising material for electrodes and super capacitators. Hydrogenated diamonds have been confirmed to exhibit negative electron affinity in vacuum and surface conductivity when exposed to air. The first ability has been proposed to induce electron emission after UV excitation and is recently investigated regarding photocatalytic application. Though the impressive potential of NDs for applications, the large diversity of material properties of NDs hinder the assignment of the observed experimental results. An ”as achieved” ND (GND) sample may variate in several properties, e.g. size, morphology, the quantity and kind of color centers inside its lattice, lattice defects, or surface functionality. Furthermore, the NDs may be contaminated with non-diamond carbon or non-carbon impurities. Thus controlled modification of NDs and the analysis of the ND properties is required, as well as an deeper understanding of the relation between the surface and optical properties of the ND. For these investigations Raman and fluorescence spectroscopy, fluorescence lifetime imaging microscopy, and pump probe experiments (ns laser photolysis) were applied. All surface modifications and optical property investigations were assisted by a comprehensive analysis of surface properties of the NDs by applying attenuated total reflection infrared spectroscopy (ATR-IR), X-ray photoelectron spectroscopy (XPS), Raman spectroscopy, zeta potential measurements, scanning electron microscopy (SEM), thermo gravimetric analysis (TGA), as well as transmission electron microscopy (TEM).

Results and Discussion

Modification of Nanodiamonds

The gas phase solid reaction has been identified as the most efficient approach for both the efficient degraphitization and functionalization of NDs. A total removal of the unwanted ubiquitous surface graphite could be achieved by the treatment of GNDs in air atmosphere. The total degraphitization of the GNDs could be achieved for a treatment at 590°C and duration times up to 16h (Fig. 1). As the properties of the GNDs may vary, these parameters needed to be

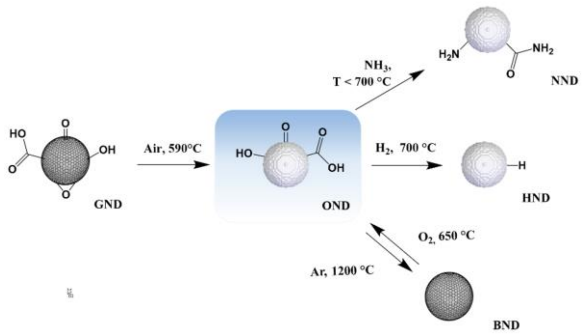

Samples	C1s [at%]	N1s [at%]	O1s [at%]
GND	88.7	0	11.2
OND	88.2	0	10.8
HND	98.2	0	1.7
NND	93.9	3.8	2.3
BND	98.6	0	1.4

Figure 1: Reaction scheme for the modification of NDs (top), atom content for different modified NDs using XPS (bottom).

determined first by applying TGA in order to guarantee the homogeneity of the formed oxidized NDs. These oxydized ND (OND) exhibit a fully degraphitized surface (as determined by TEM and Raman spectroscopy) with high content of carboxylic groups leading to a strong negative zeta potential of the particle (ξ < -30 mV). Due to the homogeneity of the surface properties of the ONDs, these particles served as educts for most of the subsequent surface modifications. By applying gas solid reactions utilizing different atmospheres, hydrogen or nitrogen termination, as well as a control graphitization of the NDs in Argon atmosphere were achieved (Fig. 1). For the hydrogen terminations of NDs (HNDs), both the temperature and treatment time regulate the surface functionalization. At lower temperatures (< 700 °C) and short duration times (<5 h) a still hydroxylated surface was determined, whereas high temperatures promote the partial graphitization of the surface. The partial graphitized/hydrogenated NDs exhibit different surface properties as indicated by a strong positive zeta potential (ξ > +20 mV) compared to non-graphitized HNDs (-20 mV > ξ < +20 mV). In case of the nitrogen termination of NDs (NND) at low temperature or short treatment times an incomplete oxygen removal was determined. At higher temperature the observation of N=N related vibrations in the IR-spectra indicated the formation of aromatic components on the surface of the NDs. Furthermore, too high temperatures led to an unwanted partial hydrogenation of the NNDs. For the graphitization of the NDs (bucky NDs, BND), a strong dependence of the formed surface graphite content morphology on the treatment temperature was found by Raman spectroscopy. At temperatures of about 1050°C (argon atmosphere) the ND surface is defunctionalized and

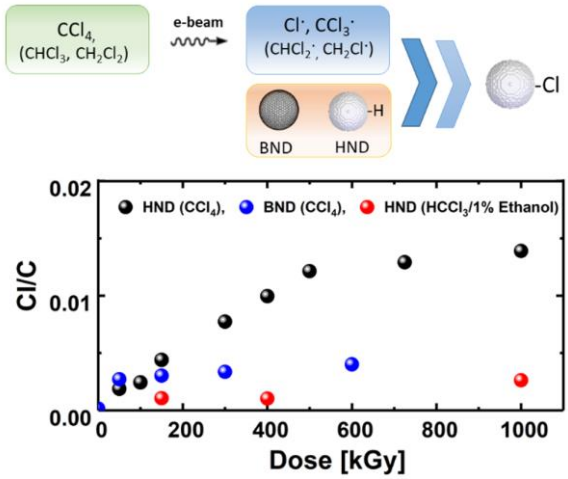

Figure 2: Chlorination of HNDs and BNDs reaction scheme (top), Cl to C ratio in dependence of the applied dose of the electron irradiation (10 MeV) determined by XPS (bottom).

a 2 nm crystalline graphite layer (according to TEM, XRD, and Raman spectroscopy) was formed. The preparation protocols were standardized in order to guarantee a propper assignment of the optical property change to the surface functionality [1].

Even if the modification of NDs were intensively investigated during the last twenty years, some functionalisations e.g. the controlled chlorination of the NDs were still challenging. In contrast to wet chemistry approaches with the disadvantages of relatively long reaction and purification times and surface contamination, a new radiation chemistry approach for the functionalisation of NDs was established [2]. Herein, NDs, in particular HNDs and BNDs, were suspended in CCl_4 or other chloromethane solvents and irradiated with 10 MeV electrons up to a dose up to 1 MGy (Fig. 2 top). The highest modification efficiency was observed for HNDs in CCl_4 (Fig. 2 bottom). According to the radiation chemistry of CCl_4 two possible radicals are formed as reactants: the $Cl^{\bullet}$ and the $CCl_3^{\bullet}$. Utilizing a theoretical DFT approach and analysis of the chlorinated NDs by in-source thermal desorption mass spectrometry, solely the $Cl^{\bullet}$ was determined to be reactive towards the hydrogenated ND surface, as confirmed by the absence of $CCl_3^{\bullet}$ related signals in the mass spectrum. Furthermore, a high stability of the chlorinated surface was determined, so even months after the functionalization, stored under air atmosphere, the chlorinated surface remains nearly unchanged, and thus is unaffected by hydrolysis. The chlorinated NDs offer great potential for subsequent modifications and the demonstrated tha radiation chemistry based modifications open up a new pathway for future modification of NDs.

NV Centers in Nanodiamonds (High-Temperature) Electron Irradiation

The creation of NV^- requires the presence of two types of impurities in the lattice, substitional nitrogen defects (P1 centers) and vacancies. A single vacancy can recombine with a P1 center to form one NV^-, provided the presence of an electron donor (e.g. another P1 center). In conventional methods, the vacancies are created by irradiation at room temperature (RT) with high energy electrons, protons or gamma rays, followed by an additional step of annealing (heating up the sample above 800°C). The RT irradiation technique is usually accompanied by the creation of unwanted paramagnetic defects due to vacancy aggregation (e.g. divacancies and vacancy clusters). In contrast, performing irradiation at or above the annealing temperature, vacancies created instantaneously become mobile and have the

Figure 3: Eperimental setup for HT electron irradiation in inert atmosphere: quartz tube under the scanning horn (top) and ceramic sample holder with diamond powders and bulk diamonds (bottom).

possibility to recombine with nitrogen atoms. Therefore, use of this high temperature (HT) irradiation technique is promising for reaching a high conversion efficiency from P1 to NV^-, keeping the concentration of undesirable defects low.

A procedure for HT irradiation was established at the 10 MeV linac (MB10-30 MP, Mevex) using a special ceramic holder in a quartz tube (Fig. 3), which provides simple temperature isolation as well as the possibility to flush the sample with Argon during the irradiation, preventing oxidation. The heating occurs by means of the energetic beam itself, allowing to reach the desired temperature of 810°C within 2 min (a more gentle increase within 12 min is adopted as standard).

Optical properties of NV centers in NDs

As mentioned above, the knowledge of the influence of the surface functionality of NDs on their optical properties is of great importance for their applicability. In order to study this influence a protocol for the well-controlled formation of the NV centers out of the single nitrogen (C center) containing OND was established via a two-step generation process involving electron irradiation and post-treatment in terms of annealing and air oxidation of the NDs (Fig. 4). The fluorescence properties of NDs containing irradiation-induced NV centers were comprehensively determined regarding the fluorescence intensity, NV^0 to

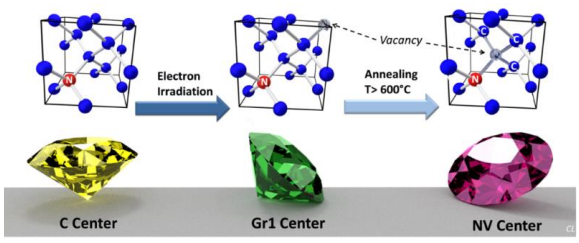

Figure 4: NV center generation via electron irradiation and annealing in inert atmosphere.

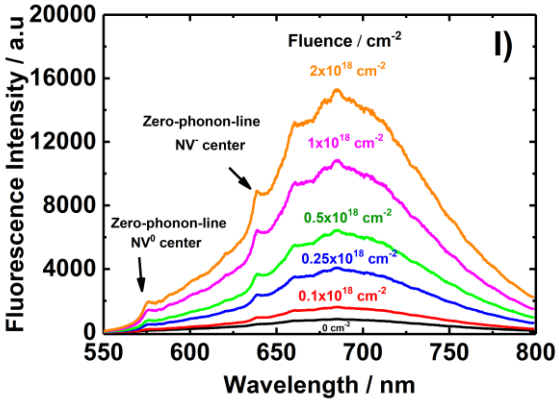

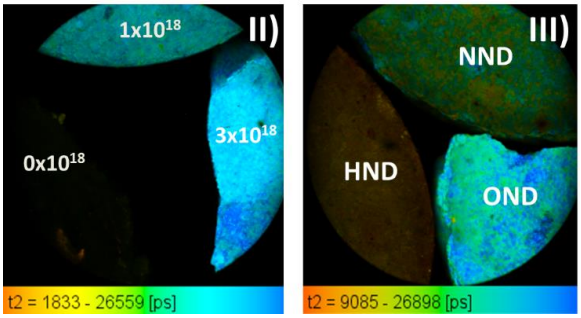

Figure 5: Fluorescence of NV center inside nanodiamonds: I) Fluorescence spectra (λex = 532 nm) of NV^0/NV^- centers inside ONDs irradiated with different fluence up to 2×10^{18} el/cm^{-2} after post-treatment (annealing at 800 °C in argon and air oxidation at 620 °C), Fluorescence lifetime images of the NV^- center (longpass filter λ > 700 nm) after excitation (514 nm, pulse width: 60 ps) inside: II) ONDs irradiated with different fluences and post-treated, III) NDs (irradiated with a fluence of 2×10^{18} el/cm^{-2} and post-treated) with different surface terminaton (OND, HND and NND).

NV^- fluorescence intensity ratio, and the charge state-related fluorescence lifetime [3]. These properties were investigated dependend on irradiation fluences, which is related to the N to NV conversion rate, as well as on the surface functionalities of the NDs (Fig. 5). The following results were obtained: With increasing irradiation fluence all fluorescence properties followed a saturation curve (investigated for OND). Herein, an up to 14-times higher fluorescence intensity, a factor 1.35 higher NV^- to NV^0 ratio, and an increase of the fluorescence lifetimes from 10 ns up to 25 ns (NV^-) and 8 ns to 33 ns (NV^0) were detected for irradiated ONDs compared to non-irradiated ONDs. The surface functionality study revealed a general decrease of the fluorescence properties in order OND > NND > HND. For irradiated HNDs (final fluence: $2\cdot10^{18}$ el/cm^{-2}), a 1.75 times lower NV^- to NV^0 ratio compared to ONDs and a decreased lifetimes of the NV^- (11.2 ns) and the NV^0 (12.4 ns) were observed. Considering literature results, these trends could be well explained by a quenching effect of single nitrogen center (C center) on the excited state of the NV centers, where the effect is more pronounced for NV^0. The effect of the

surface functionalities is related to a changed band structure of the NDs towards the particle surface.

Optical Properties of Surface functionalized NDs after two Photon Band Gap Excitation

The study of the effect of the surface functionality on the dynamics of photo-excited transients provides valuable information for the electronic and photocatalytic application of NDs. Therefore, NDs with different surface terminations were investigated via pump probe experiments in the ns - µs time range, where the pump (excitation) of the NDs was realized via a two photon excitation (TPA) at 355 nm or 266 nm in order to overcome the band gap. Investigations were performed in aqueous dispersions as electron emission from the NDs could be indicated by the formation of the solvated electron on the one hand. On the other hand, diamonds exposed to air atmosphere adsorb a water film at the surface. The high surface to volume ratio offers a good opportunity to study the surface functionality effects on formed transients. For both excitation wavelengths a transient absorption formation and decay was observed within the ns time regime (Fig 6). In case of OND, a variation of the particle concentration and the applied purging gas lead to the conclusion that the observed transient is related to the formation of separated charge carriers within the OND particles. Comparing the transient dynamics of ONDs, HNDs, NNDs and of platinum decorated NDs (the latter is expected to be an efficient electron acceptor and thus a good indicator for attribution of separated charge carriers), a clear trend of increasing transient lifetime was observed in order τ_{OND} (20 ns) < τ_{PtND} (80 ns) < τ_{NND} (210 ns) < τ_{HND} (400 ns). The trend could be explain considering: a) the electron affinity of the platinum improving the charge separation, and b) the surface band bending according to the surface transfer doping model leading to a positive surface hole layer after H termination, which aditionally forces a more efficient charge separation. Contradicting to the literature, for excited HND the electron emission followed by the formation of the solvated electron was not observed in our case and it was discussed by means of doping, surface graphitization, size effects, and the influence of the band structure (further investigation in progress).

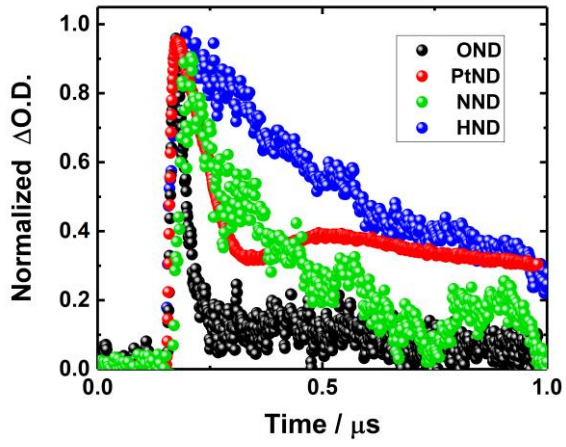

Figure 6: Normalized transient absorption time profiles detected after two-photon excitation with λ=355 nm, probed at 720 nm) of different surface functionalized NDs suspended in water: OND (black), PtND (Red), NND (Green), HND (Blue).

Conclusion

The modification of NDs with an gas-phase-solid reaction approach superior to the traditional wet chemistry was demonstrated. It offers remarkable capabilities for the purification of NDs and the controlled functionalization of NDs (H and N termination, surface graphite layer). By means of radiation chemistry an efficient chlorine termination was obtained. Raman scattering on NDs with variated surface graphite content demonstrated the effect of graphite enhanced optical heating on the Raman spectra of the NDs [4]. For the fluorescence properties of NV centers inside the NDs, a clear dependence on the formation conditions and the surface functionality was observed. The results indicated a fluorescence quenching effect of residual single nitrogen centers (C center) inside the diamond as well as an effect of the surface functionality in terms of changes of the band structure of the NDs. The controlled preparation and comprehensive charactarisation, summarized in a PhD thesis [5], is a prerequisite to future application of NDs.

Literature

[1] C. Laube, Y. M. Riyad, A. Lotnyk, F. P. Lohmann, C. Kranert, R. Hermann, W. Knolle, T. Oeckinghaus, R. Reuter, A. Denisenko, A. Kahnt, B. Abel, Materials Chemistry Frontiers 1 (2017) 2527
[2] J. Zhou, C. Laube, W. Knolle, S. Naumov, A. Prager, F. D. Kopinke, B. Abel, Diamond Relat. Mater. 82 (2018) 150
[3] C. Laube, T. Oeckinghaus, J. Lehnert, J. Griebel, W. Knolle, A. Denisenko, A. Kahnt, J. Meijer, J. Wrachtrup, B. Abel, Nanoscale 11 (2019) 1770
[4] C. Laube, J. Hellweg, C. Sturm, J. Griebel, M. Grundmann, A. Kahnt, B. Abel, Journal of Physical Chemistry C 122 (2018) 25685
[5] C. Laube, PhD thesis, Leipzig University (2019)

From Conductive Self-Assembled Monolayers to Single Molecules on Surfaces

M. Glöß, R. Pütt, S. Schmitz, M. Moors, K. Yu. Monakhov
in collaboration with
R. C. Chiechi, Stratingh Institute for Chemistry & Zernike Institute for Advanced Materials, University of Groningen, The Netherlands
W. Wernsdorfer, Physikalisches Institut (PHI), Karlsruhe Institute of Technology and Institute for Quantum Materials and Technologies (IQMT), Karlsruhe Institute of Technology, Germany
R. Waser, Peter Grünberg Institut, JARA-FIT, Forschungszentrum Jülich GmbH, Jülich and Institut für Werkstoffe der Elektrotechnik 2, RWTH Aachen University, Germany

Introduction

The implementation of metal coordination complexes with specific paramagnetic and/or redox properties as single molecules or as constituents of two-dimensional (2D) molecular monolayers into computer memory cells is a promising way to keep the miniaturization and sustainability of electronic components from colliding with the so-called “quantum limit” (sub-10-nm regime) valid. At both these levels of molecule–surface interfaces, preservation of the main molecular characteristics as identified in the bulk state, and avoidance of the agglomerative behavior of coordination compounds after their immobilization on solid support constitute important milestones in the controlled micro-spectroscopic addressing of the tunnel junction structures of molecule–electrode hybrid devices. The eventual step to practical electronic devices mandates an in-depth understanding of the adsorption, autonomous self-organization, electron charge-/spin-transport characteristics and switching mechanisms of mono- and polynuclear complexes of transition metals, lanthanides, and their mixed-metal derivatives on conductive and semi-conductive surfaces [1].

Paramagnetic Coordination Clusters

Two polynuclear cobalt(II,III) complexes, $[Co_5(N_3)_4(N\text{-}n\text{-bda})_4(bza{\cdot}SMe)_2]$ (1) and $[Co_6(N_3)_4(N\text{-}n\text{-bda})_2(bza{\cdot}SMe)_5(MeOH)_4]Cl$ (2) where Hbza·SMe = 4-(methylthio)benzoic acid and *N*-*n*-H_2bda = *N*-*n*-butyldiethanolamine, were synthesized and fully characterized by various techniques. Compound 1 exhibits an unusual, approximately C_2-symmetric $\{Co^{II}Co^{III}_4\}$ core of two isosceles Co_3 triangles with perpendicularly oriented planes, sharing a central, high-spin Co^{II} ion residing in a distorted tetrahedral coordination environment. This central Co^{II} ion is connected to four outer, octahedrally coordinated low-spin Co^{III} ions *via* oxo bridges. Compound 2 comprises a semi-circular $\{Co^{II}_4Co^{III}_2\}$ motif of four non-interacting high-spin Co^{II} and two low-spin Co^{III} centers in octahedral coordination environments. Self-assembled monolayers (SAMs) of 1 and 2 were physisorbed on template-stripped gold surfaces contacted by an eutectic gallium-indium (EGaIn) tip. The acquired current density-voltage (*I*-*V*) data revealed that the cobalt-based SAMs (Figure 1) are more electrically robust than those of the previously reported dinuclear $\{Cu^{II}Ln^{III}\}$ complexes with Ln = Gd, Tb, Dy, or Y [2]. In addition, between 170 and 220°C, the neutral, mixed-valence compound 1 undergoes a redox modification, yielding a $\{Co_5\}$-based coordination cluster (1-A) with five non-interacting, high-spin octahedral Co^{II} centers as indicated by SQUID magnetometry analysis in combination with X-ray photoelectron spectroscopy and infrared spectroscopy. Solvothermal treatment of 1 results in a high-nuclearity coordination cluster, $[Co_{10}(N_3)_2(N\text{-}n\text{-bda})_6(bza{\cdot}SMe)_6]$ (3), containing 10 virtually non-interacting high-spin Co^{II} centers [1].

Exchange-biased quantum tunneling of magnetization (QTM) in a transition metal coordination cluster showing single-molecule magnet (SMM) behavior – the characteristics which are relevant for the imple-

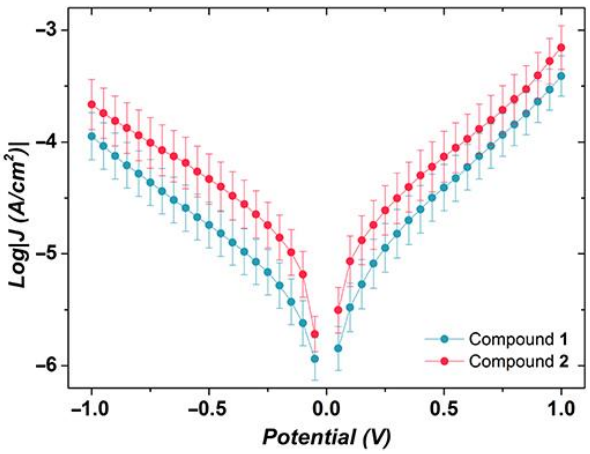

*Figure 1: Plots of logarithmic current-density against applied potential for the SAMs of compounds **1** and **2**. Values of log|J| at V = 0 V are omitted for clarity. The error bars are the 95% confidence intervals. Despite the minor difference in the shape of the J/V curves, the two SAMs are indistinguishable.*

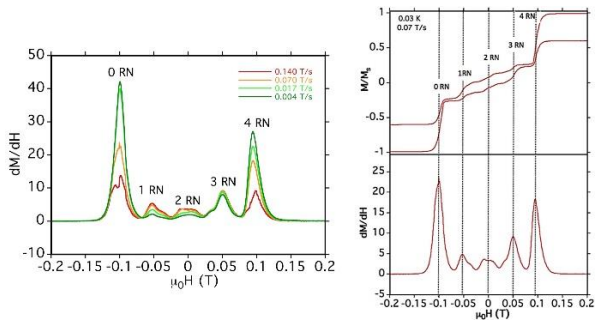

Figure 2: Left: Plots of the first derivative (dM/dH) of the magnetization versus magnetic field close to zero field at different sweep rates. The exchange bias of five situations of 0 to 4 reversed neighbors (RN) are indicated. Right: (top) Hysteresis loop measured at 30 mK and at a sweep rate of 0.07 T s^{-1}; (bottom) plot of the first derivative (dM/dH) of the magnetization against magnetic field close to zero field. The exchange bias of five situations of 0 to 4 reversed neighbors (RN) is indicated.

mentation of molecular spin qubits in quantum computing – was observed and described [3]. The SMM compound is the cubane-type Ni(II) complex with the formula [Ni(μ_3-Cl)Cl**(**HL·S)]$_4$ that is composed of the combination of two charge-neutral fragments, the {Ni_4Cl_8} core and four thio-augmented, pyridyl-alcohol HL·S ligand (= $C_{11}H_{15}NOS$)**.** The synthesis, structure, and magneto-chemistry using standard SQUID technique (0.1–5.0 T and 2.0–290 K) for this compound were reported previously [4].

Low-temperature magnetization measure-ments of [Ni(μ_3-Cl)Cl(HL·S)]$_4$ were performed on single crystals and they revealed open hysteresis loops up to 30 mK at a sweep rate of 0.07 T s^{-1}. The studied molecule exhibits intermolecular antiferromagnetic coupling J_{inter} of –0.004 K in the supramolecular environment of four other cubane-type units. Quantum tunneling of magnetization characterized by five steps at –0.1, –0.05, 0, 0.05 and 0.1 T was thus detected (Figure 2).

The usage of such non-covalent interactions in networking of the individual spin structures of metal complexes on surfaces remains challenging as **t**he interaction with a surface can exert a significant effect on the molecular geometry, electronic structure and the molecular environment, thus resulting in loss of the pristine magnetic characteristics. The obtained results prompt spectroscopy studies with regard to the spin structure and spin transport behavior of this SMM material in the form of supramolecular network on substrate surfaces in the presence of an applied magnetic field.

Diamagnetic Polyoxometalates

The first representatives of phthalocyaninato lanthanide-ligated polyoxovanadate cages {[$V_{12}O_{32}$(Cl)](LnPc)$_n$}$^{n-5}$ (n = 1 or 2, Ln = Yb^{3+}) were synthesized and fully characterized. These magnetic complexes form 2D self-assembled monolayers exhibiting electrical conductivity on gold substrate surfaces, as assessed by using an EGaIn tip (Figure 3). Complexes 1 and 2 are $n$$Bu_4N^+$-charged balanced complexes {[$V^V_{12}O_{32}$(Cl)](LnPc)}$^{4-}$ (mono^{4-}) and {[$V^V_{12}O_{32}$(Cl)](LnPc)$_2$}$^{3-}$ (bis^{3-}) where Pc is the phthalocyanine dianion. These findings offer guidance to customizing a hybrid material that can be assembled of any stable lacunary polyoxometalate core and phthalocyaninato lanthanide moieties. A comparative analysis of the molecular charge transport characteristics of the hybrid materials and their precursors (($n$$Bu_4N$)$_4$[$HV_{12}O_{32}$(Cl)] and LnPcOAc) is currently under investigation. The potential possibilities of controlled fine-tuning of their structural, electrochemical and magnetic characteristics in the applied electrode environment are expected to make 2D monolayers of such polyoxometalate-based coordination compounds suitable candidates for practical integration into memory cells. To achieve this technology transfer-oriented goal, the SAM conductivity switching response to the electric field of a scanning probe microscope as a function of oxidation and magnetic states of metal ions or temperature-controlled molecular ordering and/or adsorption geometry in monolayers are to be explored [5].

The far-reaching interplay between the speciation of polyoxometalates in the liquid phase and their adsorption characteristics on substrate surfaces yet remains to be understood. The significance of this interplay is however paramount because it indicates the degree of technical applicability of solvent pro-

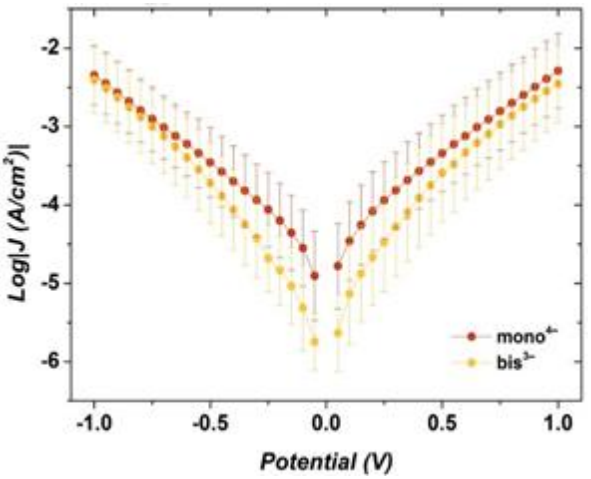

Figure 3: Plots of log current density vs applied potential for SAMs of mono^{4-} and bis^{3-} on Au^{TS}. Values of Log|J| at V = 0 V are omitted for clarity. J = I/A where I and A are the current and area of the junction, respectively. Error bars represent the standard deviation of Gaussian fits.

cessable polyoxometalate molecules. The “polyoxometalate–counterion–solvent” and “polyoxometalate–counterion–solvent–substrate” processes were elucidated due to the effective combination of small-angle X-ray scattering in solution with surface sensitive scanning tunneling microscopy and X-ray photoelectron spectroscopy measurements (Figure 4). The MeCN-solution speciation of a tris(alkoxo)-ligated Wells–Dawson-type surfactant carrying molecular 5– charge $\{[HP_2V^V_3WVI_{15}O_{59}((OCH_2)_3CCH_2OCH_2C_6H_4I)]\}^{5-}$ explored as a representative of commonly negatively charged polyoxometalate-based inorganic–organic nanostructures – was strikingly connected with the growth of porous 2D molecular layers on highly oriented pyrolytic graphite (HOPG). Low water amounts dramatically transform intermolecular relationships toward hierarchical agglomeration that inhibits the layer formation on HOPG. The obtained findings lay the groundwork for a mechanistic study of controlled nucleation and growth of polyoxometalate nanostructures on weakly interacting surfaces [6].

Elaboration of chemical and physical approaches at the level of metal-selective coordination compounds as smart successors of common transition metal oxide materials that are implemented in today’s complementary metal-oxide-semiconductor technology can help achieving the ultimate scalability of ReRAM-based electronic devices, also granting access to not-yet-developed “*More than Moore*” functionalities. The latter should ultimately allow to overcome a functional separation between storage and processing of data as is present in *von Neumann* architectures characterized by high energy dissipation. The technologically important electron modification using fully-oxidized Lindqvist-type polyoxometalate molecules $[V_6O_{13}\{(OCH_2)_3CCH_2SPh\}_2]^{2-}$ was explored. These molecules were physisorbed on the Au(111) surface, preserving their structural and electronic characteristics (Figure 5). The resistive switching cell is represented by embedding hexavanadate molecules into a model setup, in which the bottom electrode is represented by the Au(111) surface and the top electrode is the platinum tip of a scanning tunneling microscope (STM). By applying an external voltage at room temperature, the valence state of the single polyoxometalate molecule could be changed multiple times through the injection of up to 4 electrons. The molecular electrical conductivity is dependent on the number of vanadium 3d electrons, resulting in several discrete conduction states with increasing conductivity. This fundamentally important finding illustrates the far-reaching opportunities for polyoxometalate molecules in the area of multiple-state resistive (memristive) switching [7].

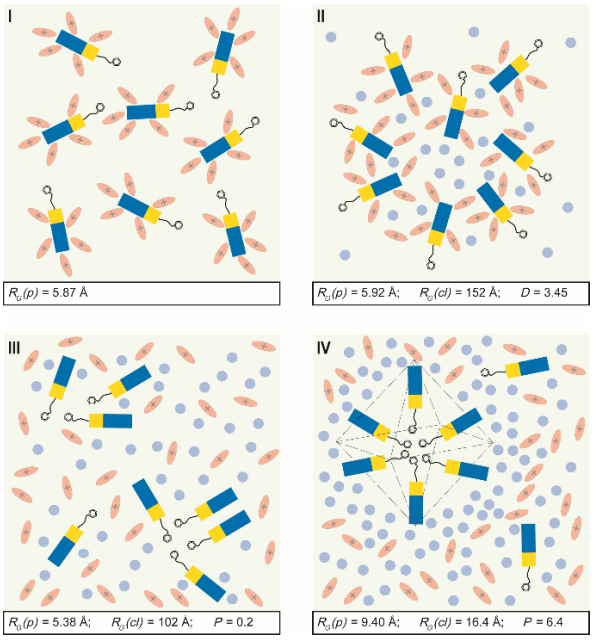

Figure 4: Deciphering the intricate behavioral properties of polyoxometalates in solution is the key to control and adjust their hierarchical assembly preferences at the nanoscale. The illustration shows such interesting abilities of a typical tris(alkoxo)-ligated Wells-Dawson-type polyoxoanion to network and to re- and de-clusterize between operational regimes in discrete solutions and on a substrate surface. This finding features the results of combined small-angle X-ray scattering, scanning tunneling microscopy and X-ray photoelectron spectroscopy experiments that may have far-reaching impact on molecular nano-engineering of polyoxometalate-based devices.

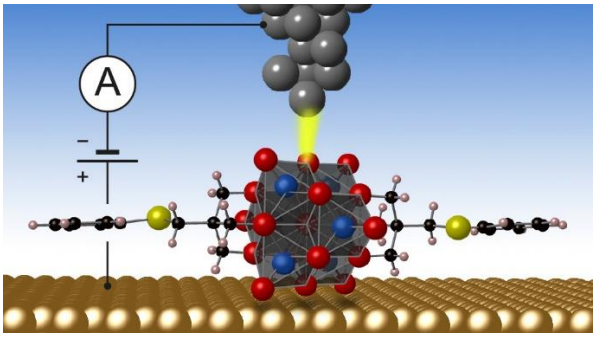

Figure 5: The electrical conductivity of a single hexavanadate molecule is remarkably dependent on the vanadium reduction states resulting in several discrete resistive states with increasing conductivity at room temperature and low operating voltages.

Literature

[1] S. Schmitz, X. Qiu, M. Glöß, J. van Leusen, N. V. Izarova, M.A. Nadeem, J. Griebel, R.C. Chiechi, P. Kögerler, K.Y. Monakhov, Front. Chem. 7 (2019), 681

[2] S. Schmitz, A. Kovalchuk, A. Martín-Rodríguez, J. van Leusen, N. V. Izarova, S. D. M. Bourone, Y. Ai,

E. Ruiz, R. Chiechi, P. Kögerler, K. Y. Monakhov, Inorg. Chem. 57 (2018), 9274–9285
[3] K. Y. Monakhov, W. Wernsdorfer, Mendeleev Commun. (2019), accepted
[4] V. Heβ, F. Matthes, D.E. Bürgler, K.Y. Monakhov, C. Besson, P. Kögerler, A. Ghisolfi, P. Braunstein, C.M. Schneider, Surf. Sci. 641 (2015), 210–215
[5] R. Pütt, X. Qiu, P. Kozłowski, H. Gildenast, O. Linnenberg, S. Zahn, R.C. Chiechi, K.Y. Monakhov, Chem. Commun. 55 (2019) 13554–13557
[6] M. Glöß, R. Pütt, M. Moors, E. Kentzinger, W. Pyckhout-Hintzen, K.Y. Monakhov, Nanoscale 11 (2019), 4267–4277
[7] O. Linnenberg, M. Moors, A. Notario-Estévez, X. López, C. de Graaf, S. Peter, C. Bäumer, R. Waser, K.Y. Monakhov, J. Am. Chem. Soc. 140 (2018), 16635–16640

Ion Conductivity Through Polymer Stabilized CsH_2PO_4 Nanoparticular Layers in Solid Acid Fuel Cells

M. Wagner, F. P. Lohmann-Richters, K. Hanus, B. Abel
in collaboration with
C. Dreßler, D. Sebastiani, Martin-Luther-Universität Halle-Wittenberg, Germany
A. Varga, BMW Group, Munich, Germany

Introduction

Fuel cells based on solid acid proton conductors, known as solid acid fuel cells (SAFCs), are a relatively new technology that carry several fundamental advantages [1-3]. An intermediate operating temperature of 513 K, at which the electrolyte CsH_2PO_4 exists in its super protonic phase, allows for fuel flexibility and excellent resistance to catalyst poisoning. So far, research has mainly focused on enhancing the activity and interconnectivity of the catalyst, overlooking the resistance of the electrolyte network within a porous powder electrode. This, however, may be limiting the performance, independent of the catalyst utilization. In this combined computational and experimental study, we explore the influence of porous electrodes on cell performance. Therefore, we synthesize three-dimensional, nanostructured, porous electrodes with varying thicknesses using a combination of spray drying and sputtering techniques to determine the impact of a porous electrolyte structure on cell performance. The influence of the stabilizing polymer additive on the average ionic resistivity is then evaluated. AC impedance measurements enable us to observe the impact of a CsH_2PO_4 network on electrode impedance. Measurements in a symmetric hydrogen atmosphere and under fuel cell conditions have been conducted and the results compared. Based on an analytical model developed through scanning microscope imaging, we adopted a combined molecular dynamics and lattice Monte Carlo approach to the specific morphological situation.

Results and Discussion

Materials, cell and electrode fabrication and measurements have been published [4]. The Kinetic rate model for proton conduction in nano-porous systems and details of the cMD/LMC method employed here are described in detail in Ref. 4. Representative SEM micrographs of CsH_2PO_4 electrolyte discs at various stages of sample preparation are presented in Fig. 1. The surface roughness decreased significantly from before polishing (a) to afterwards (b), providing a smooth surface for Pt deposition via sputtering. Fig. 1(d) shows CsH_2PO_4 particles deposited onto an electrolyte pellet via spray drying without the stabilizing polymer PVP. The particles agglomerate rapidly, even in ambient conditions.

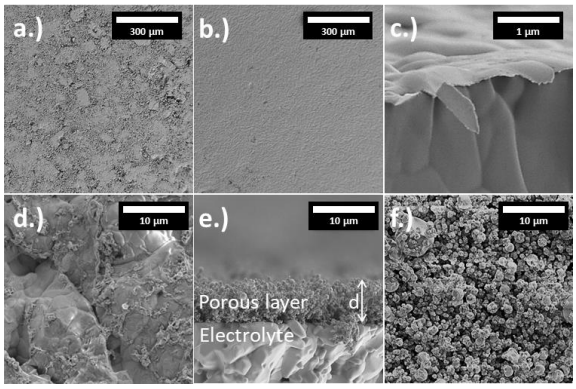

Fig. 1. Scanning electron micrographs of: a.) as pressed; and b.) a polished CsH2PO4 electrolyte pellet; c.) a cross section of a sputtered Pt thin film; d.) agglomerated pure CsH2PO4 nanostructure deposited via spray drying; e.) a cross section; and f.) a top view of a scanning electron micrograph showing a nanostructured CsH2PO4 electrode with thickness d, stabilized by the polymer PVP and deposited on a dense CsH_2PO_4 electrolyte pellet. Adapted from Ref. 4.

In contrast, the CsH_2PO_4 structure can be effectively stabilized by adding polyvinylpyrrolidone (PVP) to the precursor solution, as reported previously. Fig. 1 (e, f) shows a PVP stabilized nanostructure on a dense CsH_2PO_4 electrolyte pellet. In general, particle loading on the surface of the electrolyte pellet increases linearly with the duration of spray drying, with a slight variation across the pellet. In the initial stage, only the deposited particle density increases on the pellet surface. Here, we define the area coverage of the electrolyte surface as the ratio of the projected area of the deposited particles and the free surface area (between 0, for no coverage and 1 for full coverage). After a mixed stage, when both incomplete coverage and growth of the layer thickness d occurs, a thick porous layer is established. To quantify all stages of nanoparticle deposition, the area coverage was measured with SEM and multiplied with the average thickness of deposited particle clusters, yielding the effective layer thickness. The thermal stability of PVP and mixtures of PVP with CsH_2PO_4 and Pt nanoparticles was confirmed using TGA measurements for temperatures below 600 K in both air and nitrogen atmospheres.

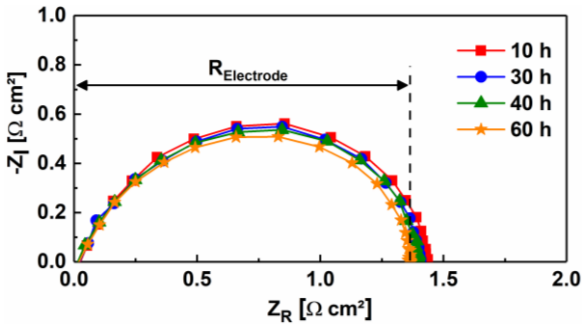

Fig. 2. Electrode impedance arcs as a function of time for a representative symmetric electrochemical cell: Pt thin-film + $CsH_2PO_4^{porous}$ |CsH_2PO_4|$CsH_2PO_4^{porous}$ + Pt thin-film showing good stability over a 60 h time period. The Pt film thickness was 30 nm and the effective layer thickness, 2.5 µm. The electrolyte impedance is subtracted and the area normalized electrode resistance, $R_{Electrode}$, is indicated as the width of the impedance arc. Adapted from Ref. 4.

Representative impedance spectra in the Nyquist form are shown in Fig. 2 for a symmetrical cell with an effective layer thickness of 2.5 µm and a Pt film thickness of 30 nm.

The width of the impedance arcs is taken as the electrode resistance. The electrolyte resistance, observed as a shift of the impedance arc along the real axis, is subtracted. For ease of comparison, the results are converted to area-normalized electrode resistances (ANRs). To verify the setup used and ensure comparability to the literature, Pt thin film electrodes were fabricated and characterized as described. The electrode resistances of the thin film electrodes are in good agreement with the data published by Louie and Haile [3]. Symmetric measurements in a hydrogen environment have often been employed to evaluate electrode structures, since they require less construction effort. However, the rate-limiting step for a hydrogen-powered fuel cell is the oxygen reduction reaction at the cathode. We compare structured and thin film cells in symmetrical and fuel cell measurements to analyze whether the structuring is yielding similar activity increases for both techniques. Therefore, two cell types, differing only by the electrode type, are compared. “Thin film cells” have 30 nm platinum thin film electrodes on both sides whereas “porous cells” have two structured electrodes with platinum sputtered on top. All cells have the same platinum content of 0.128 mg cm^{-2}. IR-corrected polarization plots for cells with Pt thin film electrodes, as well as porous electrodes under fuel cell conditions have been determined. The cells show high reproducibility among themselves. To roughly compare the two characterization techniques, the current density at a voltage of 0.5 V is taken for the fuel cell measurements and the mass normalized activity (MNA) is calculated for the symmetric measurement, which represents only the hydrogen oxidation reaction. Both the current densities as well as the MNA depend directly on the catalyst utilization. In Ref. 4 we compare the average current density at 0.5 V obtained in fuel cell measurements and the increase of the MNA obtained from symmetrical measurements in hydrogen for both electrode types. The standard deviation of the relative increase of the MNA was calculated. First it becomes clear that structuring an electrode considerably increases its activity. Through an area increase, the sputtered platinum is distributed over a larger area, increasing the active site density. As mentioned earlier, it is widely assumed, but not proven, that structure-induced improvements of the anode performance observed under symmetrical conditions are equally viable for the cathode. Since the reaction mechanism of the oxygen reduction is not yet fully understood, this assumption is not trivial. Second, a similar percental increase resulting from structuring can be seen for both the MNA and current densities. This implies that the electrode structure affects the anodic hydrogen oxidation and rate-limiting cathodic oxygen reduction in a similar way, confirming symmetric impedance measurements as a well-suited method for analysing improvements to the electrode due to spray drying. The ANR for cells with varying effective layer thicknesses and constant 30 nm Pt thin films, are shown in Figure 3. The obtained effective layer thickness depends on the spraying time and the exact position of the sample within the deposition section relative to the gas inlet. Therefore, the deposited layer thickness varies from cell to cell, as well as over each sample’s surface. The layer thickness of each cell was measured at four different points and the standard deviation was calculated as described in the experimental section. With the increasing amount of spray dried particles, the electrode impedance decreased sharply as a result of the increase in the absolute electrochemically-active surface area. However, after reaching the lowest ANR at a layer thickness of about 5 µm and complete area coverage, electrode resistance increased rapidly. One should keep in mind that this represents only the optimum for these model cells which can’t compete with high platinum loading state of the art cells in terms of power density. As reported by Suryaprakash et al. [5], the platinum deposition via sputtering only penetrates the top 5 µm of the structure. It seems that the porous layer significantly increases the ANR, given the fact that a maximum 18 µm-thick layer was applied. As CsH_2PO_4 itself serves as a frequency-independent ohmic resistor within the measurement conditions employed, the contribution of the porous electrolyte layer to the ANR is surprising.

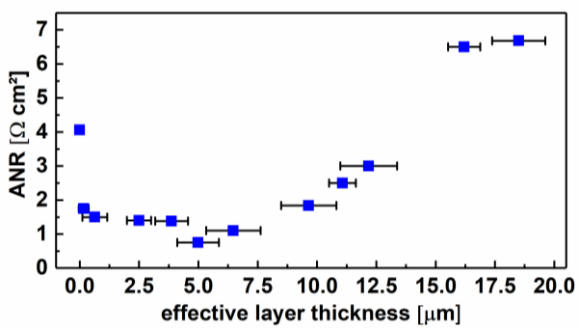

Fig. 3 Area-normalized electrode resistance (ANR) obtained via AC impedance spectroscopy plotted vs. electrode layer thickness d, showing an optimal layer thickness of ca. 5 µm, followed by an unexpected increase for larger thicknesses. All electrodes had a 30 nm Pt thin film catalyst layer deposited via DC magnetron sputtering. Adapted from Ref. 4.

In the following sections, an analytical and cMD/LCM model is introduced showing that the observed effect is mainly caused by the porosity and stabilizing agent PVP. By generating constrictions between the sprayed particles, the porous layer develops a frequency depending resistance affecting the ANR rather than the purely ohmic electrolyte resistance. For increasing layer thickness a rise in the electrode resistance from 0.75 Ωcm² to 7 Ωcm² is observed, Figure 3.

Based on SEM images of the porous structure, an analytical model is developed, not to provide precise data but to estimate the impact of the induced porosity on the resistivity of the electrode. It will be shown, that the resistance of a pure CsH_2PO_4 electrolyte network, while considering the porosity and constriction effects, fails to explain the observed resistance increase by one order of magnitude. For this model, a constant resistivity for CsH_2PO_4 at 513 K of ρ = 45.45 Ωcm is assumed. A 20 µm-thick dense electrode therefore has a resistance of 0.09 Ωcm². For a porous structure, the tortuosity as well as the porosity influences the resistance.

Analysing SEM micrographs of the two highest layer thicknesses shown in Figure 3, the porosity was estimated to be around 0.5 and the extended proton pathway due to tortuosity to be 1.4 times the layer thickness. For this rough estimate four different regions were analysed as described in the experimental section. Based on this, a 20 µm-thick porous structure is modelled by circular columns with a total area filling of 50%. According to estimations [4] the resulting area normalized resistance is 0.25 Ωcm². With the resistivity "ρ", the area of a single column "A_{Col}", the number of columns per cm² "N_{Col}" and the estimated tortuosity "x_t". Geometric constrictions created between two adjoining particles of different sizes increase the area-normalized resistance. Taking Figure 4 as a representative image, the smallest

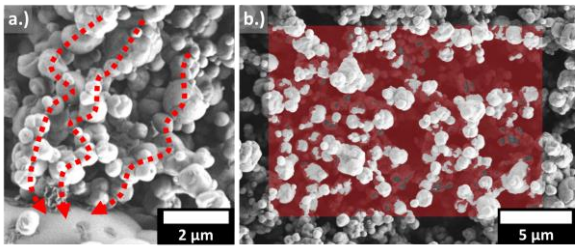

Figure 4. Representative SEM micrographs of the generated porous CsH_2PO_4 electrode network: a.) The dotted lines indicate possible pathways trough the porous network. The length is roughly 1.4 times the linear distance. b.) Top view on the porous network. The space between CsH_2PO_4 particles, which are in roughly the same plane, are colored in red. The area of CsH_2PO_4 particles compared to the void in one plane is about 50%. Adapted from Ref. 4.

constrictions have a diameter of around 300 nm. Assuming ten spherical 300 nm diameter constrictions within a 20 µm layer as an upper limit, the layer resistance increases to 0.56 Ωcm², with the length of the constriction "l_{const}" and the area of the constriction "A_{const}". Suryaprakash et al. [5] report the essential effect of the PVP for the structure's stabilization, which forms a visible shell around the CsH_2PO_4 particles during the spraying process for a very high PVP concentration of 10 g l^{-1}. As PVP is not proton conducting, such a shell would act as a barrier obstructing proton transport. To prove the significance of PVP for the overall resistivity, the electrolyte resistances of 500 µm-thick pure CsH_2PO_4 pellets are compared to a composite cell containing a 500 µm-thick pure CsH_2PO_4 layer and a 100 µm-thick dense layer of spray-dried CsH_2PO_4-PVP. The electrolyte resistance increases from 2.5 Ωcm² for the pure CsH_2PO_4 pellet to about 7.2 Ωcm² for the composite CsH_2PO_4 pellet. The resistivity of the additional 100 µm thick PVP-containing layer is thus 5.0 Ωcm, representing an almost 11 times increase compared to pure CsH_2PO_4. Assuming this increased resistivity for the calculation, we achieve a resistance increase comparable to the observed. This shows that the ANR's increase of 6.25 Ωcm² in Figure 3 between an effective layer thickness of 5 µm and 20 µm can be caused by the additional effect of the PVP stabilized porous electrolyte network. It becomes clear that the porous structure itself makes a significant contribution to the cell's performance, especially when stabilized with PVP. Although further investigations are necessary, it is important to take the thickness of the porous structure into consideration when engineering a high-performance cell. Using a cMD/LMC approach, the current density was calculated as a function of first, the proton insertion rate and second, the system length. The excess proton fraction (EPF) scales with the amount of additional hydrogen atoms attached to near-surface O atoms. Higher EPF therefore represents a more active surface. For CsH_2PO_4,

the possible number of protons per oxygen atom range from 0.5 to 1, resulting in a maximum EPF value of 0.5. Within this range, the current density shows a linear dependence [4]. According to Ohm's law, the current density is proportional to the inverse length of the system. The calculated data fits well (R = 0.9992) to the expected behaviour.

Porous systems are generated randomly by removing single 1x1x2 nm boxes from an 8x8x20 nm CsH_2PO_4 system until a defined porosity is reached. The random removal is restricted in such a way that no percolation interruption is generated. Examples for CsH_2PO_4 systems with different porosities are given in Ref. 4. The conductivity simulations are performed for a fixed EPF, corresponding to a constant platinum surface and voltage. Periodic boundary conditions in x and y directions were used for all calculations. For every porosity, three different calculations of randomly obtained systems were performed and the standard deviation for both the conductivity and resulting porosity calculated. In the analytical model, the resistance triples for a porosity of 0.5 without additional geometric constrictions, and an eightfold increase is observed with these constrictions, keeping in mind that the number of geometric constrictions were set as an upper limit. The cMD/LMC model shows a relative increase in the ohmic resistance of 4-fold for a porosity of 0.5. The analytical model was closely aligned to the observed porous structure, whereas the cMD/LMC approach aimed at random porous structures. Geometrical constrictions are the main reason for the large error, due to the strong negative effect on the resistivity. It can be concluded that the computational model is able to sufficiently characterize a porous system, as used in this work within the given margin of error.

As mentioned previously, the PVP was found to have a highly negative impact on the resistivity of CsH_2PO_4. Suryaprakash et al. [5] reported the tendency of PVP to form a shell around the CsH_2PO_4 particle during the spray drying process. With a concentration ratio of 1:33 g l^{-1} between PVP and CsH_2PO_4, it is reasonable to conclude that PVP does not form a uniform outer layer around the CsH_2PO_4 particles but reduces the contact area between two adjoining CsH_2PO_4 particles. The obstructing effect caused by the PVP was modelled by selecting four layers of CsH_2PO_4 along the z axis in an 8x8x20nm system and randomly removing boxes to simulate the area of CsH_2PO_4 covered by the PVP. According to this model, the increase of the resistivity by a factor of over 10, as observed in our cells, would represent a PVP surface coverage of 94%. Following this argumentation, at the boundary between PVP and CsH_2PO_4, a chemical double layer can develop, generating a frequency-dependent resistance. Such a resistance develops an own arc in an impedance spectrogram. In our case the impedance arc of the charge transfer reaction at the platinum-CsH_2PO_4 interface and from the PVP induced constrictions overlap, leading to a flattened overall impedance arc. This effect is shown in Ref. 4, where the impedance arc symmetry of platinum thin film electrodes and porous electrodes are compared. While thin film electrodes show an almost semicircle like symmetry, the arc's associated with the porous electrodes are deformed due to the additional frequency dependent resistance.

Conclusion

Electrodes are currently the primary performance-limiting component in low and intermediate temperature fuel cells. A proven method for improving electrode performance in solid acid fuel cells is to create ever finer nanostructures and thus increase the electrochemically-active surface area. However, this performance enhancement is limited by issues of long-term stability, as well as increasing both the electronic and ionic conduction pathways. Here, we combine a systematic experimental study with a computational model to quantify the effect of 1.) the stabilizing polymer polyvinylpyrrolidone as well as 2.) the porosity and electrode layer thickness on the average ionic conductivity of the solid acid electrolyte CsH_2PO_4 in a composite solid acid fuel cell electrode. With a multiscale simulation approach using a combined molecular dynamics and lattice Monte Carlo method, proton conduction through a porous electrode is simulated at mesoscopic timescales while retaining near-atomistic structured evolution. Electrochemical impedance spectroscopy is used to evaluate the porous electrodes obtained via spray drying. Both approaches reveal a similar and significant contribution of the porous electrolyte layer to the overall cell resistance. This indicates that geometrical parameters, as well as stabilizing materials may play an essential role when designing a high-performance solid acid fuel cell.

Literature

[1] D. A. Boysen, T. Uda, C. R. I. Chisholm, S. M. Haile, Science (2004) 303, 68-70
[2] C. R. I. Chisholm, S. M. Haile, Solid State Ionics (2000) 136-137, 229-241
[3] A. Varga, N. A. Brunelli, M. W. Louie, K. P. Giapis, S. M. Haile, J. Mater. Chem. (2010) 20, 6309-6315
[4] M. Wagner, Ch. Dreßler, F. P. Lohmann-Richters, K. Hanus, D. Sebastiani, A. Varga, B. Abel, J. Mater. Chem. A (2019) 7, 27367
[5] R. C. Suryaprakash, F. P. Lohmann, M. Wagner, B. Abel, A. Varga, RSC Adv. (2014) 4, 60429-60436

Spatially Controlled Growth and Immobilization of Peptide Fibrils on Surfaces

T. John, J. Bandak, N. Sarveson, C. Hackl, H. J. Risselada, A. Prager, C. Elsner, B. Abel

Introduction

The assembly of soluble peptide or protein monomers into fibrillar supramolecular structures, consisting of intermolecular hydrogen-bonded β-sheets, is associated with serious degenerative diseases, such as Alzheimer's disease, type 2 diabetes, and other misfolding disorders [1-3]. Despite of their physiological role, amyloid fibrils are promising tools for applications in nanoelectronics, biosensing, and separation technologies [4]. The preparation of amyloid fibrils in bulk quantities, from readily available low-cost materials, could increase their commercial potential in the near future. The advantage to control the properties of these supramolecular structures by tailoring the primary peptide sequence of the monomers is a unique feature, which enables a high flexibility in material design.

In this study, we have investigated the influence of amino acid substitutions in the primary peptide sequence of N-terminal modified NNFGAIL peptides ($IAPP_{21-27}$) on the kinetics and morphology of fibrillar structures. IAPP (islet amyloid polypeptide, amylin) is associated with type 2 diabetes. The identification of residues, which are not needed for fibril formation, could provide suitable targets for the incorporation of functionalities into the peptide, for instance molecular switches, catalytic centers, labels, or functional binding units. The $IAPP_{21-27}$ peptide (NNFGAIL) is an exception among other steric-zipper amyloid structures reported by the Eisenberg group [1].

We performed thioflavin T (ThT) fluorescence and scanning electron microscopy (SEM) measurements as well as molecular dynamics (MD) simulations to study the role of peptide modifications for the fibrillation kinetics and morphologies [5]. The hydrophobic peptide residues phenylalanine (F23), isoleucine (I26) and leucine (L27) were identified as highly relevant for peptide aggregation. Further, Btn-GNNFGAIL fibrils have been successfully immobilized on streptavidin coated surfaces [5].

Experimental and Simulations

Materials, Peptide synthesis and MALDI-TOF-MS were described in Ref. 5. Structural information for the heptapeptide NNFGAIL was obtained from the Protein Data Bank (entry 3DGJ). MD simulations were performed using GROMACS 4.5.7 and the GROMOS 54A7 united-atom force field at 300 K (see Fig. 1). All peptide bonds were constrained to their equilibrium values using the LINCS algorithm such as described in Ref. 5.

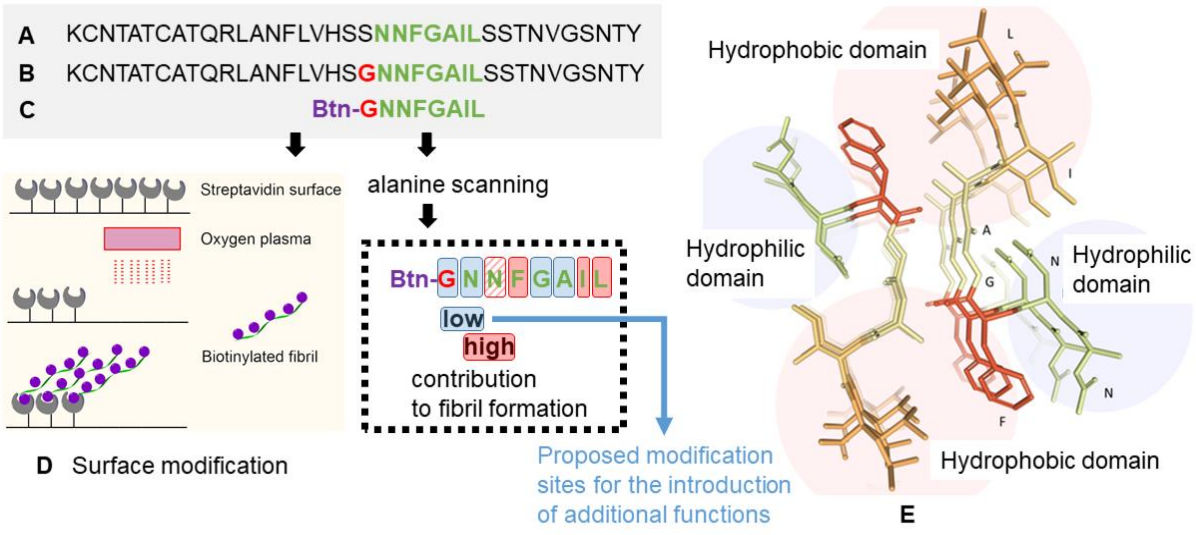

Fig. 1. Sequences and structural information on IAPP and $IAPP_{21-27}$ and their relationship to functional properties. A: Sequence of IAPP with the $IAPP_{21-27}$ segment of NNFGAIL as the assumed core structural domain for fibrillation (in green). B: Sequence of an IAPP variation found in an Asian subpopulation with accelerated diabetes type 2 (S20G shown in red). C: Studied peptide sequence for alanine scanning. D: Surface modification strategy (schematic) for spatial immobilization of biotinylated fibrils. E: NNFGAIL (PDB: 3DGJ) segment from IAPP. Hydrophilic and hydrophobic domains within the protofibril are shown. Molecular data were visualized using the WebGL based 3D viewer NGL from the RCSB PDB website. Adapted from Ref. 5.

Results and Discussion

Fibril stability of biotinylated GNNFGAIL

A peptide system with high aggregation propensity and a biotin anchor for conjugation of the fibrils to other structural elements based on the biotin-streptavidin system was established. Molecular dynamics (MD) simulations were performed in order to obtain information about the stability and the propensity to form structural fibril motifs in substituted peptides. The study involved the wildtype (wt) peptide NNFGAIL, the negative control NNGGAGL, GNNFGAIL (considering the N-terminal S20G substitution), and Btn-GNNFGAIL.

The MD starting structures consisted of five-stranded protofibrils with two β-sheets (5x2). In order to monitor the stability or disassembly of the modeled peptide oligomer structures, the systems were simulated for 100 ns. Structural representations of the protofibrils of NNFGAIL, NNGGAGL, GNNFGAIL and Btn-GNNFGAIL after 100 ns are shown in Figure 2a. The fibril structure of NNGGAGL was significantly disturbed and not stable. NNFGAIL, GNNFGAIL and Btn-GNNFGAIL had a higher fibril stability. The root-mean-square deviations (RMSD) of the peptide backbones and the root mean square fluctuations (RMSF) of the peptide residues were calculated to quantify the stability or disassembly of peptide oligomer structures (Figure 2b). The NNGGAGL protofibril had the lowest stability, confirming the importance of the hydrophobic side chains phenylalanine (F23) and isoleucine (I26) for peptide fibril formation. The extension of the wildtype sequence (GNNFGAIL, Btn-GNNFGAIL) enhanced the peptide fibril stability. In fact, Btn-GNNFGAIL had RMSD and RMSF deviations similar to NNFGAIL; however, the β-sheets were more stable than for NNFGAIL, and the deviations were caused by rearrangements to achieve an optimized structure.

Fibril formation kinetics of alanine scanning variants of Btn-GNNFGAIL

To understand the role of single amino acids within Btn-GNNFGAIL for fibril growth and morphology, alanine scanning of the Btn-GNNFGAIL peptide was carried out. Compared to glycine and proline substitutions (β-sheet breaker), it is believed that alanine scanning has a reduced impact on the peptide backbone, which is important for NNFGAIL-derived peptides since their fibrillation is promoted by backbone-backbone interactions of the individual strands (Figure 1E). The kinetics of amyloid fibril formation was followed using ThT binding assays [5]. The data show the fluorescence intensity after several time intervals under identical ambient conditions for each peptide (temperature, shaking intensity). Considering the value after one day of incubation, the peptide variants. Btn-GNN(F23A)GAIL,Btn-GNNFGA(I26A)L, Btn-GNNFGAI(L27A), and Btn-GN(N22A)FGAIL had a reduced fluorescence intensity compared to the other peptides. This suggests that the residues F23, I26, L27 and N22 are important for the formation of β-sheet rich nuclei that seed fibril formation. After one month of incubation, significant fluorescence signals were found in all samples, except of Btn-GNNFGA(I26A)L. The longest lag times of fibrillation were observed for the variants Btn-GNN(F23A)GAIL and Btn-GNNFGAI(L27A).

Morphologies of alanine scanning variants of Btn-GNNFGAIL

The peptide fibril morphologies after 1 d and 17 d were studied by SEM (Figures 5 and S3). After 1 d, large amounts of fibrils were formed for almost all alanine scanning variants, when dried on silicon wafers, with the exception of Btn-GN(N22A)FGAIL, Btn-GNN(F23A)GAIL and Btn-GNNFGAI(L27A). In these cases, mostly amorphous peptide aggregates cover the surface of the silicon wafers, which have a tendency to arrange in a more or less non-ordered phase. Btn-(G20A)NNFGAIL and Btn-G(N21A)NFGAIL formed thinner fibril structures, while Btn-GNNF(G24A)AIL, Btn-GNNFGAIL and Btn-GNNFGA(I26A)L thicker ones. The morphologies of the supramolecular structures differ from mature NNFGAIL fibrils. NNFGAIL forms extremely dense fibril associates with a crystal-like superlattice and a high degree of stiffness (Fig. 3). In contrast, single fibrils of Btn-(G20A)NNFGAIL are arranged in

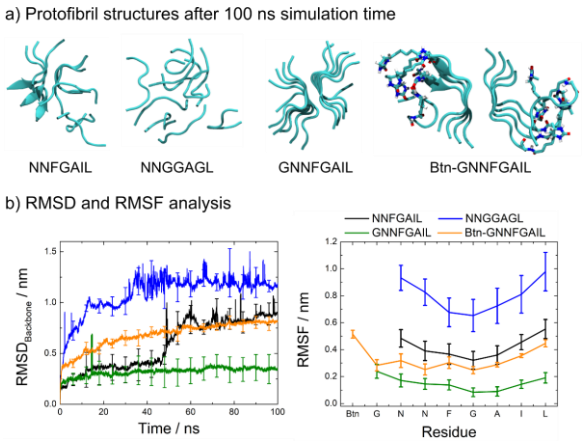

Fig. 2. (a) Double layer five-stranded peptide protofibril structures after 100 ns of simulation time are shown in cartoon representation with biotin as dynamic bonds (representative structures of the three repetitions). (b) Root-mean-square deviations (RMSD) for the peptide backbone and root mean square fluctuations (RMSF) of all peptide residues and biotin were calculated over the simulation time of 100 ns. Adapted from Ref. 5.

flexible ring shaped structures, which can be compressed to tight gels (Figure 3). The stiffness appears dramatically reduced. The same feature was ultimately found for the Btn-GNNFGAIL, indicating that the N-terminal modification has a high impact on the morphology of the fibrils, which is likely based on their intrinsic flexibility. After 17 d, the morphology slightly changed for the peptide Btn-G(N21A)NFGAIL which formed needle-like fibrils, which was not obvious after 1 d. A much higher amount of fibrils was observed for Btn-GNNFGA(I26A)L after 17 d with a comparable morphology to Btn-(G20A)NNFGAIL, Btn-GNNFGAIL, and Btn-GNNF(G24A)AIL. The double variant Btn-GNN(F23A)GA(I26A)L formed no fibrils, even after 17 d. For Btn-GNNFGA(I26A)L, no fibrils were found in the ThT fluorescence assay after 1 d, while SEM revealed some fibrillar structures. This is likely caused by surface concentration effects during sample preparation for SEM. While the peptide containing droplets air-dried on the silicon supports, the peptide concentration increased, which increased the propensity for peptide aggregation.

Our results indicate that the substitution of F23A has a large negative impact on the formation of mature fibrils. Thus, F23 is a key residue for the aggregation of Btn-GNNFGAIL. This result is consistent with previously reported MD simulations, where glycine scanning variants of the wildtype NNFGAIL were studied to understand the effect of single point substitutions on the amyloidogenic propensity in terms of the sheet-to-sheet and strand-to-strand interactions. In agreement with our experimental results, the variants NN(F23G)GAIL and NNFGA(I26G)L had a lower fibril stability followed by (N21G)NFGAIL and N(N22G)FGAIL. Our findings also agree with previous observations when IAPP (segment) mutations were investigated. For instance, the variants N(F23Y)GAILSS, SN(N22P)FGAILSS, SNNFGA (I26P)LSS and SNNFGAI(L27P) aggregated to a lower extent. No or a reduced amyloid fibril formation was observed under experimental conditions when phenylalanine was replaced with alanine in full-length IAPP and selected peptide segments. A summary on the influence of amino acid substitutions in IAPP and derived peptides from previous studies is provided in Ref. 5, emphasizing the role of each residue.

Theoretical predictions

Theoretical predictions based on the contribution of each amino acid in GNNFGAIL to the overall solubility and propensity to form fibrillar aggregates revealed that the F23A variant had the largest impact, followed by I26A and L27A. These calculations are

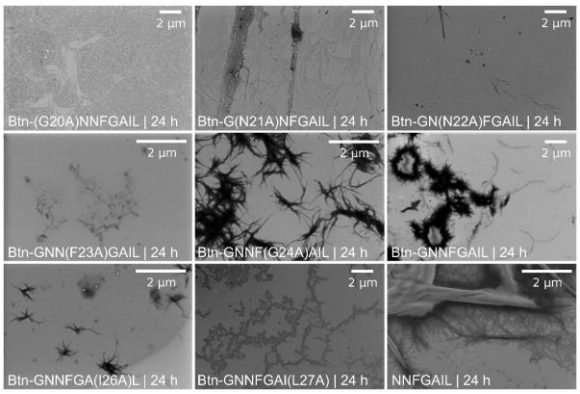

Fig. 3 SEM images of fibrils of the alanine scanning peptides of Btn-GNNFGAIL after 24 h ([peptide] in the fibrillation assay = 0.1 mg/mL). Adapted from Ref. 5.

in agreement with the experimental results obtained in the ThT kinetic assay and SEM measurements for Btn-GNNFGAIL, confirming the high relevance of the phenylalanine, isoleucine and leucine residues for peptide fibril formation, especially its early nucleation phase.

A lower solubility and higher aggregation propensity were found for the G20A, N21A, N22A and G24A variants compared to the unmodified GNNFGAIL peptide, in agreement with the ThT assay. One outlier between the predicted solubility for GNNFGAIL variants and the experimentally observed amyloid formation for Btn-GNNFGAIL after 1 d is the N22A variant. Although this variant is poorly soluble, it did not form many fibrils. This is likely due to a kinetic effect, increasing the lag time for the formation of a critical nucleus, until large amounts of fibrils were formed after 3 d.

Immobilization to streptavidin coated surfaces

Fibril-modified surfaces are of interest for different purposes, for instance their usage as a new class of morphologically and chemically engineered biomaterials, which may be involved in fibril-cell or fibril-nanoparticle interactions. Since the amount of biological sample materials is limited, microfluidic approaches are readily advantageous over conventional laboratory techniques. The spatially controlled immobilization of fibrils to surfaces is the first step towards their integration into multifunctional microfluidic systems [6]. A streptavidin coated glass slide was used as a model to demonstrate the spatial immobilization of biotinylated fibrils to surfaces as a first proof-of-concept; however, even other binding concepts may be suitable.

To achieve the goal, the streptavidin coated slide was exposed to an atmospheric oxygen plasma through a mask allowing for streptavidin inactivation

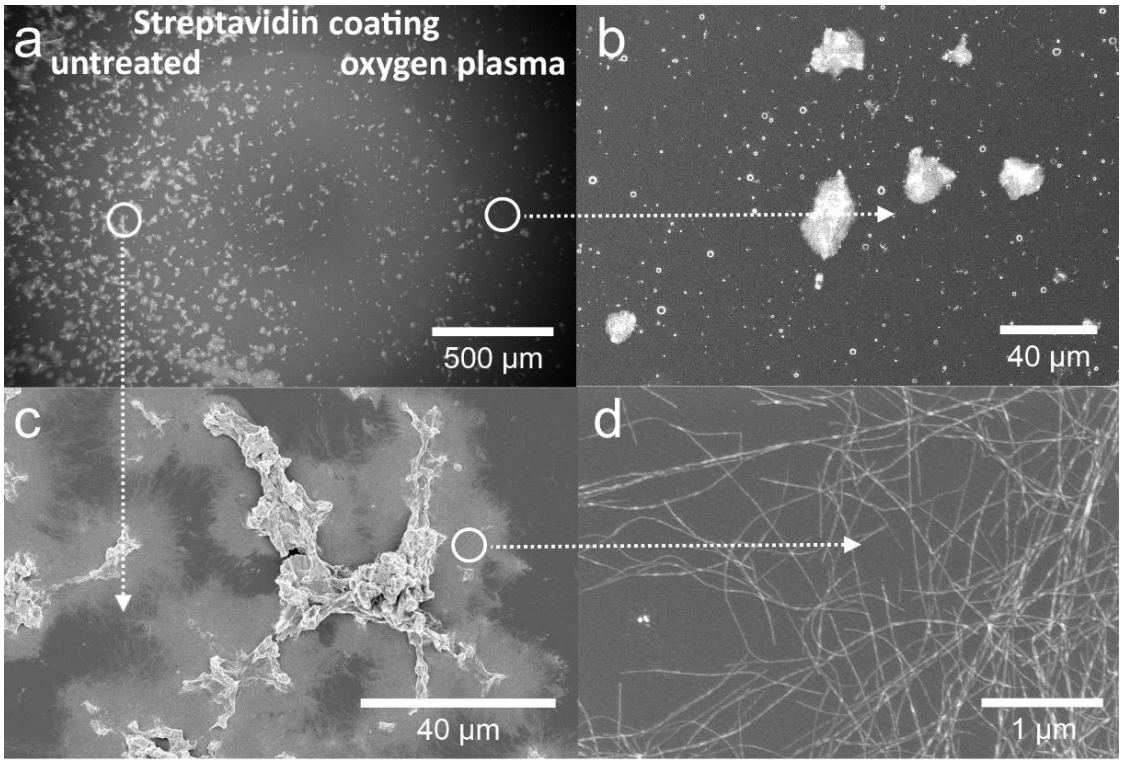

Figure 4. SEM images of spatially immobilized fibrils of Btn-GNNFGAIL on a streptavidin coated glass slide. (a) While the left side of the streptavidin coated glass slide was untreated, the right side was cleaned under an oxygen plasma. Amyloid fibrils were largely immobilized in the streptavidin coated area. Image analysis (Matlab R2018b, Gwyddion 2.52) revealed a fibril surface coverage of at least 24 % on the streptavidin coated (untreated) area and 5 % fibril coverage on the plasma treated side (see Figure S5 for masked images). (b) Typical SEM image of an area that was oxygen-plasma treated with not many immobilized peptide fibrils. (c) Typical SEM image of a streptavidin coated (untreated) area with many immobilized peptide fibrils. (d) Magnified area of the bound amyloid fibrils showing the typical fibril structure. Adapted from Ref. 5.

and degradation at the exposed areas. Different surface modification techniques, such as laser structuring, could also be applied at this stage. After treatment, exposed and unexposed areas were incubated with a peptide solution of Btn-GNNFGAIL under fibrillation conditions (Figure 4). SEM revealed a higher degree of immobilized fibrils in the streptavidin coated areas, whereas plasma-cleaned areas showed a much lower degree of bound fibrils (Figure 4). Instead of a homogeneous surface coverage, the fibrils formed islets of a few tenth of micrometers (Figure 4c). The herein presented approach is highly compatible with our recently developed method of inverse microfluidic printing (cryoprinting [6]). Cryoprinting enables the fabrication of microfluidic systems on a time scale of a few minutes by aqueous printing and freezing of microstructures using the drop-on-demand technology, which are subsequently encapsulated in a photocured polymer within milliseconds. Fibrillar nanostructures and their gels could thus be integrated into microfluidic systems under spatial control in the near future [6].

Conclusion

Key residues for fibril formation of the N-terminal biotinylated $IAPP_{21-27}$ peptide (Btn-GNNFGAIL) were identified using an alanine scanning approach combined with molecular dynamics simulations, thioflavin T fluorescence measurements, and scanning electron microscopy. A significant contribution of phenylalanine (F23) for the fibrillation of the short peptide segment was identified. The fibril morphologies of the peptide variants differed depending on their primary sequence, ranging from flexible and semi-flexible to stiff and crystal-like structures. These insights could advance the design of new functional hybrid bionanomaterials and fibril-engineered and coated surfaces using short peptide segments. To validate this concept, fibrils were immobilized on streptavidin coated surfaces under spatial control.

Literature

[1] D.Eisenberg, A. D. McLachlan, Solvation Energy in Protein Folding and Binding, Nature (1986) 319 (6050), 199–203
[2] T. John, A Gladytz, C. Kubeil, L. L. Martin, H. J. Risselada, B. Abel, Nanoscale (2018) 10 (45), 20894–20913
[3] A. Gladytz, B. Abel, H. J. Risselada, Angew. Chemie - Int. Ed. (2016) 55 (37), 11242–11246
[4] J. Bandak, J. Petzold, H. Hatahet, A. Prager, B. Kersting, C. Elsner, B. Abel, RSC Adv. (2019) 9 (10), 5558–5569
[5] T. John, J. Bandak, N. Sarveson, C. Hackl, H. J. Risselada, A. Prager, C. Elsner, B. Abel, Biomacromolecules (2020) 21, 2, 783-792
[6] C. Elsner, et al., Verfahren zur Herstellung eines Mikrosystembauteils, DE Patent 102017130947.0 (A1), Dezember 21, 2017

Photoemission Electron Microscopy – a Tool Analyzing the Polymer Surface Morphology

F. Niefind, A. Neff, S. Karande, F. Frost, B. Abel, A. Kahnt
in collaboration with
S.C.B. Mannsfeld, Center for Advancing Electronics Dresden (cfaed), Technische Universität Dresden, Germany

The Bigger Picture

The energy consumption of the world is rising since decades and is reaching new highs nearly every year. The most of this energy is still originating from non-renewable sources such as burning oil, natural gas and coal, which all contributes to the human carbon dioxide footprint with foreseeable and already recognizable harmful impact on the worlds ecosystem. The challenge minimizing these adverse effects in the future is the transition of the economy away from the consumption of fossil fuels towards the usage of sustainable sources, which are renewable. As it is foreseeable, solar light to power conversion will make a major contribution to achieve this goal. Major successes were already attained in the past, utilizing very efficient silicon or perovskite based solar devices. However, such devices are impractical in applications where other properties such as semitransparency or mechanical flexibility is a major factor. Here devices based on semiconducting polymers are emerging as feasible candidates and thus the determination of the nanoscale structure of polymer films becomes a key factor.

Introduction

Semiconducting polymers have drawn attentions in the scientific community since several decades and are assumed as promising candidates for organic transistors, organic light emitting diodes and organic photovoltaics. In the case of the latter – organic photovoltaics – semiconducting polymers will have its niche in applications where the mechanical flexibility is a necessary feature e.g., in the emerging field of wearables. The flexibility and efficiency of organic photovoltaic devices is dictated by the sub-micrometer morphology of the polymer film. As a rule over thumb, on the one hand side, the more crystalline and well aligned the polymers are, the more efficient is the overall light to power conversion. On the other hand side, the more random the polymers are coiled, the more flexible the film is, but such films exhibit lower light conversion efficiencies. In order to control the polymer film structure, a technique is required that enables to image the morphology on the nanometer and micrometer scale. Photoemission Electron Microscopy (PEEM) has emerged as techniques that enables the determination of the morphology on the relevant scale. Furthermore, PEEM is a fast and in particular non-destructive technique making it supreme over other approaches like near edge X-ray absorption fine structure spectroscopy (NEXAFS), scanning transmission X-ray microscopy (STXM) or polarized X-ray scattering (PoXS).

As a microscopic technique, PEEM delivers images of the photoelectron intensity, and when measured with polarized light the intensity contains information on the orientation of the polymer chain. In order to make the chain orientation obtained from PEEM images of different samples comparable; a method is needed that allows breaking the orientation information from PEEM images down to a single value or a simple graph. In the following we report on our published results establishing the orientation persistence length (OPL) as a measure for the order of polymer films and with this information on hand, we report on the solvent influence on the surface morphology in spin coated P3HT thin films. [1,2]

Results

As already shown in the past, polarized light, e.g., originating from a laser allows the imaging of the morphology in polymer films in respect of their chain orientation and local degree of order. [3] As an example regioregular poly(3-hexylthiophene-2,5-diyl) (RR-P3HT) was chosen and spin-coated on silicon wafer and FTO-coated glass. The PEEM measurements of both samples (figure 1) exhibited domains in the micrometer range with polymer chains with a similar orientation. However, even by eye it is clearly visible that the domains of similar order are smaller for the polymer coated on FTO compared to the domain sizes for the Si based sample (compare figure 1a and 1c).

As a way to quantify this by eye visible difference in the PEEM images, the orientation persistence length was used in order to determine the average distance starting from a random pixel in the PEEM image until the change of the polymer chain orientation is overcoming a selected threshold angle $\Delta\beta$. For both PEEM images (figures 1a and 1c) 10000 pixels from the centers of the images – to avoid boundary effects – were randomly selected and the chain orientation for every of this pixel was determined. Than for every pixel in a random direction the distance to the first pixel where the chain orientation differs more than the threshold angle $\Delta\beta$ was determined. The average

values obtained for different selected threshold angle Δβ for both samples is shown in figure 2 depicting clearly substantially larger orientation persistence length values – independent from the selected threshold angle Δβ – for the RR-P3HT spin coated on Si.

With the OPL as a measure to quantify the order of polymer chains from PEEM images on hand, the influence of the solvent from which the films were spun was investigated. Previous literature published results indicated a strong solvent dependence on the polymer film morphology and film quality. [4]

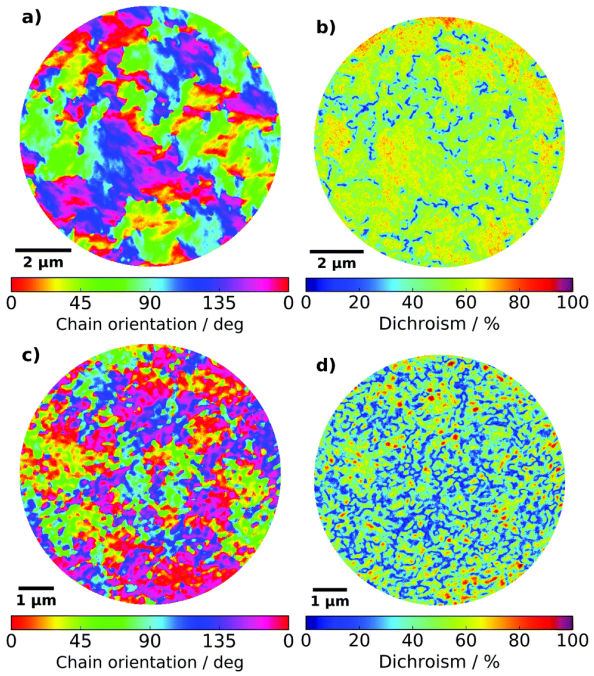

Figure 1: Maps of orientation (a and c) and dichroism (b and d) resulting from laser-PEEM measurements of RR-P3HT films on a silicon substrate (a and b) and on an FTO-coated glass (c and d) (F. Niefind, A. Neff, S. C. B. Mannsfeld, A. Kahnt and B. Abel, Phys. Chem. Chem. Phys. 21, 21464 (2019). - Reproduced by permission of the PCCP Owner Societies).

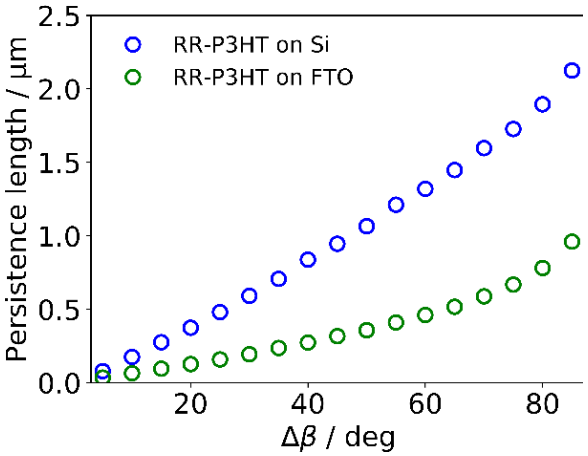

Figure 2: Dependence of orientation persistence length of measurements shown in figure 1 on the threshold angle Δβ (F. Niefind, A. Neff, S. C. B. Mannsfeld, A. Kahnt and B. Abel, Phys. Chem. Chem. Phys. 21, 21464 (2019) - Reproduced by permission of the PCCP Owner Societies).

Especially the boiling point of the solvent from which the films were spun was assumed as the dominating factor for the film quality – in terms of ordered structure size – and the performance of the devices made from it. The rational for this is that films obtained from solutions with solvents of higher boiling points will exhibit higher crystallinity since the higher the boiling point, the longer is the evaporation period and thus it grants the polymer more time to arrange in a crystalline morphology. However, when measuring PEEM images for RR-P3HT films spun from different organic solvents with boiling points ranging from 60 to 214°C derivations from this trend were obvious. As one can already see by the eye from the PEEM images in figure 3, the size of the domains with the same orientation in thiophene and chlorobenzene is larger than in 1,2,4-trichlorobenzen, even though the boiling point of 1,2,4-trichlorobenzen is with 214°C

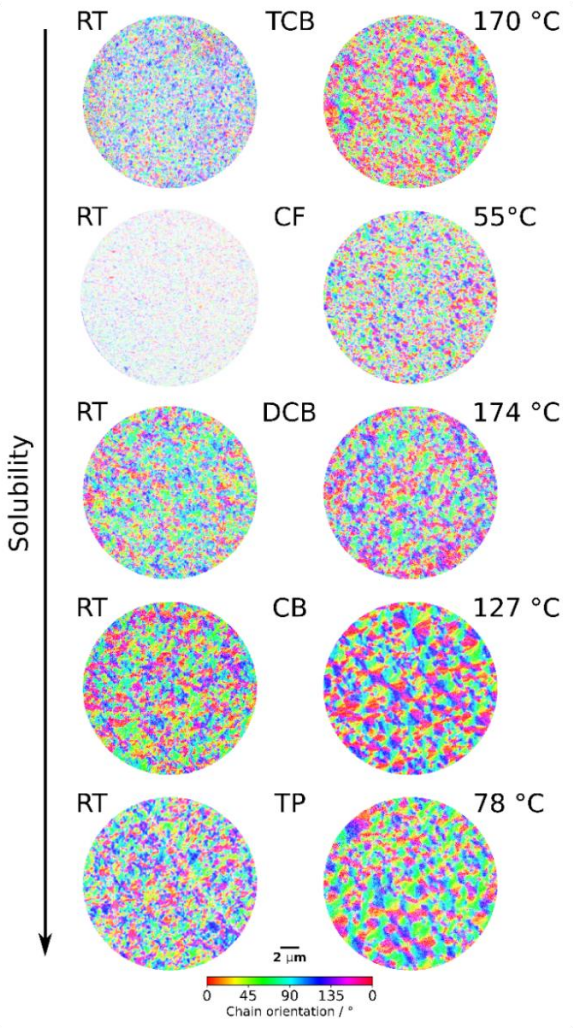

Figure 3: Evaluated PEEM image series showing the combination of chain orientation and local degree of order of P3HT films spun from different solvents: Cholorbenzene (CB), o-dichlorobenzene (DCB), 1,2,4 trichlorobenzene (TCB), thiophenen (TP) and chloroforme (CF) on Si. The left side shows the results for the films spun at room temperature, while the right hand side shows the results for the films spun from elevated temperatures (F. Niefind, S. Karande, F. Frost, B. Abel and A. Kahnt, Nanoscale Adv. 1, 3883 (2019) - Published by The Royal Society of Chemistry).

higher than the boiling point for thiophene (84°C) and chlorobenzene (132°C). This finding is strongly contradicting the notion that the boiling point is the (exclusive) key factor determining the film crystallinity. Noteworthy is the fact that for all solvents it is clearly visible that the domain size and therefor the crystallinity is increased when the films were spun from solutions at elevated temperatures. Bearing in mind that with the elevation of the temperature also the solubility increases, this finding indicates that the solubility of P3HT in the selected solvent contributes to the domain size in the films.

Using the OPL as a measure for the crystallinity of the films figure 4 depicts the correlation between the OPL and the P3HT solubility. As a general finding – disregarding chloroform – one sees an increase of the OPL with increasing solvability of P3HT. Chloroform however shows rather small domains and is a clear outliner breaking this global trend, and requires separate considerations. Compared to the other solvents used, chloroform exhibits a much higher vapor pressure, which leads too much shorter drying times, leaving the polymer chains less time to aggregate properly and thus resulting in smaller domains of the same orientation. These findings stresses clearly that the polymer film morphology depends on multiple factors and the solvability of the polymer together with the boiling point, seems to be a substantial if not the key factor controlling the domain size and the overall film morphology.

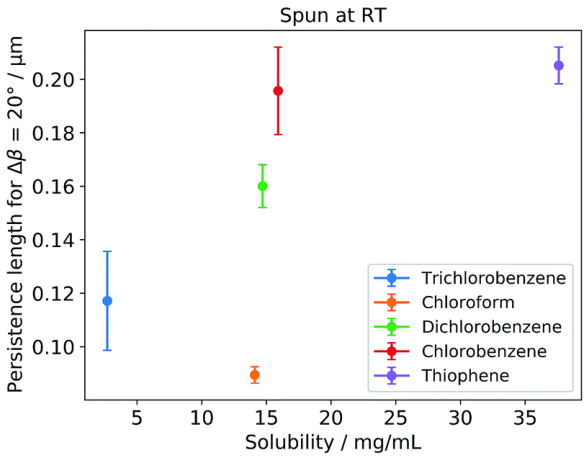

Figure 4: Dependence of the OPL for Δβ = 20° plotted against the solubility of P3HT in different solvents. The values represent the mean value gathered from multiple spots on the same sample. The error bars express the standard deviation (F. Niefind, S. Karande, F. Frost, B. Abel and A. Kahnt, Nanoscale Adv. 1, 3883 (2019) - Published by The Royal Society of Chemistry).

Conclusion

In conclusion, we report on a method, which allows to quantify the average domain size and thus the crystallinity of polymer films from PEEM images taken with polarized light. With this method on hand further key factors dictating the polymer crystallinity for spin coated films were determined.

Experimental Section

All PEEM measurements were performed in an IS-PEEM from FOCUS GmbH with an ultimate resolution of ≈ 40 nm. The laser radiation was generated with a Coherent Fidelity-2 laser. The fundamental wavelength (1070 nm) was frequency doubled to 535 nm by an APE Harmonixx. The samples were illuminated using a normal incidence rhodium mirror inside the Focus PEEM. The polarization direction and the pulse energy were adjusted by a combination of a λ/2-waveplate and a polarizer. For the presented measurements the laser power was set to 17.5 mW before entering the vacuum chamber through a window, except for chlorobenzene, where the laser power used was 10 mW. For further details see Ref. 1 and 2.

Acknowledgement

The work was funded in part by the German Science foundation (DFG) through SFB-TR102. Dr. Falk Niefind gratefully acknowledges funding from the DBU. Dr. Andreas Neff was funded by the Beilstein-Institut zur Förderung der Chemischen Wissenschaften. Prof. Dr. Bernd Abel thanks the Miller Institute of the UC Berkeley for a Somorjai-Miller-Guest-Professorship Award 2018. Dr. Axel Kahnt and Prof. Dr. Bernd Abel thank APE Angewandte Physik und Elektronik GmbH for support with the Harmonixx. All authors are deeply indebted to Dr. Katrin Siefermann for her contributions in the early stages of this project. The authors thank Dr. Mike Hambsch for insightful discussions concerning the film preparation.

Literature

[1] F. Niefind, A. Neff, S. C. B. Mannsfeld, A. Kahnt, B. Abel, Phys. Chem. Chem. Phys. 21, 21464 (2019)
[2] F. Niefind, S. Karande, F. Frost, B. Abel and A. Kahnt, Nanoscale Adv. 1, 3883 (2019)
[3] A. Neff, F. Niefind, B. Abel, S. C. B. Mannsfeld, and K. R. Siefermann, Adv. Mater. 29, 1701012 (2017)
[4] H. Yang, T. J. Shin, L. Yang, K. Cho, C.Y. Ryu, Z. Bao, Adv. Funct. Mater. 15, 671 (2005)

TALIF Diagnostics of Rare Gas Densities in Gridded Ion Sources

C. Eichhorn, F. Scholze, C. Bundesmann, D. Spemann, H. Neumann
in collaboration with
H. Leiter, ArianeGroup GmbH, Lampoldshausen, Germany

The knowledge of neutral particle densities within or near the exit plane of grid systems is of substantial importance for the estimation of the lifetime of gridded ion sources. In two-grid ion optics, the impingement of secondary ions, produced in charge exchange processes between primary ions and thermal neutral particles, on the accelerator grid is commonly known as the main cause of grid erosion. Long grid lifetimes are essential for the design of ion optics for electric space propulsion, where multi-year operation of gridded ion thrusters is required to achieve mission objectives of orbiting satellites or interplanetary probes.

Two-photon absorption laser induced fluorescence (TALIF) spectroscopy is a powerful non-intrusive diagnostic technique to measure ground state densities of atoms or molecules [1]. Since in many low-temperature plasma applications the depletion of the ground state may be neglected, the method allows for a direct measurement of neutral particle species like xenon or krypton, which are common process gases in surface engineering, as well as propellants for space applications. The principle of the method is the spatially resolved state-selective two-photon excitation of the plasma species of interest using the output of a Nd:YAG pumped dye laser, and detecting the subsequent fluorescence with a photomultiplier, which is processed in a boxcar integrator (Fig. 1).

Measurements using a newly installed TALIF set-up at IOM have recently been carried out in the plume of the ion thruster RIT-10, which has been provided by ArianeGroup GmbH [2,3]. An example of a radial

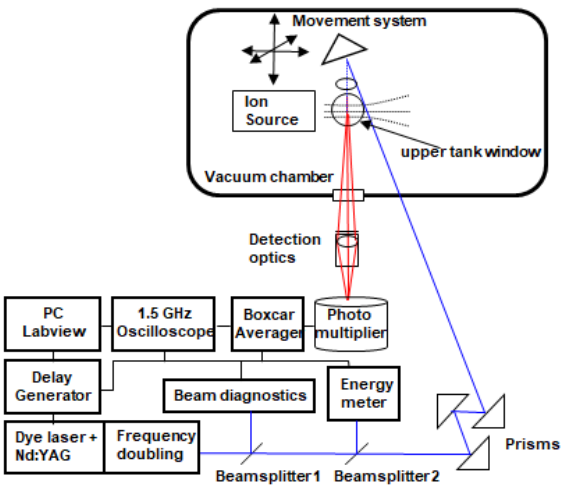

Figure 1: TALIF experimental set-up.

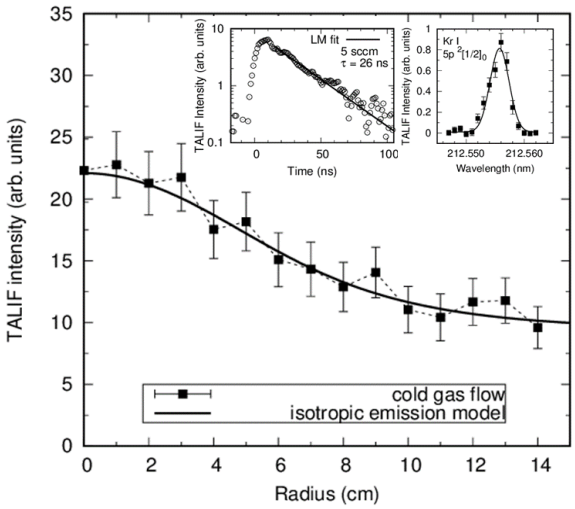

Figure 2: Radial neutral density profile in the plume of the RIT-10, including time- and spectrally resolved signals.

profile of the neutral density of krypton in the plume of the thruster measured with TALIF is shown in Fig. 2. As can be seen, the neutral density in the plume can be clearly resolved from an offset, which results from the krypton background density in the vacuum chamber. The set-up allows for an analysis of the lineshape of the absorption line, as well as of the lifetime of the excited level, which is measured using a fast oscilloscope of 1.5 GHz bandwidth.

Besides such axial and radial neutral density mapping in xenon and krypton, further investigations deal with the application of the TALIF method on the plasma inside the discharge chamber of gridded ion sources. Here, in experiments using the institute-built ISQ40 RF source equipped with quartz glass chamber walls, quantitative TALIF spectroscopy on neutral particle densities has been demonstrated.

Financial support from the Deutsche Forschungsgemeinschaft DFG through grant EI978/1-1 is gratefully acknowledged.

Literature

[1] D. J. Bamford, L. E. Jusinski, W. K. Bischel, Phys Rev A 34 (1986) 185
[2] Eichhorn, C., Scholze, F., Bundesmann, C., Spemann, D., Neumann, H., Leiter, H., J. Propul. Power 35 (2019) 1175
[3] Eichhorn, C., Scholze, F., Bundesmann, C., Spemann, D., Neumann, H., Leiter, H., 36th International Electric Propulsion Conference, Wien, IEPC Paper-2019-503, 2019

Setting up a New Laboratory for Plasma Engineering

A. Anders, C. Bundesmann, W. Diyatmika, C. Eichhorn, U. Gey, D. Kalanov, J. Knipper, K. Oh, T. Pröhl, M. Rudolph, D. Spemann, Y. Unutulmazsoy, R. Woyciechowski

Plasma and ion beams are often used to assist in physical vapor deposition in order to obtain films or nanostructures with the desired properties. Those properties are the result of the intrinsic material properties and the micro (and nano) structure. For plasma-assisted deposition, it seems obvious that the plasma should be engineered but in practice the plasma source is often used “as-is” and the effects are primarily tuned via substrate bias affecting ion and electron fluxes to the substrate. Therefore, to have a better control over the final properties of surfaces, coatings, and nanostructures, a lab is set up in which the engineering of the plasma is at the center of future research activities. This is done with surface effects being monitored, too. In other words, the activities at the lab aim to simultaneously diagnose and adjust the properties of the plasma (such as the flux of ions to a substrate in terms of energy and charge states) and monitor plasma effects on surfaces and films.

As model plasma sources we have set up a high power impulse magnetron (HiPIMS) source, which will be supplemented in 2020 with pulsed filtered arc sources.

The Plasma Lab, located in 17.1/0.06, occupies the formed BN-MBE lab, which has not be operational for some time. In 2018/19, the outdated equipment was removed and the room prepared to accommodate three vacuum chambers, two of them were put in service by the end of the reporting period (Fig. 1).

The large chamber has been named “pi-PVD” (pulsed ionized physical vapor deposition) since its main purpose is to expand the established technique

Figure 1: Vacuum chamber “pi-PVD” in the new Plasma Lab, December 2019

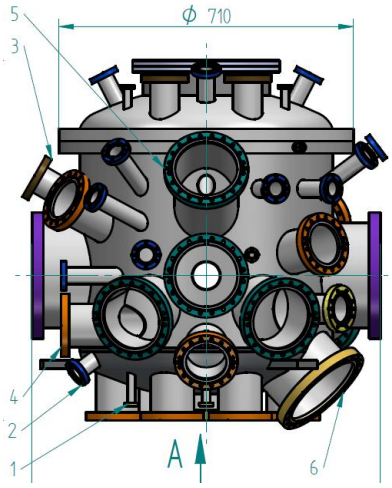

Figure 2: Vacuum chamber for SAB-Project “Modular Plasma Deposition Platform”, designed in 2019, to be manufactured and installed in 2020.

of “i-PVD” to a pulsed system, thereby opening new process parameters (high pulse power, adjustable pulse length, duty cycle, pulse reversal). The concept of “pi-PVD” is the basis for a project of the “Leibniz Collaborative Excellence” that was jointly prepared with the RWTH Aachen University. In this project, which started in 2019, we plan to study the effect of ion charge on the microstructure and properties of compound films such as VAlN. The second chamber, which is much smaller, is designed for preparatory experiments, including high power impulse magnetron sputtering (HiPIMS); it will also be used for the training of graduate students.

The third vacuum chamber, funded by a grant of the SAB, has been designed (Fig. 2).

This chamber is specifically designed to simultaneously accommodate plasma diagnostics and surface measurements, therefore a large set of carefully selected ports had to be placed.

With these preparations, and the acquisition of modern diagnostic equipment, the Plasma Engineering Group is positioned to execute various projects, most notable the Leibniz Collaborative Excellence and the SAB-funded project.

Highly Porous Silver Thin Films for Biosensing Applications

C. Grüner, S. Grüner, B. Rauschenbach
in collaboration with
I. Abdulhalim, Ben-Gurion University of the Negev, Israel

Precious metal thin films, generated by Glancing Angle Deposition (GLAD), provide highly unique physical properties. One of these properties is the extreme enhancement of specific optical effects, which can be taken advantage of for sensing applications [1]. While effects like surface enhanced Raman scattering (SERS), surface enhanced fluorescence (SEF), and surface enhanced infrared absorption (SEIRA) can also be found in the vicinity of smooth, compact metal films, GLAD films on the one hand exhibit a very high porosity and large effective surface area, which maximizes the contact between the test medium and the metal itself. On the other hand, GLAD films consist of very thin nanostructures. This further increases i.e. the Raman efficiency due to the strong electric field observed close to the highly curved surfaces of such nanostructures.

GLAD, in principle, is a straightforward technique. Deposition equipment and conditions are used that are common with most physical vapour deposition (PVD) techniques. The main difference is that the material flux does not arrive at normal incidence at the substrate, but instead in a highly oblique manner. This leads to a geometric self-shadowing effect during deposition, which finally yields the self-organized growth of nanostructures on the surface. The shape of the nanostructures and the integral properties of the porous thin film can be controlled by the deposition geometry (angle of incidence, substrate rotation) and the usual PVD parameters (like material flux, substrate temperature or residual gas pressure).

The extremely high enhancement factors, achievable with Ag GLAD films, are in the 10^{10} range and a possibility to make these films specific to a previously

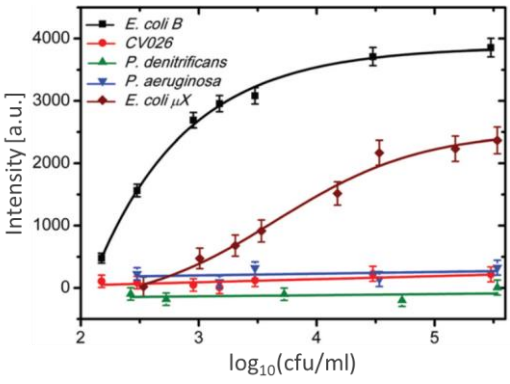

Figure 1: SERS signal intensity obtained at different concentrations of various bacteria strains using Ag GLAD films.

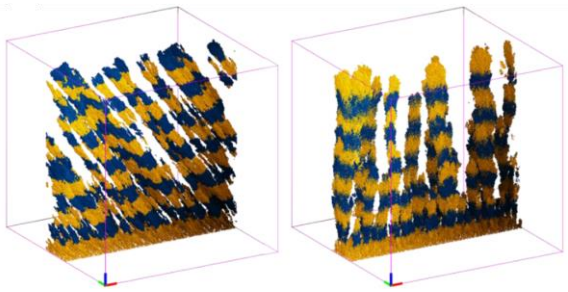

Figure 2: Computer simulations of tilted (left) and upright (right) nanostructures, grown under oblique material incidence without and with substrate rotation, respectively.

chosen test agent is mandatory. This can be accomplished by further surface functionalization with antibodies or bacteriophages. In Figure 1 the SERS signal intensity measurement of E. coli bacteria is shown. The sensor consists of a 350 nm thick Ag film with around 30% overall porosity. Specificity is provided by applying bacteriophages. The results reveal, that already small concentrations, down to 1 bacterium per 10 µl volume can be safely detected. Other than the targeted bacteria strains do not lead to a change in signal intensity, demonstrating the selectivity of this sensor type.

Optimization of such sensors requires fundamental knowledge of the underlying growth processes. On one side, the growth process itself must be studied. This is realized by accompanying computer simulations (see Figure 2) and theoretic modelling [2]. An underlying general relationship could already be found, that links the angle of incidence with morphological film parameters, such as porosity. On the other side, material properties strongly influence the GLAD process. Therefore, GLAD metal films have been intensively studied. It could be shown that for most metals a growth temperature window exists, in which the nanostructures grow single crystalline, forming a biaxially textured porous thin film [3].

Literature

[1] C. Grüner, I. Abdulhalim, B. Rauschenbach, Encyclopedia of Interfacial Chemistry, Editor: K. Wandelt, Elsevier: Oxford. (2018) pp. 129
[2] C. Grüner, S. Liedtke, J. Bauer, S.G. Mayr, B. Rauschenbach, ACS Appl. Nano Mater. 1 (2018) 1370
[3] S. Liedtke-Grüner, C. Grüner, A. Lotnyk, J.W. Gerlach, B. Rauschenbach, Phys. Stat. Solidi A 217 (2020) 190063

Reactive Ion Beam Etching of Highly Dispersive, High-Efficiency Transmission Gratings for the VIS Range

A. Finzel, G. Dornberg, F. Frost
in collaboration with
F. Koch, D. Lehr, T. Glaser, Carl Zeiss Jena GmbH, Germany

With the growing importance of ultrashort pulse lasers the demand for particularly tailored optical components arises. Different dispersive elements can be utilized for the temporal stretching and recompression of short pulses. Transmission surface relief gratings in fused silica are particularly popular due to their high-laser-induced damage threshold as well as the ability to utilize them in the Littrow configuration [1].

For the realizationn of the monolithic transmission gratings with 3000 L/mm the resist-coated and soft-baked fused silica substrateswere exposed to the stabilized interference pattern and afterward wet-chemically developed [2].

The optimizedresist profiles show no residual resist layer left at the grooves and a sufficiently large duty cycle of 0.4 [2]. Typical resist profiles show no residual resist layer left at the grooves, a height of 280 nm and a duty cycle (ratio between ridge width and period) of 0.4. The pattern transfer of the resist profile into the fused silica substrate was performed by reactive ion beam etching (RIBE) [3]. A commercially RIBE plant equipped with a broad beam Kaufman-type ion source was used. The ion source was operated with a beam voltage of 700 V, resulting in an ion energy of 850 eV (discharge voltage: 150 V) and a beam current of 70 mA. The chosen gas mixtures were 3.75 sccm CHF_3 / 0.94 sccm Ar / 0.31 sccm O_2, and 4.06 sccm CHF_3 / 0.94 Ar to achieve a high selectivity. The acceleration voltage of the ion source was set to −100 or −1000 V to study the effect of different angular distributions of ions within the broad beam.

Comparing the etch gas mixture with oxygen (samples A, C, and E) and without oxygen (B, D, and F, see Figure 1), it can be seen that the duty cycle of the structures is smaller when the etching was performed with oxygen. The reason for this is the faster degradation of the photoresist and its higher lateral etch rate. A comparison of the samples A and E (3.75 sccm CHF_3 / 0.94 sccm Ar / 0.31 sccm O_2) shows a reduction of the duty cycle from 0.36 (sample A) to 0.30 (sample E) with increasing acceleration voltage. The higher divergence of the incoming ions (U_{acc} = −1000 V) causes a higher side-wall removal and hence smaller duty cycles. For the samples D and F (4.06 sccm CHF_3 / 0.94 sccm Ar) an increase of the

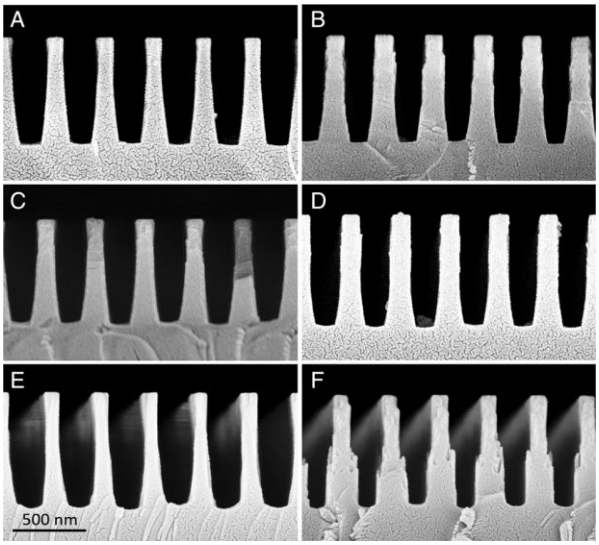

Figure 1: SEM measurements of the different gratings (A-F). Etching parameters are mentioned in the text.

acceleration voltage leads to similar changes of the profile shape. In addition, a higher acceleration voltage (samples E and F) causes almost binary profiles with side-wall angles of 0° compared to a lower acceleration voltage of −100 V (samples A, B, C, and D). The minimum duty cycle of 0.30 corresponds to a ridge width of 100 nm resulting in an aspect ratio of 7.9 (grating depth: 790 nm). Regarding the measured diffraction efficiencies, the samples etched with −100 V acceleration voltage (samples A, B, C, and D) achieve higher values (91.2% to 94.9%) than the samples etched with −1000V acceleration voltage (samples E and F) (83.4% and 90.2%). The relatively low efficiencies of sample E and F result from the nearly binary profiles. In the case of a binary profile, the tolerancing of the optimal profile depth and duty cycle is very small. For higher side-wall angles, the tolerance window for duty-cycle and depth is larger and consequently samples A, B, C, and D reach higher efficiencies.

Literature

[1] H.T. Nguyen, B.W. Shore, S.J. Bryan, J.A. Britten, R.D: Boyd, M.D. Perry, Optics Letters 22(3) (1997) 142
[2] F. Koch, D. Lehr, O. Schönbrodt, T. Glaser, R. Fechner, F. Frost, Microelectric Engineering 191 (2018) 60
[3] A. Finzel, F. Koch, G. Dornberg, D. Lehr, F. Frost, T. Glaser, Optical Engineering 58(9) (2019) 092614

Laser Annealing of Block Copolymer (BCP) Films for Fast and Localized Nanopattern Fabrication

K. Zimmer, J. Zajadacz, F. Frost
in collaboration with
A. Mayer, HC. Scheer, Universität Wuppertal, Germany

Nanopatterning of technical surfaces is challenging for laser processing in particular for patterns below 100 nm due to the limited optical resolution. Self-assembly processes provide a mechanism of pattern generation down to molecular size thus offering an alternative fabrication method. Different approaches of rapid and laser-based annealing of BCP films already demonstrated [1].

Here we focuses on CO_2 laser annealing of PS-b-PMMA block copolymer (PS-b-PMMA, poly(styrene-block- methyl methacrylate) films on fused silica samples to achieve self-assembly into vertical lamellas with periods of approximately 50 nm that can be used as masks for pattern transfer. In preliminary study was found that with rapid, high temperature annealing processes (hot plate, 280 °C) the annealing of BCP films can be accomplished within seconds. This gave the approach for laser annealing by scanning a focussed CO_2 laser across the sample annealing locally the film forming vertical aligned lamellas by microphase separation of in the BCP film in the laser spot (see Fig. 1).

PS-b-PMMA BCP films were prepared according to Ref [2] onto silicon and fused silica samples. These films were subject to CO_2-laser exposure in air with a focussed beam studying the impact of the laser power (2...15 W), the scan velocity (1...250 mms^{-1}) and the repeated laser scanning (see [2]). Basically, the lamellas observed in the centre of the laser track due to the laser-induced temperature distribution. The laser annealing turns the disordered virgin film into ordered state within an irradiation times below 0.1 s as proved by thermal simulations. Due to the random nature of the process the domains with different orientations and disordered interfaces are

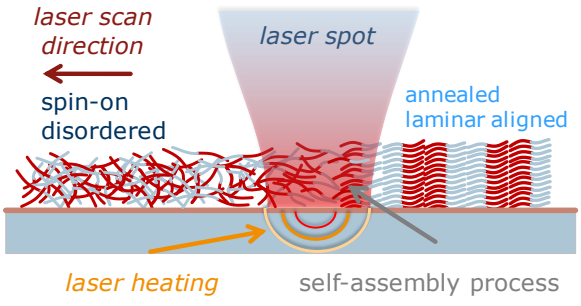

Figure 1: Laser annealing of PS-b-PMMA BCP films for "writing" of vertical aligned lamellas.

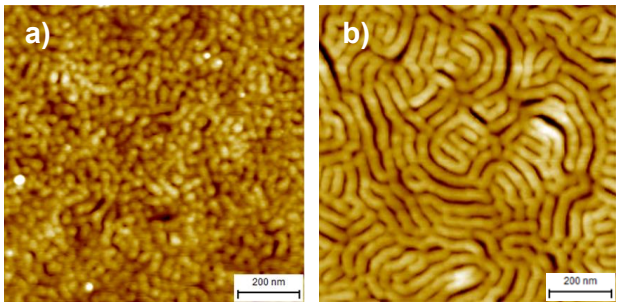

Figure 2: BCP surface morphology after a) spin on, b) optimal annealing.

formed. Less optimized laser-exposure (either over or under exposure) results in partial annealing and dewetting. Selected experimentally achieved surface topographies are shown in Fig. 2. In addition to the observed self-assembly into domains surprisingly a self-development has been observed during laser annealing. This phenomenon is related to the degradation PMMA phase due to the laser-induced, high temperatures. This reduces not only the number of process steps as standard annealed BCP film needs to be developed (VUV and wet developing) but also reduced the risk of pattern collapse at wet processing.

The pattern transfer into functional materials can be performed by reactive ion beam etching (RIBE) that enables the utilization for different applications. In particular the pattern transfer into fused silica [3] has been demonstrated that enabling application of UV optics.

This approach of combining self-assembly processes with direct writing allows localised nano- or hierarchical patterning that is called for by various applications related to superhydrophobicity, self cleaning or friction reduction.

Literature

[1] S.R. Nowak, K.G. Yager, Adv. Mater. Interfaces, (2019) 1901679
[2] K. Zimmer, J. Zajadacz, F. Frost, A. Mayer, C. Steinberg, H.F. Chang, J.Y. Cheng, H.C. Scheer, Appl. Surf. Sci., 470 (2019) 639-644
[3] J. Zajadacz, P. Lorenz, F. Frost, R. Fechner, C. Steinberg, H.-C. Scheer, K. Zimmer, Microelectron. Eng., 141 (2015) 289-293

Improving Molecular Compounds of Solar Cells Based on Computational Screening

S. Zahn
in collaboration with
H. Krautscheid, Universität Leipzig and Thomas Heine, TU Dresden, Germany

Efficient n-type dye-sensitized solar cells are known since the seminal work of O'Reagan and Grätzel in 1991. However, highly efficient p-type dye-sensitized solar cells were not developed so far. This hinders the construction of tandem dye-sensitized solar cells which can surpass the performance of n-type devices. We have investigated if a temporary link between a transition metal-based redox mediator and a sensitizer can increase the efficiency of p-type dye-sensitized solar cells [1]. This link should result in a close distance of counter charges after photoreduction of the dye stabilizing the reduced dye (Fig. 1) and, thus, slow down charge recombination processes between sensitizer and semiconductor. Additionally, the neighboured counter charges should accelerate the electron transfer from the dye to the redox mediator. If the transferred electron occupies an antibonding d-orbital of the transition metal complex, the link between redox mediator and the coordinated dye can be broken facilitating the regeneration of the dye.

Complexes based on Co, Ni and Cu where selected for computational screening. In all cases a significantly weakened bond between the transition metal and the dye was observed after reduction. Furthermore, the investigated Cu complexes showed the preferred push-pull MO structure where the highest occupied molecular orbital resides close to the semiconductor while the lowest unoccupied orbitals are located at the linked redox mediator. Unfortunately, a working device was obtained only for the Co complexes. In case of the investigated Ni and Cu complexes, a reduction to immobile Ni(0) and Cu(0) could not be excluded additionally to an overall low stability of the transition metal complexes visible by the high air sensitivity of the synthesized Ni complexes. A quenching of the excited state could be observed for the Co complexes inhibiting a fast electron transfer from the dye to the redox mediator.

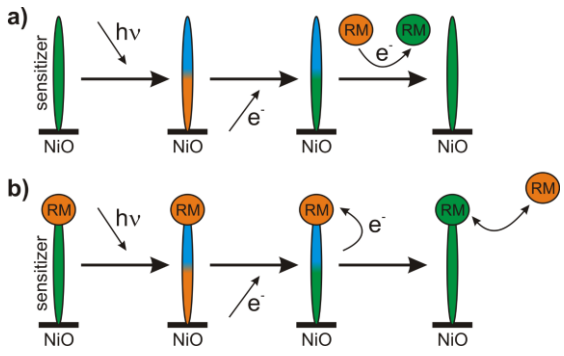

Figure 1: Schematic illustration to highlight the advantages of temporary docking of the redox mediator (RM) at the sensitizer. a): Mode of action used so far. b): Investigated concept of temporary docking of the RM at the dye. Green illustrates uncharged components while blue/red illustrates regions of negative/positive charge.

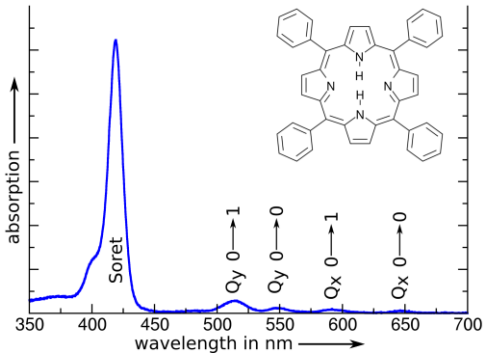

Figure 2: Typical absorption spectra of Tetraphenylporphyrin showing the characteristic Soret and Q-bands.

Additionally, solar cells based on surface-mounted metal organic frameworks (SURMOF) were screened by computational approaches for which porphyrins are among the most promising molecular compounds [2]. However, Q-bands of porphyrins possess an overall low extinction coefficient, see Fig. 2. Computational screening showed that a modification of attached phenyl groups in meso position hardly affects light absorbing properties as long as strong nonplanar deformations are not induced by additional substituents. The latter as well as increasing or decreasing the conjugated π-system resulted in a red shift and an increased extinction coefficient of the modified porphyrins. Additional effects within the crystal structure were identified by computational screening in the Heine group.

Literature

[1] S. Merker, H. Krautscheid, S. Zahn, J. Mol. Model. 24 (2018) 317
[2] R. Haldar, K. Batra, S.M. Marschner, A.B. Kuc, S. Zahn, R.A. Fischer, S. Bräse, T. Heine, C. Wöll, Chem. Eur. J. 25 (2019) 7847

Near-Infrared Hyperspectral Imaging for Monitoring the Thickness Distribution of Thin PEDOT:PSS Layers

O. Daikos, M. Naumann, C. Bundesmann, U. Helmstedt, T. Scherzer

PEDOT:PSS consisting of poly(3,4-ethylenedioxythiophene) (PEDOT) and polystyrene sulfonate (PSS) is a well-known conductive polymer with excellent transparency, high conductivity and high chemical stability. This macromolecular polyelectrolyte complex forms stable aqueous suspensions, which can be applied by a wide range of processing methods such as spin coating, gravure printing, ink jetting, slot-die coating or with a doctor blade. The latter techniques allow continuous roll-to-roll application to flexible substrates such as polymer films.

Layers used as transparent electrode materials should be as thin and as homogeneous as possible. For an effective control of the applied thickness, continuous monitoring of the properties of the deposited layers is inevitable. White-light interferometry allows measurements with very high precision but is of limited suitability for space-resolved investigations, especially if large areas have to be scanned. In this study, NIR hyperspectral imaging was shown to be a powerful method for such investigations in spite of the very low thickness of conductive polymer layers (~50 to 350 nm).

The prediction of quantitative thickness data from NIR reflection spectra was based on chemometric models using the partial least squares (PLS) algorithm. Calibration was carried out by means of spin-coated layers of PEDOT:PSS, whose thickness was determined by white-light interferometry and stylus profilometry. Finally, this resulted in calibration models with root mean square errors of prediction (RMSEP) of less than 10 nm. These models were used for quantitative imaging of the thickness distribution in PEDOT:PSS layers on glass discs (Figure 1). Results reveal the typical inhomogeneities of spin-coated layers such as the hump in the center and the ridge at the edge. The precision of the predicted values was confirmed by comparison with data from various reference methods.

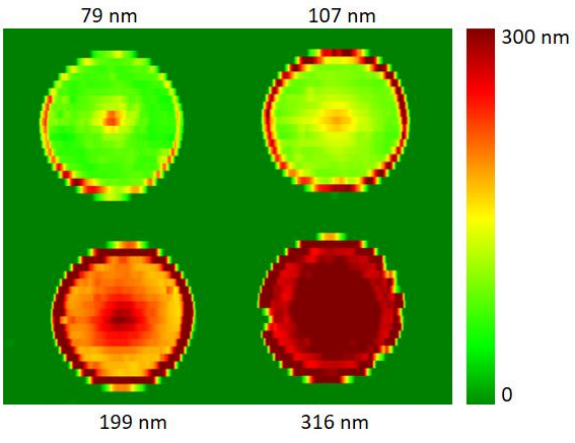

Figure 1: Hyperspectral images of spin-coated PEDOT:PSS layers on glass. The thickness distribution was predicted from NIR spectra using a PLS calibration model.

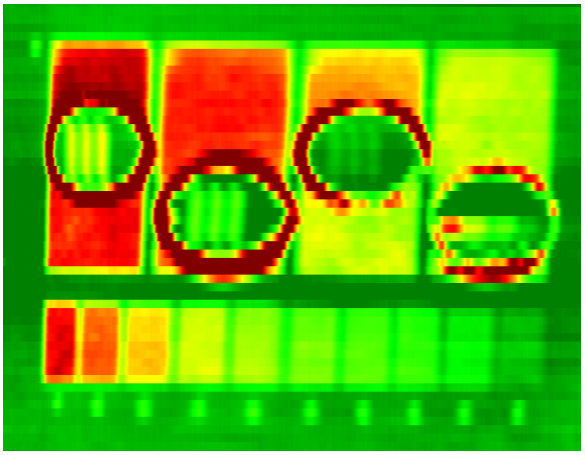

Figure 2: Hyperspectral image of a test pattern of PEDOT:PSS printed on transparent PET film.

Moreover, it was shown that this approach can be also used for hyperspectral imaging of the thickness of thin gravure printed layers and structures of PEDOT:PSS on polymer films with excellent thickness resolution. Figure 2 shows the hyperspectral image of a test pattern printed on polyester film. It is obvious that even the thinnest layers (right boxes in the lower line) as well as labels can be clearly detected by this method. Reproduction is only limited by the *spatial* resolution of the hyperspectral camera (2.6 mm/track).

This analytical approach opens new possibilities for in-line process control by large-scale monitoring of thickness and homogeneity of ultrathin layers of conductive polymers and other systems [1,2].

Literature

[1] G. Mirschel, U. Helmstedt, T. Scherzer, U. Decker, L. Prager, Ind. Eng. Chem. Res. 53 (2014) 16813-16819
[2] G. Mirschel, O. Daikos, T. Scherzer, Progr. Org. Coat. 132 (2019) 116-124

Surface Modification of Gas Barrier Films for Direct and Dry Graphene Transfer – A Way to Transparent Flexible and Conductive Encapsulation Foils

P. With, J. Lehnert, R. Heller, L. Prager, U. Helmstedt

Wider adoption of flexible (organic) electronic devices e.g. in solar energy harvesting, smart packaging or displays, is limited by short device lifetimes due to degradation by atmospheric gases. Transparent conductive encapsulation foils are therefore of high interest providing high flexibility, transparency, electrode stability and elasticity. Carbon-based electrode materials such as graphene and carbon nanowires are promising materials for conductive thin films since they are highly flexible (bendable and stretchable), transparent, highly abundant and show excellent electrode stability. It is though challenging to adjust the surface and interface properties of the target substrate so that surface energy and roughness ensure sufficient electrode adhesion throughout subsequent processing steps. Furthermore, electrode deposition onto gas barrier films should be carried out in a dry processing step in order to prevent degradation of encapsulated sensitive electronic components by outgassing water. Several dry graphene transfer methods have been reported in the literature [1]. For most of them high temperatures (>80 °C) are necessary, which is not compatible with state of the art low-cost PET-based gas barrier films. Others involve an additional polymer substrate/thermal release tape for the final graphene transfer, increasing the number of processing steps. We present the direct and dry transfer of graphene grown on copper surfaces to gas barrier films at temperatures below 80 °C.

Sufficient graphene adhesion on the target substrate has to be ensured for realization of a large-area transfer process [2], which requires adaptation of the surface energy and a compensation of roughness differences between the respective films. We have thus performed a systematic study in order to evaluate the impact of surface energy and glass transition temperature (T_g) for different types of coatings on SiO_x/PET gas barrier films, the latter being prepared by a photochemical roll-to-roll process developed at IOM [3]. The study was performed with alkylsilazanes, alkylsiloxanes and acrylate systems with varying side chains. In particular, soft acrylate-based coatings with low T_g showed high adhesion to graphene areas of several centimetres in size. Further advantages regarding processing of these acrylate-based coatings are their high chemical stability and

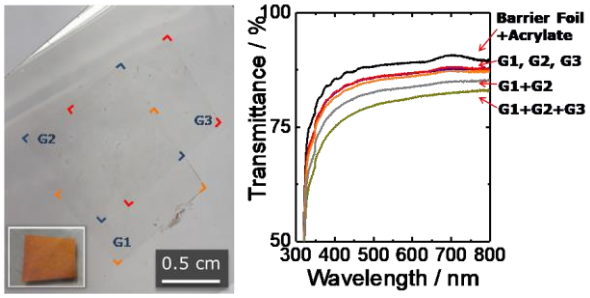

Figure 1: Photo of three overlapping graphene layers (G1, G2, G3) successively transferred to a gas barrier film (left), recovered copper foil after peeling off graphene; (left, inset) and UV/VIS transmittance at different positions of the overlapping graphene layers (right).

that they can be photochemically cured at ambient conditions and on various organic and inorganic substrates (e.g. polyesters, glass).

We were able to successfully carry out a simple and fast (<10 s) lamination process of graphene on pre-oxidized copper films [4] onto soft acrylate surface modified barrier films at temperatures of 20 to 60 °C (Fig. 1, left). The copper substrate could then simply be peeled off and is available for further graphene growth (Fig. 1, left, inset). A cost-intensive and wet chemical dissolution of copper can be omitted. The presence of graphene on barrier films was confirmed by RAMAN spectroscopy and the loss in transmission (at λ= 550 nm) corresponds to the theoretically expected value of 2.4% per monolayer graphene (Fig. 1, right).

With the method presented, not only larger pieces of graphene in the cm range can be transferred, but graphene layers can also be stacked on top of each other (patchwork approach), which increases area coverage and enables the introduction of dopants between individual graphene layers in order to produce transparent and flexible high-performance electrodes [5].

Literature

[1] J. Kang, D. Shin, S. Bae, B.H. Hong, Nanoscale 4 (2012) 5527
[2] Martins et al., PNAS 110 (2013) 17762
[3] L. Prager et al., Thin Solid Films 570 (2014) 87
[4] P.R. Whelan et al., Carbon 117 (2017) 75
[5] US 201801423

Tailor-made Drug Delivery Systems for Medical Application by Electron Beam Polymerization

S. Glaß, B. Abel, A.Schulze

Hydrogels are three-dimensional polymeric networks synthesized from highly hydrophilic monomers. They are used as drug delivery systems in medical applications. Nowadays, they are commonly synthesized by UV curing using organic photoinitiators. However, organic photoinitiators are often cytotoxic and not suitable for medical applications. Therefore, new synthesis strategies using non-cytotoxic TiO_2 as photoinitiator [1] and an initiator-free method - electron beam polymerization [2] - were developed.

Electron beam polymerization enables to manipulate the crosslinking density of the hydrogels. Since the crosslinking density is crucial for the drug delivery (see Figure 1), the velocity and amount of the released substance can be adjusted. Highly crosslinked hydrogels released the drugs slowly, while hydrogels with low crosslinking densities set it free fast. This enables a defined application of hydrogels for specific medical problems and therefore, an individualized therapy will be possible.

The so-prepared hydrogels were loaded with various photoactive drugs, so called photosensitizers [3]. Selected examples for photosensitizer-loaded hydrogels are displayed in Figure 2. The photosensitizers generate antimicrobial singlet oxygen upon irradiation with light. Thus, the application of photosensitizers is a promising therapy for infections with antibiotic-resistant bacteria. Therefore, the here-described hydrogels can be applied on infected wounds, especially on those infected with (multi-)resistant bacteria.

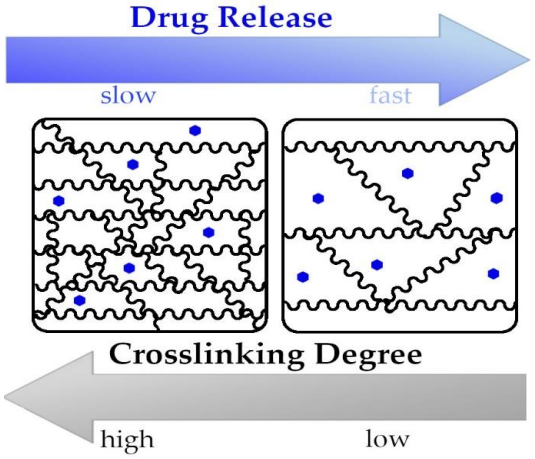

Figure 1: Specialized drug release was achieved varying the crosslinking density of the hydrogel.

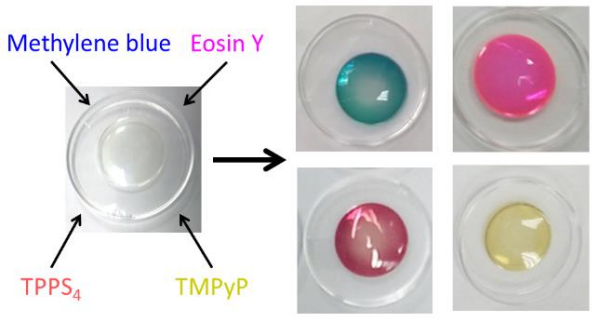

Figure 2: Examples of hydrogels loaded with different photosensitizers.

Additionally, an irreversible immobilization of the photoactive drugs was achieved by electron beam irradiation. Irreversible immobilization of photoactive substances and drugs is not possible using UV polymerization. Therefore, the electron beam technology enables further applications of photosensitizers in hydrogels, such as antimicrobial or antifouling surfaces e.g. for food packaging.

To determine the performance of the photosensitizer-loaded hydrogels a singlet oxygen test was designed. The photosensitizers were highly active after release from the hydrogels. Thus, they generated a sufficient amount of singlet oxygen for the treatment of bacteria. Interestingly, the method can be used for further photoactive polymer systems like membranes.

In conclusion, electron-beam irradiation was demonstrated to be a powerful tool to control the properties of biomaterials such as hydrogels. The photosensitizer-loaded hydrogels can be applied in infections with (multi-)resistant bacteria.

Literature

[1] Glass, S.; Trinklein, B.; Abel, B.; Schulze, A. Front. Chem. 6 (2018) 340
[2] Glass, S.; Kühnert, M.; Abel, B.; Schulze, A., Polymers 11 (2019) 50
[3] Glass, S.; Rüdiger, T.; Griebel, J.; Abel, B.; Schulze, A. RSC Adv. 8 (2018) 41624–4

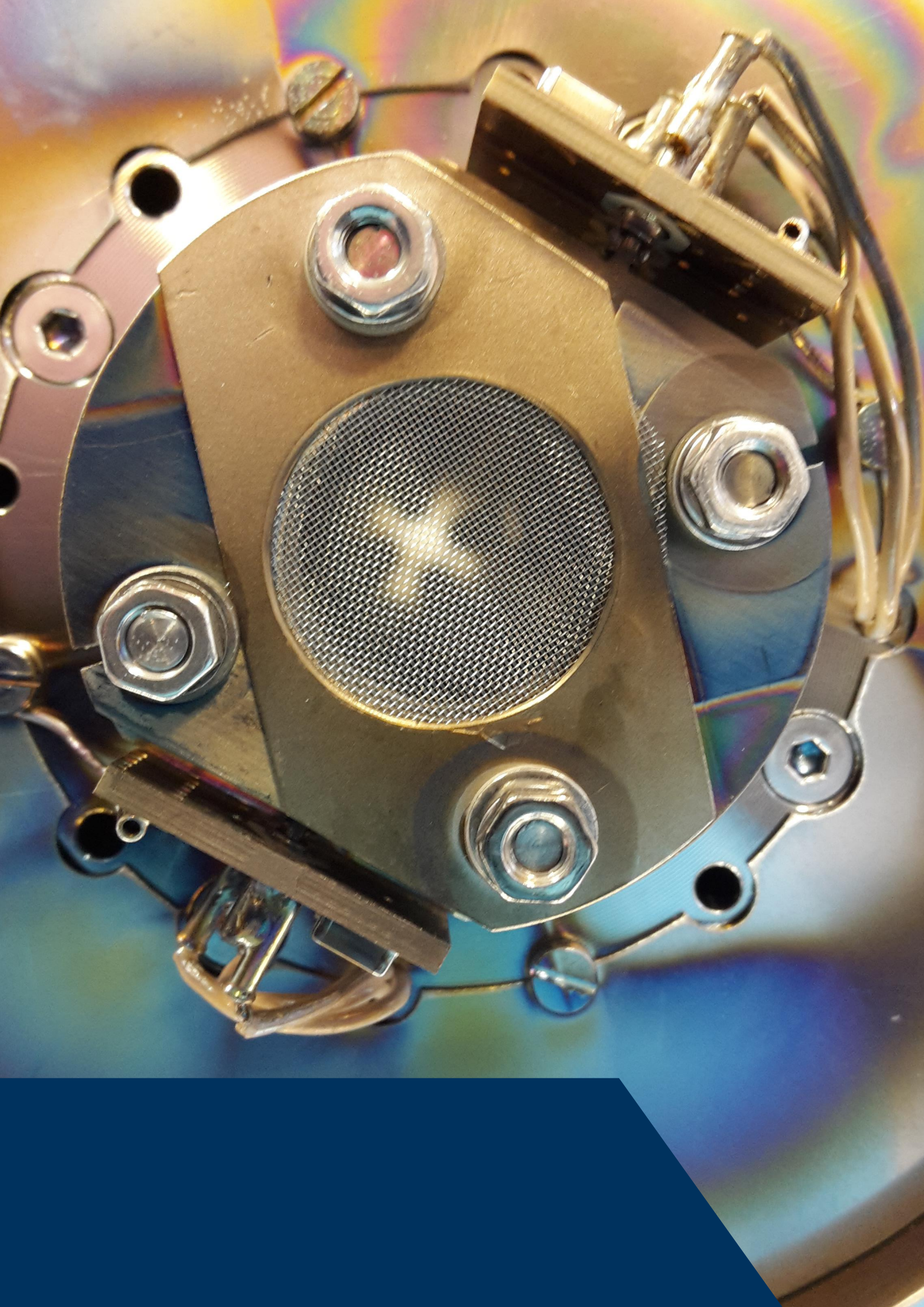

Equipment for Research and Application

APPLICATION CENTER OF THE IOM

MISSION

The Application Center of the IOM is a technology platform for the efficient and sustainable transfer of IOM research results to industrial partners. Radiationbased high technologies, new process technologies, and products can be developed at the IOM for industry under industry-relevant conditions. The aim is to transfer technological developments from pilot scale to scale up, especially in the fields of optical and chemical industry, semiconductor technology, mechanical engineering and medical technology.

TASKS

- Provision of research and development services in the form of contract research
- Cooperative research together with users
- Pilot plants, sampling and small series production

FACILITIES

REACTIVE ION BEAM ETCHING (RIBE)

Reactive ion beam etching (RIBE) is a sophisticated technology enabling the fabrication of e.g. optical elements with sub-atomic precision. Within the extended research infrastructure a new state-of-the-art RIBE facility was established. An integrated 5 axes-motion system enables now uniform etching of large workpieces with diameters up to 450 mm and a maximum weight of 50 kg. The RIBE system is equipped with a Kaufman-type ion source, configured for Fluorine-containing etching gases, and can be upgraded with different optical and masspectroscopic in-situ measurement technologies which guarantee high process stability and reliability. With the RIBE 450 etching plant, newly developed IOM etching processes for ultraprecise and innovative structured functional surfaces can be further scaled up to industrially relevant sizes.

Expertise

- Ion beam driven self-organization
- RIBE for pattern transfer
- IBE/RIBE on large surfaces
- Ion beam assisted surface smoothing

PLASMA JET PROCESS FOR ULTRA-PRECISION SURFACE TREATMENT

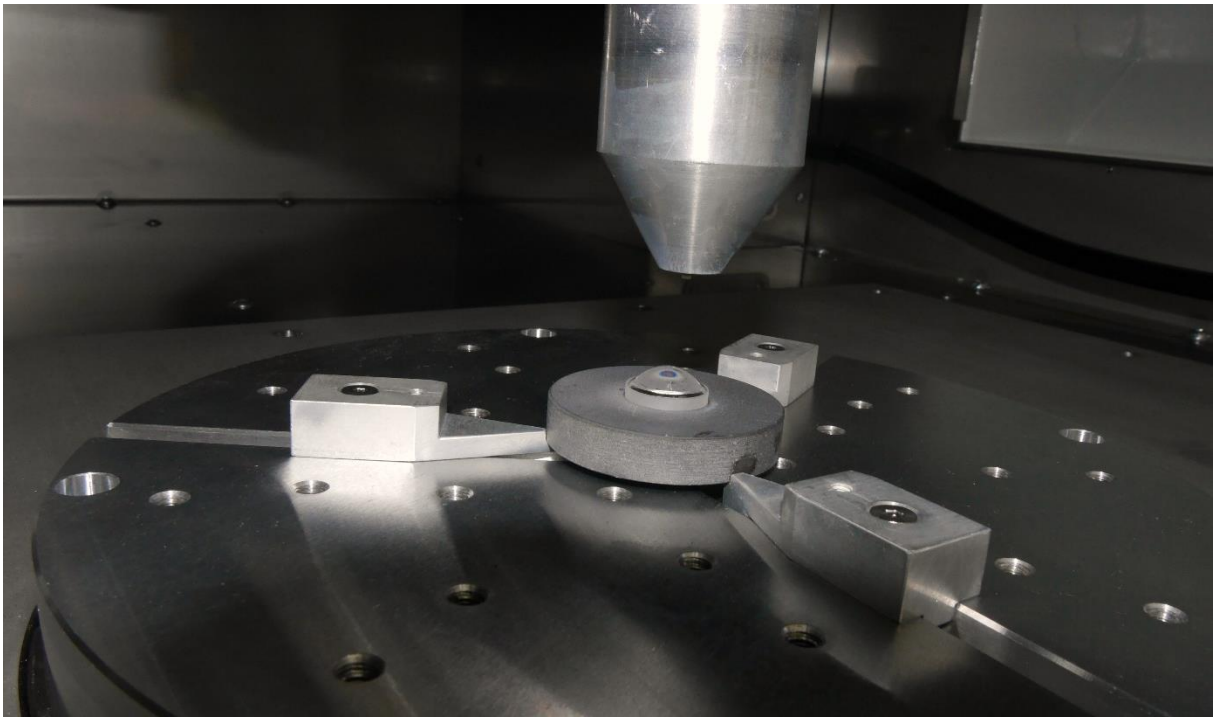

Plasma jet-based processing chains for the manufacturing of optical freeform surfaces of fused silica are comprised of several machining steps including plasma jet polishing. The main advantage of the plasma jet polishing process is its action independent of surface curvature. Hence, shape-preserving smoothing is achieved even on surfaces with variable surface curvatures like aspheres or freeforms. The new plasma jet polishing machine is based on a 4-axes CNC platform equipped with a specially designed microwave-driven inert plasma jet source. The machine allows to treat fused silica surfaces with lateral dimensions up to 250 mm in diameter obtaining micro-roughness values of less than 0.3 nm RMS.

Expertise

- Plasma jet machining of surfaces
- Plasma assisted polishing of surfaces
- Ion beam figuring
- Reactive plasma jet sources

ELECTRON BEAM BASED MEMBRANE MODIFICATION IN ROLL-TO-ROLL PROCESS

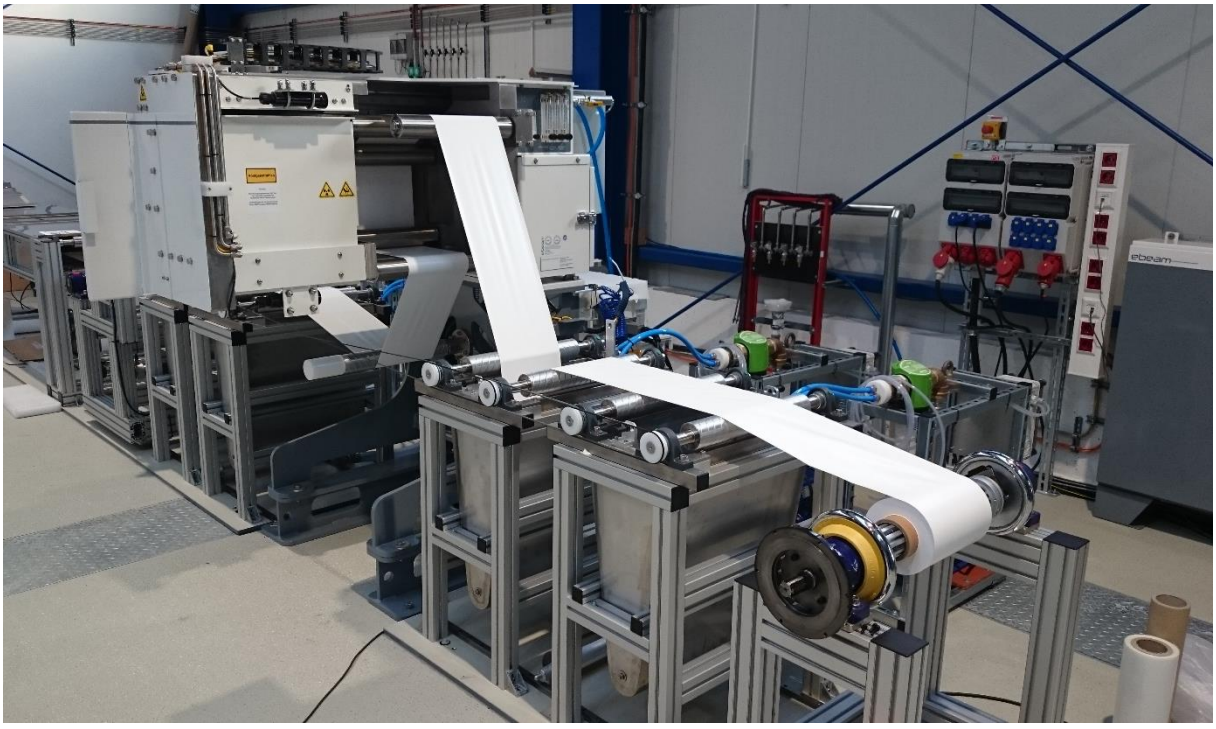

Porous polymer membranes are of increasing importance regarding modern separation technologies such as waste water treatment, sterilization filtration, hemodialysis, dairy industry, etc. To comply with required process conditions these polymer membranes are predominantly fabricated from synthetic hydrophobic polymers. However, these materials are prone to fouling. Electron beam technology can be efficiently used for the hydrophilization of polymer membranes by directed grafting of hydrophilic small molecules/polymers to the membrane surface. This new machine (80 – 200 keV) enables an upscaling (roll-to-roll) of our method using hollow fibres or flat sheet membranes with individual pre- and post-treatment.

Expertise

- Electron beam modification of polymer membranes
- Photocatalytically active membrane surfaces
- Bioactive membrane surfaces

PILOT-SCALE COATING MACHINE FOR FLEXIBLE GAS BARRIER FILMS IN ROLL-TO-ROLL PROCESS

Development of cost-efficient flexible gas-barrier films for encapsulation of sensitive thin-film photovoltaics is currently a challenge facing industry when aiming on higher quota of renewable energy production. Recently, a photochemical process working at normal pressure and low temperature has been developed at IOM. The process involves UV-initiated conversion of a thin polysilazane layer into silica. A pilot-scale coating machine has been designed and constructed with the aim to further develop gas-barrier films and their production technology. The machine enables scale-up to wider substrates, demonstrations in true technical scale, and resilient economical evaluation of the production process.

Expertise

- Low-temperature processes for preparation of metal oxide thin films
- Silicon oxide thin films for flexible transparent high gas permeation barrier
- Lamination of single laye films (up to 500 mm web width)

The research facilities were financial supported by the German Federal Ministry of Education and Research, the Ministry of Science and Art of the Free State of Saxony and the European Union.

Gefördert durch
STAATSMINISTERIUM FÜR WISSENSCHAFT UND KUNST
Freistaat SACHSEN

European Union

Europe funds Saxony.
EFRE
European Regional Development Fund

GEFÖRDERT VOM
Bundesministerium für Bildung und Forschung

HERTZ ELECTRON BEAM LABORATORY

MISSION

The Hertz electron beam laboratory houses a 10 MeV electron accelerator for material modification as well as time-resolved basic investigations on the kinetics and dynamics of reactive processes. This enables the production of new materials for a wide variety of high-tech applications in close proximity to industry. This unique accelerator infrastructure is used for research and development in the field of material sciences, in joint projects with external university and non-university cooperation partners as well as industry.

EQUIPMENT

The accelerator at the IOM is based on a technological platform providing computer-controlled stable average beam currents up to 1 mA (10 kW beam power) for material modification. The high energy of

10 MeV allows synthesis and modification of 3D-samples up to a thickness of 5 cm (single-sided irradiation). Scanning and transport system provide homogeneous irradiation up to sample sizes of 0.6 m × 2 m. A modification of the accelerator for short (15 ns) single pulses of high pulse current (1A) allows state-of-the-art time-resolved spectroscopy (pulse radiolysis) of electron-induced primary processes for basic research in radiation chemistry.

Expertise

- Curing of polymers (thin films and bulk)
- Cross-linking (PE, hydrogels, cryogels …)
- Material modification (e.g. diamonds, semiconductors)
- Cryo-irradiation (> 77K)
- Sterilisation
- Radiation and radical chemistry
- Analytics during irradiation
- Single pulse and pulse train investigations
- Timescales: ns up to min

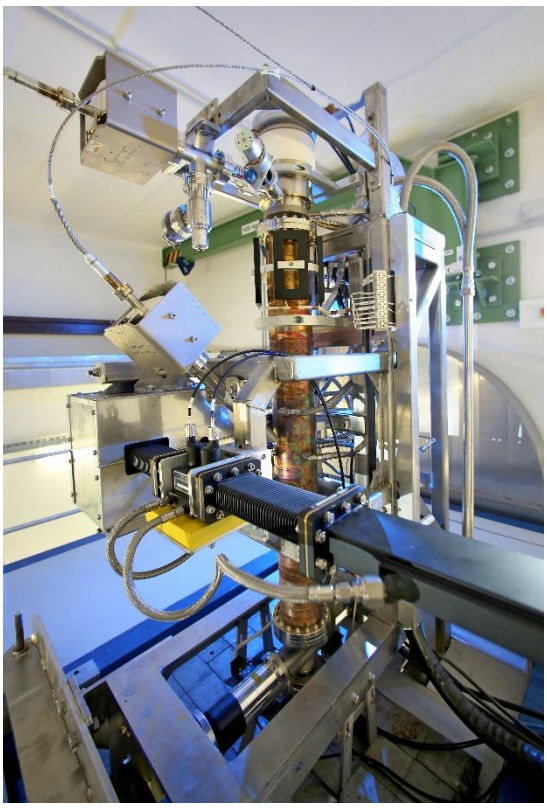

Gefördert durch
STAATSMINISTERIUM FÜR WISSENSCHAFT UND KUNST
Freistaat SACHSEN

GEFÖRDERT VOM
Bundesministerium für Bildung und Forschung

LASER LABORATORY

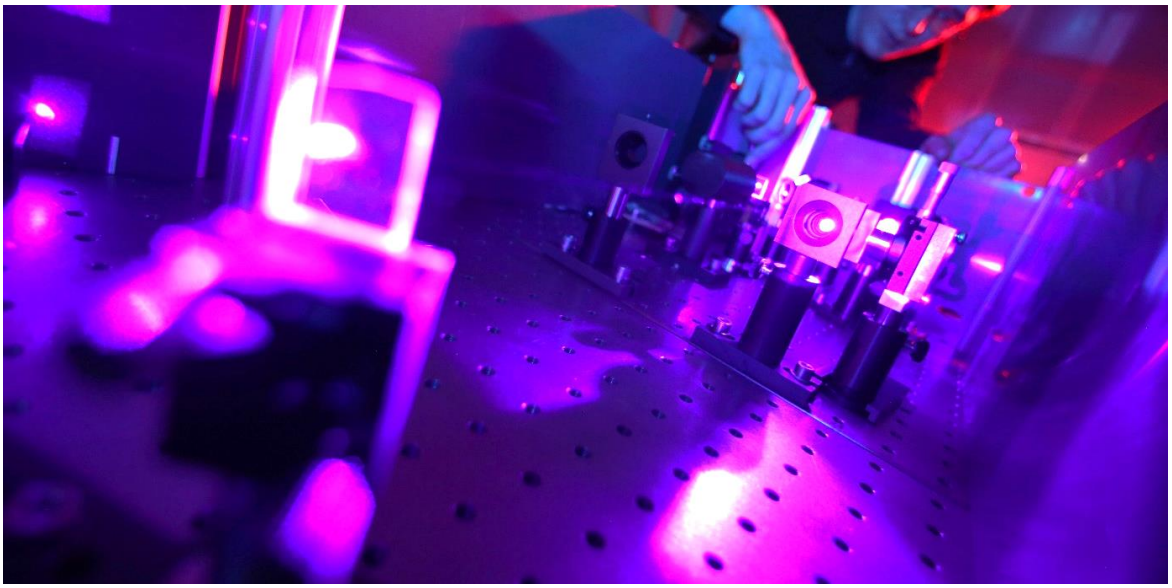

MISSION

Lasers are a versatile tool for materials processing that integrate well into production processes enabling a large variety of patterning, modification or deposition processes.
The IOM laser machining (LAMA) group aims to the development of laser micro processing techniques for high quality, high precision and low damage laser processing of materials.
The application-related research bases on the understanding of basic principles of laser material processes, the versatile control of the laser beam and the tuning of the laser machining processes to the particular needs of the application. Application-related work is performed in close cooperation with different industrial partners.

Special attention is paid to:

- Texturing of plane and cylindrical surfaces
- Scribing of thin films for electronic devices, e.g. photovoltaics
- Machining of transparent materials for optical applications
- Surface functionalization for wetting, diffraction or mechanical applications

EQUIPMENT

The IOM's Laser laboratories are equipped with standard industrial laser sources for materials processing that are integrated into workstations for the full control of the laser machining process. IOM completed these workstations with equipment for material processing at specific conditions or with in process analysis options.

- Modern workstations with pulsed lasers with wavelengths from UV 193 nm to NIR 1,55 µm and ns, ps and fs pulse length
- Modules for cylinder machining with ps laser
- Off and in process measurement subsystems for process control and optimization

Expertise

- Qualifying laser machining processes (laser ablation, etching, and surface modification) on state-of-the-art laser workstations including advanced analytics
- Developing and qualifying laser micro processing techniques for high quality, high precision and low damage machining
- Developing, optimizing and implementing application-specific machining processes including the processing strategy
- Application of beam shaping techniques for high speed and/or high quality machining
- Hybrid processing: combining of laser processing with other beam-based or standard processing technologies
- Adapting of laser processing to existing process chains

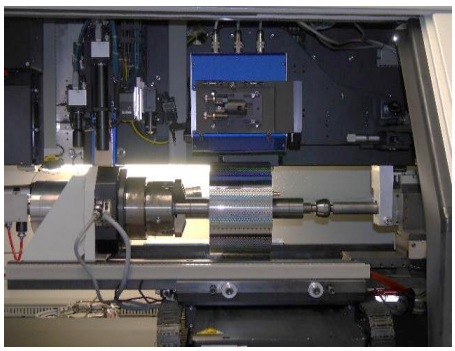

FURTHER EQUIPMENT

HIGH CURRENT ION IMPLANTER

Ion implantation beyond doping concentration for adjustment of structural, mechanical, electronic or optical properties necessitates high ion currents which became only recently technically feasible.

The low energy high current ion implanter provides ion energies between 5 and 200 keV with a beam current of up to 1 mA. A standard hot filament ion source allows the use of a variety of ions from gaseous precursors while an additional evaporator enlarges the accessible range of elements which can be implanted using solid precursors. Mass separation permits the direct implantation of the required ion species without contaminations. Using the available cold and hot stages, ion implantation temperatures between – 150 and + 600 °C are possible. The accessible substrate size is up to 3 inch.

SYSTEM FOR DETERMINISTIC SINGLE ION IMPLANTATION

Deterministic ion implantation, i.e. the implantation of a pre-defined, counted number of single ions with a lateral accuracy of a few nanometers, is a promising technique to realize a functionalization of single atoms in a solid state material. In the framework of a mutual project, the Leibniz Joint-Lab “Single Ion Implantation” of the IOM and the Applied Quantum Systems Department of Leipzig University was equipped with an advanced high resolution focused ion beam system containing a high precision laser interferometer stage for accurate and reproducible sample positioning. This development system has been equipped with an electron beam ion source and will be extended with a sophisticated single ion detector in order to fabricate quantum devices or sensors based on functionalized single atoms.

MODULAR RESEARCH PLATFORM FOR PLASMA-BASED THIN FILM DEPOSITION TECHNIQUES

IOM provides a new and unique tool to modify surfaces and synthesize new functional materials and thin films by applying different physical and chemical non-equilibrium processes. The platform is flexible and modular in design in order to be applicable to different material systems in the long term and to be able to react to research needs that emerge through new developments in fundamentals and applications. First tests with the platform will be carried out on material systems from the fields of switchable layers at low temperatures (controllable surface physics) and energy conversion and storage (electrochemically active surfaces).

UNIVERSAL DIAGNOSTIC PLATFORM FOR REACTIVE ION BEAM PROCESSES

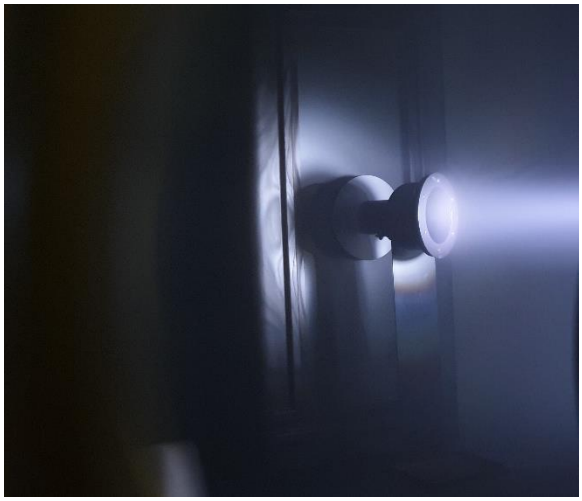

Ion beam-based ablation processes for shaping, structuring and smoothing surfaces are now established key technologies, e.g. in high-end optics manufacturing. The basic prerequisite for this high-tech sector is to meet the constantly increasing accuracy requirements (shape accuracy, roughness, process stability and control). Of central importance are highly developed and process-adapted reactive gas-suitable ion sources, which must meet certain requirements regarding stability, process-adapted beam composition, maintenance times, etc. Due to the necessity of the application, the development and optimization of process-adapted broad beam ion sources will be intensified in the future.

The research facilities were financial supported by the Ministry of Science and Art of the Free State of Saxony and the European Union.

Gefördert durch
STAATSMINISTERIUM FÜR WISSENSCHAFT UND KUNST
Freistaat SACHSEN
European Union
Europe funds Saxony.
EFRE
European Regional Development Fund

MATERIAL CHARACTERIZATION AND ANALYTICS

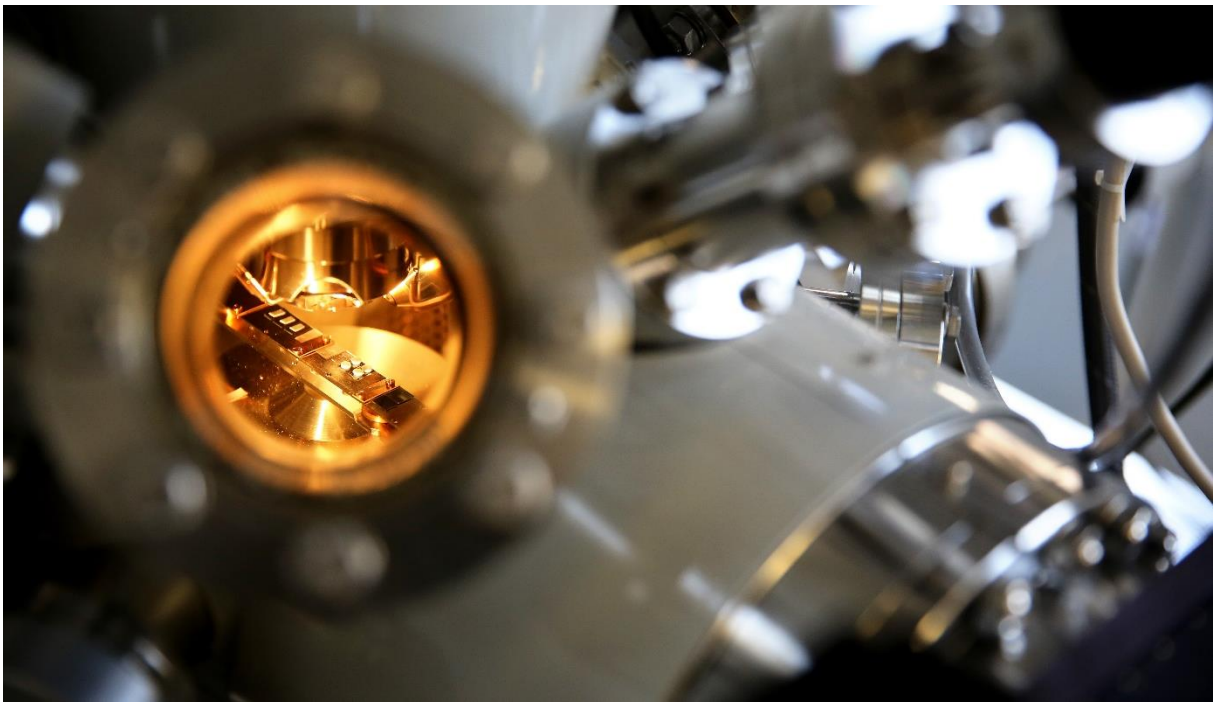

MISSION

The experimental infrastructure comprises a broad portfolio of instrumental methods to allow a comprehensive physical and chemical characterization of materials. A main focus is set to surface-related analytical techniques. Therefor imaging methods show a huge versatility together with a high performance. Several additional techniques are available for the determination of the elemental and the chemical composition, the analysis of molecular, crystalline, and phase conditions as well as to characterize functional properties of materials.

Expertise

- Surface analysis: microscopy, topography, wetting
- Material characterization: material composition, phase and thermal analysis
- Molecular structure: structure determination, substance separation, mass spectrometry
- Analysis of crystalline solids: crystalline structure, phase distribution, real structure
- Functional material properties: viscoelastic properties, thin film characterization

LEIPZIGER nanoANALYTIKUM (LenA)

Nanoscale analysis of artificially produced materials is an important prerequisite for understanding the relationship between material structure and material properties. The design of materials with desired functionalities can only be achieved through precise knowledge of their real structure. The research area of LenA focuses on the structural and chemical analysis of thin films, interfaces and nanostructures using advanced methods of transmission electron microscopy (TEM).

Expertise

- TEM: Probe Cs-corrected Titan³ G2 60-300 S/TEM (FEI) equipped with a X-FEG shottky emitter, Super-X EDX-detector and GIF Quantum imaging energy filter systems as well as with specimen holders for *in situ* TEM biasing and heating
- TEM specimen preparation: Focused ion beam (FIB) milling (Zeiss Auriga FIB-SEM crossbeam system, Fishione NanoMill system)
- Additional equipment: Environmental scanning electron microscope (FEI ESEM Quanta 250)

Gefördert durch
STAATSMINISTERIUM FÜR WISSENSCHAFT UND KUNST | Freistaat SACHSEN
European Union
Europe funds Saxony.
EFRE
European Regional Development Fund

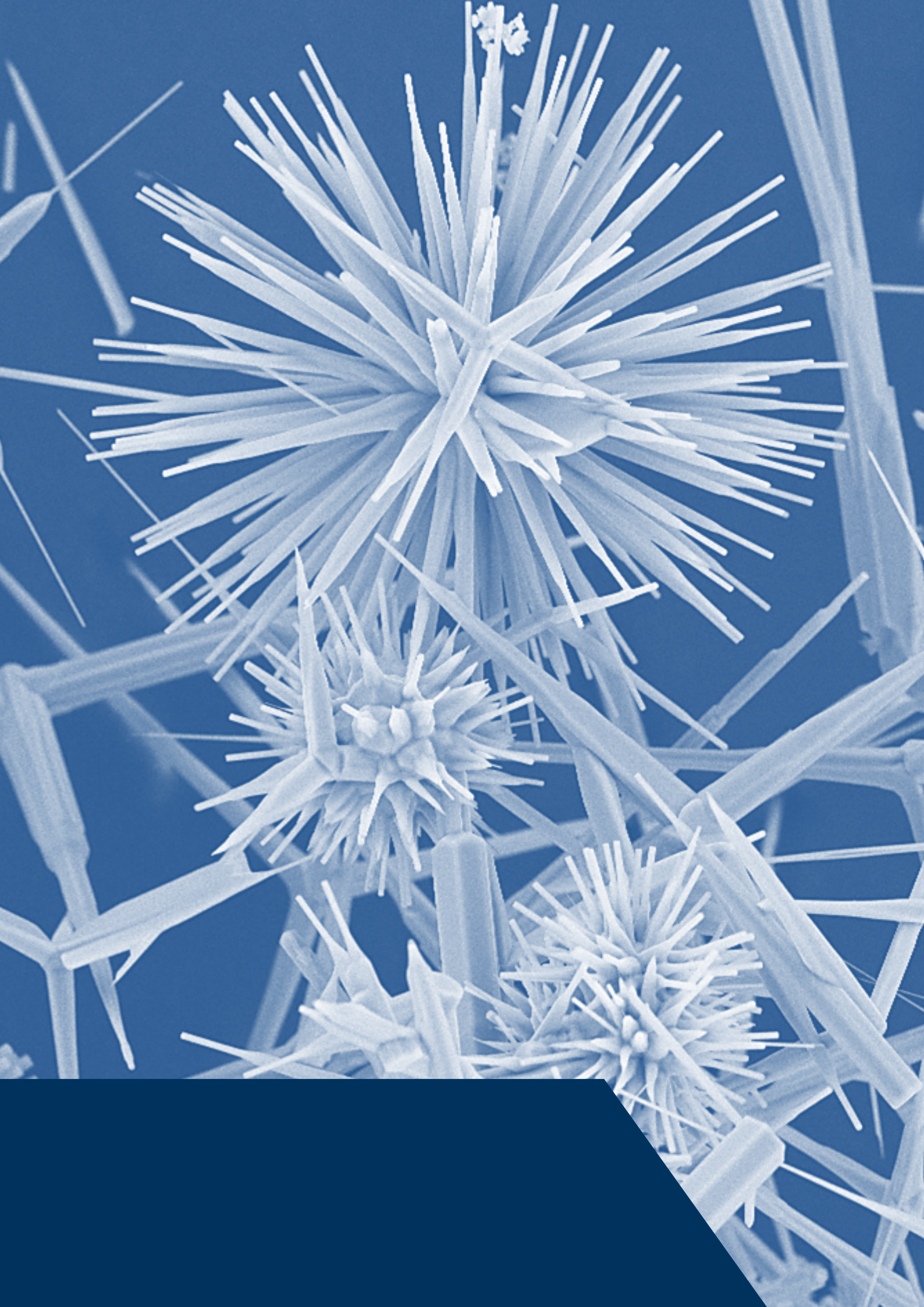

Personnel Activities

Graduation

Committee Work

Honors

Habilitations

2019

Kahnt, Axel, Dr.
Time resolved investigations on nanomaterials
Friedrich-Alexander-Universität Erlangen-Nürnberg (FAU), Naturwissenschaftliche Fakultät, 2019

Doctoral Theses

2018

Hilmi, Isom
Epitaxial chalcogenide Ge-Sb-Te thin films and superlattices by pulsed laser deposition
Universität Leipzig, Fakultät für Physik und Geowissenschaften, 2018

Hintzen, Daniel
Erythrosin B als Sonde für Wasserstoffbrückenbindungen in verschiedenen molekularen Umgebungen
Universität Leipzig, Fakultät für Chemie und Mineralogie, 2018

Lautenschläger, Thomas
Systematic investigation of the ion beam sputter deposition of TiO_2
Universität Leipzig, Fakultät für Physik und Geowissenschaften, 2018

Lohmann-Richters, Felix
Fundamentals and applications of advanced solid acid fuel cell electrodes
Universität Leipzig, Fakultät für Chemie und Mineralogie, 2018

2019

Bandak, Juhaina
Amyloid fibril-based hybrid materials: characterization and application
Universität Leipzig, Fakultät für Chemie und Mineralogie, 2019

Glaß, Sarah
Characterization and application of hydrogels containing photoactive molecules
Universität Leipzig, Fakultät für Chemie und Mineralogie, 2019

Grüner, Christoph
Oblique angle deposition of thin films – theory, modelling, and application
Universität Leipzig, Fakultät für Physik und Geowissenschaften, 2019

Laube, Christian
Surface modification and electron irradiation treatment of nanodiamonds
Universität Leipzig, Fakultät für Chemie und Mineralogie, 2019

Lehnert, Jan
Synthesis of graphene using carbon ion implantation in copper
Universität Leipzig, Fakultät für Physik und Geowissenschaften, 2019

Liedtke-Grüner, Susann
Growth of obliquely deposited metallic thin films
Universität Leipzig, Fakultät für Physik und Geowissenschaften, 2019

Niefind, Falk
Nanoscale morphology of semiconducting polymer films by photoemission electron microscopy
Universität Leipzig, Fakultät für Chemie und Mineralogie, 2019

Riedel, Stefanie
High-energy electron-treatment of collagen and gelatin hydrogels: Biomimetic materials, stimuli-responsive systems and funktional surfaces
Universität Leipzig, Fakultät für Physik und Geowissenschaften, 2019

Schumacher, Philipp
Realization of ion mass and energy selected hyperthermal ion-beam assisted deposition of thin epitaxial nitride films: Characterization and application
Universität Leipzig, Fakultät für Physik und Geowissenschaften, 2019

Diploma and Master Theses

2018

Abadie, Jean-Baptiste
Untersuchung zur Plasmajet-gestützten Politur von Quarzglas- und N-BK7-Substraten
TU Dresden, Fakultät Maschinenwesen, 2018

Jacobs, Paul-Philipp
Untersuchung der Glanzwinkeldeposition von Nickel-Eisen-Nanostrukturen
Westsächsische Hochschule Zwickau, Fakultät für Physikalische Technik/ Informatik, 2018

Lorenz, Oliver
Aktivierung von Platindünnfilmelektroden von Festsäurebrennstoffzellen durch in situ Cyclovoltammetrie
Universität Leipzig, Fakultät für Chemie und Mineralogie, 2018

Petzold, Johannes
Peptide fibrils on surfaces - templates for metallic nanowires, networks, and high surface area electrode materials
Universität Leipzig, Fakultät für Chemie und Mineralogie, 2018

Sarveson, Nilushiya
Investigations of amyloid fibrillation kinetics of alanine scan mutants of N-terminal modified NNFGAIL and the influence of AuNPs in the fibrillation process
Universität Leipzig, Fakultät für Chemie und Mineralogie, 2018

Schemel, Christian
Lasermikrostrukturierung polymerer Nanokomposite
Universität Leipzig, Fakultät für Chemie und Mineralogie, 2018

Surjuse, Swati
Towards epitaxial Al_2O_3 (0001)/ Cu (111) template development for ion implantation assisted graphene growth
TU Chemnitz, Fakultät für Elektrotechnik und Informationstechnik, 2018

Tadsen, Meike
Micropatterning of high energy crosslink gelatin hydrogels
Universität Leipzig, Fakultät für Physik und Geowissenschaften, 2018

Tema, Tshepiso Lawrence
One step synthesis of silver nanoparticle-filled acrylate coatings for UV-laser-microstructuring
Universität Leipzig, Fakultät für Chemie und Mineralogie, 2018

Ullmann, Jason
Untersuchungen zur strahlenchemischen Immobilisierung bio- und photokatalytisch aktiver Nanokomposite auf Polyvinylidenfluorid-Membranen
Universität Leipzig, Fakultät für Chemie und Mineralogie, 2018

2019

Abel, Tobias
TEM investigation to optimize optical switching of epitaxial $Ge_2Sb_2Te_2$ thin films
Universität Leipzig, Fakultät für Physik und Geowissentschaften, 2019

Bernstein, Jacques
Schichtabscheidung von SiO_2-Dünnschichten mit reaktiven Ionenstrahlen
Universität Leipzig, Fakultät für Physik und Geowissentschaften, 2019

Dietrich, Johannes
Simulation of contact-resonance atomic force microscopy with the finite element method and comparison with experiments
Universität Leipzig, Fakultät für Physik und Geowissentschaften, 2019

Fella, Johannes
Entwurf und Inbetriebnahme einer Apparatur zur Synthese von Nanopartikeln durch Inertgaskondensation mittels Sputterquellen
Universität Leipzig, Fakultät für Physik und Geowissentschaften, 2019

Herath, Sören
TEM Charakterisierung von ionenstrahl-gestützt epitaktisch gewachsenen GaN-Dünnschichten
Universität Leipzig, Fakultät für Physik und Geowissentschaften, 2019

Niavarani, Zahra
Development of adsorber membranes with MIP modification for the removal of micropollutants from water
Technische Universität Chemnitz, Fakultät für Naturwissenschaften, 2019

Schütte, Friedrich
Electron beam modified collagen fibers - synthesis and characterization of global and local mechanical response
Universität Leipzig, Fakultät für Physik und Geowissentschaften, 2019

Tietz, Matthias
Untersuchung des Temperatureinflusses auf die photochemisch initiierte Umsetzung von Tetraisobutylorthotitanat
Universität Leipzig, Fakultät für Chemie und Mineralogie, 2019

Wang, Rui
Untersuchung zum lateralen Alignment der Werkzeugfunktion beim Plasma Jet Machining
TU Dresden, Fakultät Maschinenwesen, 2019

Wu, Junfang
Untersuchungen zur plasmagestützten Schichtabscheidung dünner Schichten an Atmosphärendruck zur Formkorrektur optischer Oberflächen
TU Dresden, Fakultät Maschinenwesen, 2019

Committee Work

Anders, André, Prof. Dr.

- Editor-in-Chief, Journal of Applied Physics, published by AIP Publishing, New York, USA
- Chair, The Journals' Editor Conference, AIP Publishing, New York, USA
- Treasurer, Symposia on Discharges and Electrical Insulation in Vacuum (ISDEIV), an IEEE-co-sponsored series of conferences
- Member of the Advisory Board, International Conference on Metallurgical Coatings and Thin Films (ICMCTF)
- Member of the Advisory Board of the International Conference on Plasma Surface Engineering (PSE)
- Chair, Plathinium, The Plasma, Thin Films and Related Processing Union Meeting
- Member of the International Scientific Committee, International Conference on High Power Impulse Magnetron Sputtering (HIPIMS Conf.)
- Member, MPEX Advisory Board, Oak Ridge National Laboratory, Oak Ridge, TN, USA
- Member, Advisory Committee, European Research Society for Thin Films (EFDS)
- Member, Coordinating Committee, Society "Plasma Germany"
- Fächerübergreifende Arbeitsgemeinschaft Halbleiterforschung Leipzig (FAHL, Interdisciplinary Workgroup on Semiconductor Research Leipzig), Representative of the member institute

Abel, Bernd, Prof. Dr.

- Co-editor of "Zeitschrift für Physikaische Chemie - International journal of research in physical chemistry and chemical physics", De Gruyter Verlag
- Reviewers in the Review Board „Physikalische Chemie" of the DFG
- Management Board oft the Wilhelm-Ostwald-Gesellschaft
- Co-Editor of Scientic Reports
- Elected member of the DFG review panel „Physikalische und Theoretische Chemie" of the DFG (Fachkollegium 303)
- Reviewer in various ERC review panels
- Founder and co-owner of Advanded Microfluidic Systems GmbH (2018)
- Board of Graduate School BuildMoNa, University Leipzig
- Board of the CRC TR102 "Polymers under Constraints"

Arnold, Thomas, Prof. Dr.

- Member of the Nanotechnologie Kompetenzzentrum Ultrapräzise Oberflächenbearbeitung e.V. (CC UPOB e.V.)

Bundesmann, Carsten, Dr.

- Arbeitskreis Ellipsometrie (AKE) – Paul Drude e.V. (German Association on Ellipsometry), Member of the extended executive board
- Fächerübergreifende Arbeitsgemeinschaft Halbleiterforschung Leipzig (FAHL, Interdisciplinary Workgroup on Semiconductor Research Leipzig), Personal member

Elsner, Christian, Dr.

- Member of EFDS-Fachausschuss „Oberflächen für die Bio- und Medizintechnik"
- Advisory Board „Nanotechnology" IOP Science

Frost, Frank, Dr.

- Member of the Programm committee „EOS Conferences at the World of Photonics Congress (WPC2019): Conference on Manufacturing of Optical Systems"
- Fächerübergreifende Arbeitsgemeinschaft Halbleiterforschung Leipzig (FAHL, Interdisciplinary Workgroup on Semiconductor Research Leipzig), Personal member

John, Torsten

- Board Member of the International Younger Chemists Network (IYCN)
- Selection Committee Member for the Historical Landmarks Award of the European Chemical Society (EuChemS)
- Board Member (Secretary) of the European Young Chemists' Network (EYCN)

Knolle, Wofgang, Dr.

- Member of the Editorial Board "Radiation Physics and Chemistry"

Lotnyk, Andriy, Dr.

- Second speaker of the working group High-Resolution Transmission Electron Microscopy (German Society for Electron Microscopy)

Mändl, Stephan, Dr.

- Member of the International Committee "Plasma Based Ion Implantation and Deposition"
- Guest Editor Surf. Coat. Technol. Proc. 14th International Conference on Plasma-Based Ion Implantation and Deposition
- Guest Editor Surf. Coat. Technol. Proc. 15th International Conference on Plasma-Based Ion Implantation and Deposition

Mayr, Stefan, Prof. Dr.

- Scientific Board at the Leibniz MMS Days 2018
- Reviewer in the Review Board of the DFG

Monakhov, Kirill, Dr.

- Member of the International Research Network IRN-POM Smart Molecular Oxides
- Member of the German Chemical Society (GDCh)
- Guest Editor on the research topic "Nanoscale Imaging of Coordination Compounds and Their Assemblies" in Frontiers in Chemistry

Scherzer, Tom, Dr.

- Advisory Board of the European European Symposium of Photopolymer Science
- Advisory Board of the International Symposium on Photopolymerization

Zimmer, Klaus, Dr.

- Member of the Editorial Board "Surfaces and Interfaces" Elsevier

Honors

Abdul Latif, Amira and Fischer, Kristina, Dr.

- Saxon Environmental Award 2019, Category D: Voluntary work and environmental education

Abel Bernd, Prof. Dr.

- Gabor A. and Judith K. Somorjai Visiting Miller Professorship Award in 2018 at the University of California, Berkley, USA

Behrens, Mario, Dr.

- Best Poster Award at the Microscopy Conference MC 2019, Berlin, Germany

Böhm, Georg, Dr. and Paetzelt, Hendrik

- IQ Innovation Prize Central Germany 2018, Category: Cluster Prize Chemistry/ Plastics
- IQ Innovation Prize Central Germany 2018, Category: Local Innovation Award Leipzig

Glaß, Sarah, Dr.

- Polymers Travel Award 2018 runner-up
- Polymers Travel Award 2019

John, Thorsten

- Finalist for the European Young Chemist Award (EYCA), EuChemS, 2018
- IUPAC Periodic Table of Younger Chemists (Pb) Award, IUPAC, 2018
- Australia Awards–Endeavour Research Fellowship, Australian Government Department of Education and Training, 2018

Laube, Christian, Dr.

- Young Scientist Award 2019 (Award of the IOM)

Lotnyk, Andriy, Dr.

- Best Poster Award at the 6th Nano Today Conference 2019, Lisbon, Portugal

Maywald, Cornelia, Dr. and Schönherr, Nadja

- Non-Scientist Award 2018 (Award of the IOM)

Reeck, Pascal

- Jugend forscht competition 2018, 1st place in the regional competition Northwest Saxony, Leipzig, Germany

Riedel, Stefanie, Dr.

- Young Scientist Award 2018 (Award of the IOM)
- Publication Prize of the Graduate School BuildMoNa at the Leipzig University, 2018

Schulze, Agnes, Dr.

- Kurt-Schwabe Prize 2018 of the Saxon Academy of Sciences in Leipzig
- IQ Innovation Prize Central Germany 2018 in Silver, Category: Cluster Prize Chemistry/ Plastics

Ulitschka, Melanie

- Best Oral Award at the Euspen Conference Special Interest Group Meeting: "Structured and Freeform Surfaces" 2018 in Paris-Saclay, France

Woyciechowski, Ronny

- Non-Scientist Award 2019 (Award of the IOM)

Scientific Events

Scientific Meetings

Institute Colloquia

Lecture Series

Seminar Series

Scientific Meetings co-organized by IOM

3rd Leibniz MMS Days “Mathematical Modeling and Simulation”
28.02.-02.03.2018, Leibniz Institute of Surface Engineering (IOM), Leipzig, Germany

XXV. Erfahrungsaustausch Oberflächentechnologie mit Plasma- und Ionenstrahlprozessen
20.-23.03.2018, Mühlleithen, Germany

4nd International Summer School “Trends in Ultra-precision optical surface engineering Manufacturing methods and applications”
03.-07.09.2018, Leibniz Institute of Surface Engineering (IOM), Leipzig, Germany

7th Russian-German Conference “Electric Propulsions - New Challenges”
21.-26.10.2018, Gießen, Germany

XXVI. Erfahrungsaustausch Oberflächentechnologie mit Plasma- und Ionenstrahlprozessen
05.-07.03.2019, Mühlleithen, Germany

GRAVOMER – Kompetenzregion mikrostrukturierte Funktionsoberflächen (Alliance kick-off meeting)
18.09.2019, Leibniz Institute of Surface Engineering (IOM), Leipzig, Germany

Vom Labor in die Praxis – mit Innovationen Unternehmen stärken: „Oberflächen nach Maß - Mikrostrukturierte Funktionsoberflächen“
12.11.2019, Leibniz Institute of Surface Engineering (IOM), Leipzig, Germany

International Conference on Laser Interaction with Material and Applied Laser 2019 (LIMA)
27.-29.11.2019, Shanghai, China

Institute Colloquia

Prof. Dr. Thomas Höche (12.12.2019)
Fraunhofer Institute for Microstructure of Materials and Systems IMWS Halle, Germany
Mikrostrukturbasierte Material- und Prozessentwicklung

Prof. Dr. Koen Vandewal (05.12.2019)
Instituut voor Materiaalonderzoek, Diepenbeek, Belgium
Fundamentals and applications of intermolecular charge-transfer states

Prof. Ferdinand Schmidt-Kaler (17.10.2019)
Johannes Gutenberg-Universität Mainz, *Institut für Physik, Germany*
Trapped ion quantum computing and single ion implantation for novel quantum technologies

Prof. Dr. M. Sommer (11.07.2019)
TU Chemnitz, Germany
N-type copolymers for organic photovoltaics, field-effect transistors and thermoelectrics

PD Dr. habil. Yogendra K. Mishra (27.06.2019)
Kiel University, Institute for Materials Science, Germany
Flame based ZnO tetrapod nanomaterials for multifunctional applications

Dr. Sven Schröder (20.06.2019)
Fraunhofer Institute Applied Optics and Precision Engineering IOF, Jena, Germany
Rauheit und Streulicht ultrapräziser optischer Oberflächen und Schichten

Prof. Dr. F. Jelezko (13.06.2019)
Ulm University, Germany
Quantum sensing enabled by color centres

Dr. Cristina Díaz Jiménez (06.06.2019)
Asociación de la Industria Navarra, Spain
Surface functionalization and coatings for advanced biomaterials

Dr. J. Warneke (23.05.2019)
Leipzig University, Wilhelm-Ostwald-Institut für Physikalische und Theoretische, Germany
From isolated ions to functional compounds and materials using ion soft-landing

Prof. Matthias Wuttig (16.05.2019)
RWTH Aachen University, *I. Physikalisches Institut (IA), Germany*
Phase change materials by design: Taming bond No.6

Dr. Marcelo Lozada-Hidalgo (09.05.2019)
University of Manchester, UK
Proton transport through atomically-thin electron clouds

Dr. Denise Erb (25.04.2019)
Helmholtz-Zentrum Dresden-Rossendorf, Germany
Self-assembled surface nanopatterns for magnetic anisotropy engineering

Prof. Dr. Claudia S. Schnohr (11.04.2019)
Leipzig University, Felix-Bloch-Institut für Festkörperphysik, Germany
Structural and compositional inhomogeneity in complex semiconductors used for thin film solar cells

Dr. Michael Zürch (24.01.2019)
Friedrich-Schiller-Universität Jena, Institut für Optik und Quantenelektronik, Germany
Excitation dynamics in bulk and twodimensional semiconductors on the electronic timescale

Prof. Dr. Sebastian Günther (10.01.2019)
TU München, Germany
Towards the ultimate electron transparent membrane

Dr. Carsten Baldauf (06.12.2018)
Leipzig University, *FHI Berlin, Germany*
Biomolecules in thin air

Dr. Jörg Krüger (29.11.2018)
Bundesanstalt für Materialforschung und Prüfung (BAM), Germany
Femtosecond laser-assisted photovoltaic bottom-up strategies

Dr. Franziska Hess (15.11.2018)
Massachusetts Institut of Technology, USA
Materialien im Nichtgleichgewicht: Modellierung von Katalysatordesaktivierung und-stabilisierung in heterogener und Elektrokatalyse

Dr. Konstantin Shportko (08.11.2018)
Institute for Semiconductor Physics of NAS, Ukraine
Optical properties of chalcogenide-based phase-change materials: Challenges and opportunities

Dr. Carsten Bundesmann (27.09.2018)
Leibniz Institute of Surface Engineering (IOM), Leipzig, Germany
Mehr als 50 Jahre Ionenquellenentwicklung am Wissenschaftsstandort Permoserstraße in Leipzig (Ein Beitrag zur Geschichte des IOM)

Dr. Houda Ennaceri (16.08.2018)
Humboldt-Forschungsstipendium
Self-cleaning coatings for CSP solar modules

Prof. Dr. Jörg Matysik (12.07.2018)
Leipzig University, Institut für Analytische Chemie, Germany
Collective events in biomolecular machines

Dr. Kerstin Thorwarth (05.07.2018)
Laboratory for Nanoscale Materials Science Empa Swiss Federal Laboratories for Materials Science and Technology, Switzerland
Smarter implants by PVD: Needs and challenges

Dr. Klaus Mann (28.06.2018)
Laser Laboratorium Göttingen e. V. (LLG), Germany
Vom tiefen UV in den Röntgenbereich: Überblick über die Arbeiten der Abteilung Optik/ Kurze Wellenlängen des LLG

Prof. Dr. Manfred Albrecht (21.06.2018)
Universität Augsburg, Institut für Physik, Germany
Ferrimagnetic Tb-Fe based heterostructures: Intriguing properties and applications

Prof. Dr. Jochen Balbach (14.06.2018)
Martin-Luther-Universität Halle-Wittenberg, Germany
High-resolution NMR-spectroscopy of biomolecules: From formation of structures to structural and dynamic interaction

Dr. Jean Dijon (31.05.2018)
CEA-LITEN, Grenoble, France
Platinum as a material of choice to grow and dope single layer graphene

Frank Siewert (24.05.2018)
Helmholtz Zentrum Berlin, Germany
On the current state of ultra-precise optical elements for Synchrotron- and FEL-application

Prof. Dr. Thomas Heine (17.05.2018)
Leipzig University, Wilhelm-Ostwald-Institut, Germany
Computational theoretical chemistry: Understanding and predicting novel 2D-materials

Dr. Timothy E.L. Douglas (26.04.2018)
Lancaster University, UK
Mineralised hydrogels for bone regeneration

Prof. Dr. Oliver Kühn (19.04.2018)
University of Rostock, Germany
First principles approach to the x-ray spectroscopy of transition metal complexes

Prof. Dr. Bernd Herzog (01.02.2018)
BASF Ludwigshafen, Germany
Recent developments in the photoprotection of human skin - UV-absorbers, nanoparticles and thin films

Dr.-Ing. Anke Dalke (25.01.2018)
TU Bergakademie Freiberg, Germany
Plasmanitrieren - Stand der Technik und neue Möglichkeiten

Prof. Jochen M. Schneider (18.01.2018)
RWTH Aachen University, Germany
Quantum mechanically guided materials design for surface engineering

Prof. Dr. Jan Münch (11.01.2018)
University Ulm, Germany
Simulation of light-induced processes: Molecular materials and proteins

Lecture Series

Abel, Bernd, Prof. Dr.

- *Physikalische Chemie für Fortgeschrittene*
  Universität Leipzig, Fakultät für Chemie und Mineralogie
  Summer 2018, Summer 2019
- *Aktuelle Themen der Physikalischen Chemie*
  Universität Leipzig, Fakultät für Chemie und Mineralogie
  Summer 2018, Summer 2019
- *Allgemeine Chemie für das Nebenfach*
  Universität Leipzig, Fakultät für Chemie und Mineralogie
  Winter 2018/19, Winter 2019/20

Anders, André, Prof. Dr.

- *Plasmas Physics, Thin Film Deposition and Characterization*
  Universität Leipzig, Fakultät für Physik und Geowissenschaften
  Winter 2019/20

Arnold, Thomas, Prof. Dr.

- *Mikro- und Ultrapräzisionsbearbeitung*
  Technische Universität Dresden, Fakultät Maschinenwesen
  Winter 2017/18, Winter 2018/19

Frost, Frank, Dr.

- *Analytik und Spektroskopie: Oberflächen- und Dünnschichtanalytik (Aufbaustudium)*
  Universität Leipzig, Fakultät für Chemie und Mineralogie
  Winter 2018/19

Helmstedt, Ulrike, Dr.

- *Modul "Dünne Schichten" in "Funktionskontrolle an komplexen Oberflächen“*
  Universität Leipzig, Fakultät für Chemie und Mineralogie
  Winter 2019/20

Mändl, Stephan, Dr.

- *Plasmas Physics, Thin Film Deposition and Characterization*
  Universität Leipzig, Fakultät für Physik und Geowissenschaften
  Winter 2019/20

Mayr, Stefan G., Prof. Dr.

- *Experimentalphysik 5 - Festkörperphysik*
  Universität Leipzig, Fakultät für Physik und Geowissenschaften
  Winter 2017/18, Winter 2018/19, Winter 2019/20
- *Advanced Solid State Physics*
  Universität Leipzig, Fakultät für Physik und Geowissenschaften
  Summer 2018

Schulze, Agnes, Dr.

- *Funktionskontrolle an komplexen Oberflächen*
  Universität Leipzig, Fakultät für Chemie und Mineralogie
  Winter 2018/19

Spemann, Daniel, Dr.

- *Kernphysik*
  Universität Leipzig, Fakultät für Physik und Geowissenschaften
  Summer 2018, Summer 2019
- *Experimentalphysik VII – Kern- und Teilchenphysik*
  Universität Leipzig, Fakultät für Physik und Geowissenschaften
  Winter 2018/19, Winter 2019/20

With, Patrick, Dr.

- *Modul "Photochemische Methoden" in "Funktionskontrolle an komplexen Oberflächen“*
  Universität Leipzig, Fakultät für Chemie und Mineralogie
  Winter 2019/20

Zahn, Stefan, Dr.

- *Postgraduales Aufbaustudium "Analytik & Spektroskopie"*
  Universität Leipzig, Fakultät für Chemie und Mineralogie
  Winter 2018/19

Seminar Series

Anders, André, Prof. Dr.

- *Plasmas Physics, Thin Film Deposition and Characterization*
  Universität Leipzig, Fakultät für Physik und Geowissenschaften
  Winter 2019/20

Helmstedt, Ulrike, Dr.

- *Modul "Dünne Schichten" in "Funktionskontrolle an komplexen Oberflächen“*
  Universität Leipzig, Fakultät für Chemie und Mineralogie
  Winter 2019/20

Mändl, Stephan, Dr.

- *Plasmas Physics, Thin Film Deposition and Characterization*
  Universität Leipzig, Fakultät für Physik und Geowissenschaften
  Winter 2019/20

Mayr, Stefan G., Prof. Dr.

- *Seminar „Oberflächenphysik“*
  Universität Leipzig, Fakultät für Physik und Geowissenschaften
  Winter 2017/18, Summer 2018, Winter 2018/19, Summer 2019, Winter 2019/20
- *Hauptseminar – “Modern Developments in Solid State Physics”*
  Universität Leipzig, Fakultät für Physik und Geowissenschaften
  Winter 2017/18, Winter 2018/19, Winter 2019/20
- *Seminar zu Experimentalphysik 5 - Festkörperphysik*
  Universität Leipzig, Fakultät für Physik und Geowissenschaften
  Winter 2017/18, Winter 2018/19, Winter 2019/20

Riedel, Stefanie, Dr.

- *Hauptseminar – “Modern Developments in Solid State Physics”*
  Universität Leipzig, Fakultät für Physik und Geowissenschaften
  Winter 2019/20

Schulze, Agnes, Dr.

- *Funktionskontrolle an komplexen Oberflächen*
  Universität Leipzig, Fakultät für Chemie und Mineralogie
  Winter 2018/19

Spemann, Daniel, Dr.

- *Kernphysik*
  Universität Leipzig, Fakultät für Physik und Geowissenschaften
  Summer 2018, Summer 2019
- *Teilchenphysik*
  Universität Leipzig, Fakultät für Physik und Geowissenschaften
  Summer 2018, Summer 2019
- *Experimentalphysik VII – Kern- und Teilchenphysik*
  Universität Leipzig, Fakultät für Physik und Geowissenschaften
  Winter 2018/19, Winter 2019/20

With, Patrick, Dr.

- *Modul "Photochemische Methoden" in "Funktionskontrolle an komplexen Oberflächen“*
  Universität Leipzig, Fakultät für Chemie und Mineralogie
  Winter 2019/20

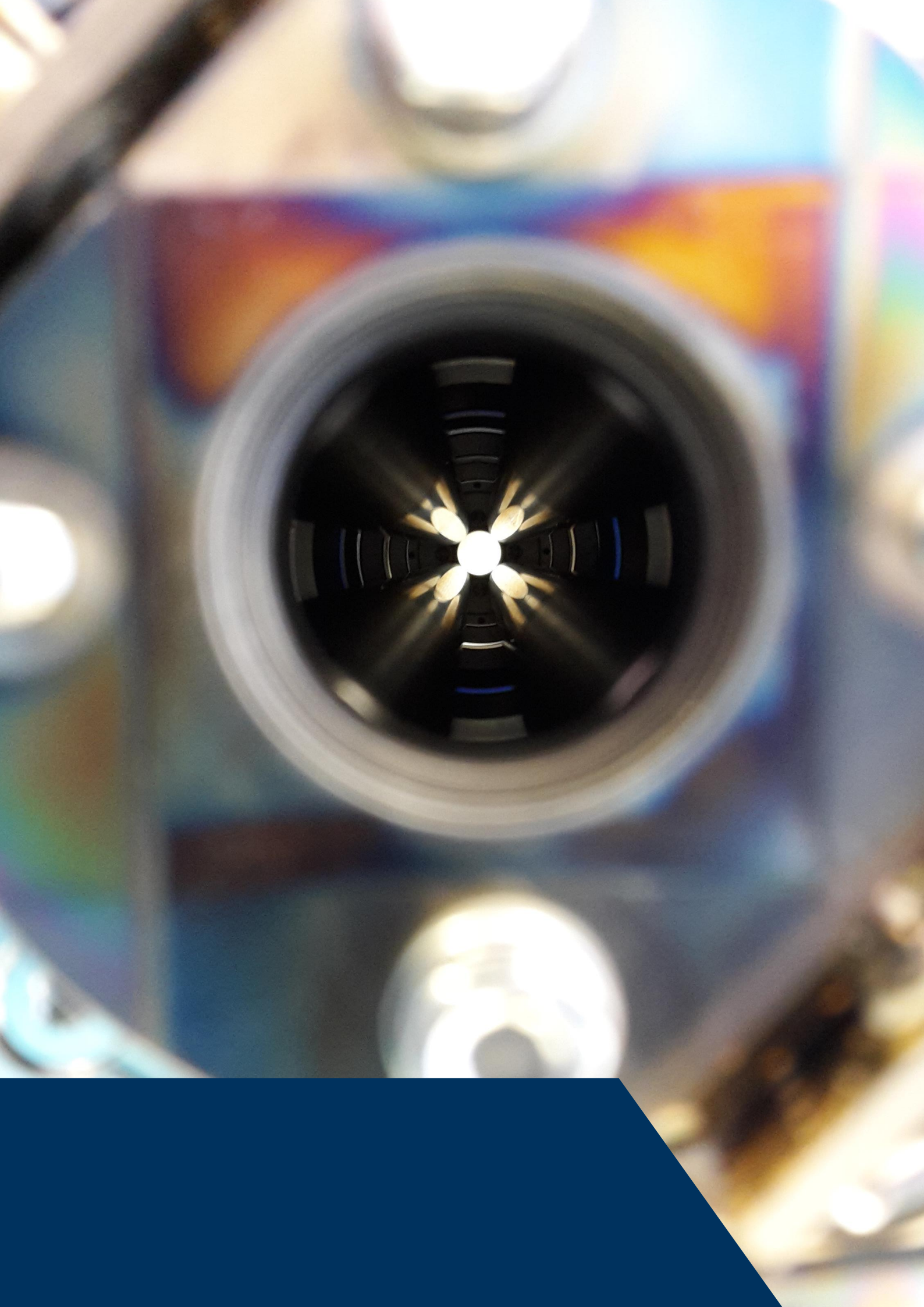

Publications and Presentations

Publications in Journals and Books

Conference Proceedings

Talks

Posters

Patents

Publications in Journals and Books

2018

A. Anders, Y. Yang
Plasma studies of a linear magnetron operating in the range from DC to HiPIMS
J. Appl. Phys. 123 (2018) 043302

J. Appun, F. Stolz, S. Naumov, B. Abel, C. Schneider
The rapid, modular, and highly efficient synthesis of dipyrroloquinolines: A combined cxperimental and analytical study
J. Org. Chem. 83 (2018) 1737-1744

P.A. Atanasov, N.N. Nedyalkov, R.G. Nikov, C. Grüner, B. Rauschenbach, N. Fukata
SERS analysis of Ag nanostructures produced by ion-beam deposition
J. Phys.: Conf. Ser. 992 (2018) 012050

P.A. Atanasov, N.N. Nedyalkov, Ru.G. Nikov, N. Fukuta, W. Jevasuwan, T. Subramani, D. Hirsch, B. Rauschenbach
SERS analyses of thiamethoxam assisted by Ag films and nanostructures produced by laser techniques
J. Raman Spectrosc. 49 (2018) 397-403

T. Bahners, B. Gebert, A. Prager, N. Hartmann, U. Hagemann, J.S. Gutmann
UV-light assisted patterned metallization of textile fabrics
Appl. Surf. Sci. 436 (2018) 1093-1103

P. Bassereau, R. Jin, T. Baumgart, M. Deserno, V.A. Frolov, P.V. Bashkirov, H. Grubmüller, R. Jahn, H.J. Risselada, L. Johannes, M.M. Kozlov, R. Lipowsky, T.J. Pucadyil, W.F. Zeno, J.C. Stachowiak, D. Stamou, A. Breuer, L. Lauritsen, et al.
The 2018 biomembrane curvature and remodeling roadmap
J. Phys. D: Appl. Phys. 51 (2018) 343001

J. Bauer, M. Ulitschka, F. Pietag, T. Arnold
Improved ion beam tools for ultraprecision figure correction of curved aluminum mirror surfaces
J. Astron. Telesc. Instrum. Syst. 4 (2018) 046003

M. Behrens, A. Lotnyk, J.W. Gerlach, I. Hilmi, T. Abel, P. Lorenz, B. Rauschenbach
Ultrafast interfacial transformation from 2D- to 3D-bonded structures in layered Ge-Sb-Te thin films and heterostructures
Nanoscale 10 (2018) 22946-22953

M. Behrens, A. Lotnyk, U. Roß, J. Griebel, P. Schumacher, J.W. Gerlach, B. Rauschenbach
Impact of disorder on optical reflectivity contrast of epitaxial $Ge_2Sb_2Te_5$ thin films
CrystEngComm 20 (2018) 3688-3695

C. Bundesmann, H. Neumann
Tutorial: The systematics of ion beam sputtering for deposition of thin films with tailored properties
J. Appl. Phys. 124 (2018) 231102

M.V. Cakir, U. Allenstein, M. Zink, S.G. Mayr
Early adhesion of cells to ferromagnetic shape memory alloys functionalized with plasma assembled biomolecules - a single cell force spectroscopy study
Mater. Des. 158 (2018) 19-27

R. Chanson, L. Zhang, S. Naumov, Yu.A. Mankelevich, T. Tillocher, P. Lefaucheux, R. Dussart, S. De Gendt, J-F. de Marneffe
Damage-free plasma etching of porous organo-silicate low-k using micro-capillary condensation above -50 ºC
Sci. Rep. 8 (2018) 1886

D. Chen, G. Yang, J. Li, D. Hirsch, Y. Liu, F. Frost, Y. Hong
Terrace morphology on fused silica surfaces by Ar^+ ion bombardment with Mo co-deposition
Appl. Phys. Lett. 113 (2018) 033102

M. D`Agostino, H.J. Risselada, L.J. Endter, V. Comte-Miserez, A. Mayer
SNARE-mediated membrane fusion arrests at pore expansion to regulate the volume of an organelle
The Embo Journal 37 (2018) e99193

O. Daikos, K. Heymann, T. Scherzer
Monitoring of thickness and conversion of thick pigmented UV-cured by NIR hyperspectral imaging
Progr. Org. Coat. 125 (2018) 8-14

M. Ehrhardt, P. Lorenz, B. Han, R. Zhu, K. Zimmer
Laser-induced backside wet etching of SiO_2 with a visible ultrashort laser pulse by using $KMnO_4$ solution as an absorber liquid
J. Laser Micro Nanoen. 13 (2018) 47-54

M. Ehrhardt, P. Lorenz, L. Bayer, B. Han, K. Zimmer
Studies of the confinement at laser-induced backside dry etching using infrared nanosecond laser pulses
Appl. Surf. Sci. 427 (2018) 686-692

C. Elsner, M. Lohan, J. Griebel, U. Decker
Photo-stimulated leaving group isomerization of acyl donor esters in protease-catalyzed hydrolysis reactions
Biocat. Biotrans. 36 (2018) 444-449

H. Ennaceri, A. Ghennioui, A. Benyoussef, A. Ennaoui, A. Khaldoun
Direct normal irradiation-based approach for determining potential regions for concentrated solar power installations in Morocco
Int. J. Ambient Energy 39 (2018) 78-86

E. Fasshauer, M. Forstel, M. Mucke, T. Arion, U. Hergenhahn
Corrigendum to 'theoretical and experimental investigation of electron transfer mediated decay in ArKr clusters' [Chem. Phys. 482 (2017) 226238]
Chem. Phys. 501 (2018) 138

K. Fischer, P. Schulz, I. Atanasov, A. Abdul Latif, A. Prager, J. Griebel, A. Schulze
Synthesis of high crystalline TiO_2 nanoparticles on a polymer membrane to degrade pollutants from water
Catalysts 8 (2018) 376

S. Glaß, T. Rüdiger, J. Griebel, B. Abel, A. Schulze
Uptake and release of photosensitizers in a hydrogel for applications in photodynamic therapy: The impact of structural parameters on intrapolymer transport dynamics
RSC Adv. 8 (2018) 41624-41632

S. Glaß, B. Trinklein, B. Abel, A. Schulze
TiO_2 with dual function: Photoinitiator and photosensitizer in the synthesis of photoactive TiO_2-PEGDA hydrogels
Front. Chem. 6 (2018) 340

C. Grüner, I. Abdulhalim, B. Rauschenbach
Glancing angle deposition for biosensing applications
Encyclopedia of Interfacial Chemistry - Surf. Sci. Electrochem. (2018) 129-137

C. Grüner, P. Reeck, P.-P. Jacobs, S. Liedtke, A. Lotnyk, B. Rauschenbach
Gold coated metal nanostructures grown by glancing angle deposition and pulsed electroplating
Phys. Lett. A 382 (2018) 1287-1290

C. Grüner, S. Liedtke, J. Bauer, S.G. Mayr, B. Rauschenbach
Morphology of thin films formed by oblique physical vapor deposition
ACS Appl. Nano Mater. 1 (2018) 1370-1376

F. Haase, D. Manova, D. Hirsch, S. Mändl, H. Kersten
Dynamic determination of secondary electron emission using a calorimetric probe in a plasma immersion ion implantation experiment
Plasma Sources Sci. Technol. 27 (2018) 044003

T. Herzig, P. Räcke, N. Raatz, D. Spemann, W. Redjem, J.W. Gerlach, J. Meijer, G. Cassabois, M. Abbarchi, S.Pezzagna
Creation of quantum centers in silicon using spatial selective ion implantation of high lateral resolution
Proc. 22nd Int. Conf. on Ion Implantation Technology (2018) 136-139

E. Jahangiri, I. Thomas, A. Schulze, B. Seiwert, H. Cabana, D. Schlosser
Characterisation of electron beam irradiation-immobilised laccase for application in wastewater treatment
Sci. Total Environ. 624 (2018) 309-322

T. John, A. Gladytz, C. Kubeil, L.L. Martin, H.J. Risselada, B. Abel
Impact of nanoparticles on amyloid peptide and protein aggregation: A review with a focus on gold nanoparticles
Nanoscale 10 (2018) 20894-20913

T. John, B. Abel, L.L. Martin
The quartz crystal microbalance with dissipation monitoring (QCM-D) technique applied to the study of membrane-active peptides
Aust. J. Chem. 71 (2018) 543-546

F. Koch, D. Lehr, O. Schönbrodt, T. Glaser, R. Fechner, F. Frost
Manufacturing of highly-dispersive, high-efficiency transmission gratings by laser interference lithography and dry etching
Microelectron. Eng. 191 (2018) 60-65

C. Laube, J. Hellweg, C. Sturm, J. Griebel, M. Grundmann, A. Kahnt, B. Abel
Photoinduced heating of graphitized nanodiamonds monitored by the Raman diamond peak
J. Phys. Chem. C 122 (2018) 25685-25691

J. Lehnert, D. Spemann, S. Surjuse, M. Mensing, C. Grüner, P. With, P. Schumacher, A. Finzel, D. Hirsch, B. Rauschenbach
Preparation and characterisation of carbon-free Cu(111) films on sapphire for graphene synthesis
J. Phys.: Conf. Ser. 992 (2018) 012024

S. Liedtke, C. Grüner, J.-W. Gerlach, A. Lotnyk, B. Rauschenbach
Crystalline Ti-nanostructures prepared by oblique angle deposition at room temperature
J. Vac. Sci. Technol. B 36 (2018) 031804

S. Liedtke, Ch. Grüner, J.W. Gerlach, B. Rauschenbach
Comparative study of sculptured metallic thin films deposited by oblique angle deposition at different temperatures
Beilstein J. Nanotechnol. 9 (2018) 954-962

O. Link, E. Lugovoy, B. Abel
Interface solvated electrons
Encyclopedia of Interfacial Chemistry - Surf. Sci. Electrochem. (2018) 433-442

O. Linnenberg, M. Moors, A. Notario-Estévez, X. López, C. de Graaf, S. Peter, C. Bäumer, R. Waser, K. Yu. Monakhov
Adressing multiple resistive states of polyoxovanadates: Conductivity as a function of individual redox states.
J. Am. Chem. Soc. 140 (2018) 16635-16640

Y. Liu, D. Hirsch, R. Fechner, Y. Hong, S. Fu, F. Frost, B. Rauschenbach
Nanostructures on fused silica surfaces produced by ion beam sputtering with Al co-deposition
Appl. Phys. A 124 (2018) 73

F.P. Lohmann-Richters, C. Odenwald, G. Kickelbick, B. Abel, Á. Varga
Facile and scalable synthesis of sub-micrometer electrolyte particles for solid acid fuel cells
RSC Advances 8 (2018) 21806-21815

F.P. Lohmann-Richters, B. Abel, Á. Varga
In situ determination of the electrochemically active platinum surface area: key to improvement of solid acid fuel cells
J. Mater. Chem. A 6 (2018) 2700-2707

P. Lorenz, L. Bayer, T. Tachtsidis, K. Zimmer
Laser patterning of hierarchical structures on metal cylinders for UV-NIL replication
Proc. 10th CIRP Conference on Photonic Technologies [LANE 2018] (2018)

P. Lorenz, M. Klöppel, I. Zagoranskiy, K. Zimmer
From statistic to deterministic nanostructures in fused silica induced by nanosecond laser radiation
Procedia CIRP 74 (2018) 371-375

A. Lotnyk, I. Hilmi, U. Ross, B. Rauschenbach
Van der Waals interfacial bonding and intermixing in GeTe-Sb_2Te_3-based superlattices
Nano Res. 11 (2018) 1676-1686

H.V. Lutze, J. Brekenfeld, S. Naumov, C. von Sonntag, T. Schmidt
Degradation of perfluorinated compounds by sulfate radicals - New mechanistic aspects and economical considerations
Water Research 129 (2018) 509-519

R. Macchieraldo, L. Esser, R. Elfgen, P. Voepel, S. Zahn, B.-M. Smarsly, B. Kirchner
Hydrophilic ionic liquid mixtures of weakly and strongly coordinating anions with and without water
ACS Omega 3 (2018) 8567-8582

J.-F. de Marneffe, B.-T. Cha, M. Spieser, G. Vereecke, S. Naumov, D. Vanhaeren, A.-W. Knoll
Conversion of a patterned organic resist into a high performance inorganic hard mask for high resolution pattern transfer
ACS Nano 12 (2018) 11152-11160

L.L. Martin, C. Kubeil, S. Piantavigna, T. Tikkoo, N.P. Gray, T. John, A.N. Calabrese, Y. Liu, Y. Hong, M.A. Hossain, N. Patil, B. Abel, R. Hoffmann, J.H. Bowie, J.A. Carver
Amyloid aggregation and membrane activity of the antimicrobial peptide uperin 3.5
Pept. Sci. 110 (2018) e24052

M. Mateev, T. Lautenschläger, D. Spemann, A. Finzel, J.W. Gerlach, F. Frost, C. Bundesmann
Systematic investigation of the reactive ion beam sputter deposition process of SiO_2
Eur. Phys. J. B 91 (2018) 45

S. Merker, H. Krautscheid, S. Zahn
Can a temporary bond between dye and redox mediator increase the efficiency of p-type dye-sensitized solar cells?
J. Mol. Model. 24 (2018) 317

G. Mirschel, O. Daikos, T. Scherzer, C. Steckert
Near-infrared chemical imaging used for in-line analysis of functional finishes on textiles
Talanta 188 (2018) 91-98

G. Mitri, F. Postberg, J.M. Soderblom, P. Wurz, P. Tortora, B. Abel, J.W. Barnes, M. Berga, N. Carrasco, A. Coustenis, J.P. Paul de Vera, A. D`Ottavio, F. Ferri, A.G. Hayes, P.O. Hayne, J.K. Hillier, S. Kempf, J.-P. Lebreton, R.D. Lorenz, et al.
Explorer of Enceladus and Titan (E^2T): Investigating ocean worlds`evolution and habitability in the solar system
Planet. Space Sci. 155 (2018) 73-90

M. Mitterbauer, P. Knaack, S. Naumov, M. Markovic, A. Ovsianikov, N. Moszner, R. Liska
Acylstannanes - a new generation of cleavable and highly reactive photoinitiators for curing at wavelengths above 500 nm with excellent photobleaching behavior
Angew. Chemie Int. Ed. 57 (2018) 12146-12150

A. Müller, A. Preuß, T. Bornhütter, I. Thomas, A. Prager, A. Schulze, B. Röder
Electron beam functionalized photodynamic polyether-sulfone membranes photophysical characterization and antimicrobial activity
Photochem. Photobiol. Sci. 17 (2018) 1346-1354

O. Naumov, S. Naumov, B. Abel, A. Varga
The stability limits of highly active nitrogen doped carbon ORR nano-catalysts: a mechanistic study of degradation reactions
Nanoscale 10 (2018) 6724-6733

V. Nikolaou, F. Plass, A. Planchat, A. Charisiadis, G. Charalambidis, P.-A. Angaridis, A. Kahnt, F. Odobel, A.-G. Coutsolelos
Effect of the triazole ring in zinc porphyrin-fullerene dyads on the charge transfer processes in NiO-based devices
Phys. Chem. Chem. Phys. 20 (2018) 24477-24489

J.-C. Oliveira, F. Ferreira, A. Anders, A. Cavaleiro
Reduced atomic shadowing in HiPIMS: Role of the thermalized metal ions
Appl. Surf. Sci. 433 (2018) 934-944

L. Pietzonka, T. Lautenschläger, D. Spemann, A. Finzel, J.W. Gerlach, F. Frost, C. Bundesmann
Ion beam sputter deposition of TiO_2 films using oxygen ions
Eur. Phys. J. B 91 (2018) 252

F. Postberg, N. Khawaja, B. Abel, G. Choblet, C.R. Glein, M.S. Gudipati, B.L. Henderson, H.-W. Hsu, S. Kempf, F. Klenner, G. Moragas-Klostermeyer, B. Magee, L. Nölle, M. Perry, R. Reviol, J. Schmidt, F. Stolz, G. Tobie, M. Trieloff, J.H. Waite
Macromolecular organic compounds from the depths of Enceladus
Nature 558 (2018) 564-568

P. Räcke, D. Spemann, J.W. Gerlach, B. Rauschenbach, J. Meijer
Detection of small bunches of ions using image charges
Sci. Rep. 8 (2018) 9781

A. Reinhardt, I. Thomas, J. Schmauck, R. Giernoth, A. Schulze, I. Neundorf
Electron beam immobilization of novel antimicrobial, short peptide motifs leads to membrane surfaces with promising antibacterial properties
J. Funct. Biomater. 9 (2018) 21

E. Reisz, C. von Sonntag, A. Tekle-Röttering, S. Naumov, W. Schmidt, T. Schmidt
Reaction of 2-propanol with ozone in aqueous media
Water Research 128 (2018) 171-182

C. Richter, D. Hollas, C.-M. Saak, M. Förstel, T. Miteva, M. Mucke, O. Björneholm, N. Sisourat, P. Slavicek, U. Hergenhahn
Competition between proton transfer and intermolecular Coulombic decay in water
Nat. Comm. 9 (2018) 4988

S. Riedel, K. Bela, E.I. Wisotzki, C. Suckfüll, J. Zajadacz, S.G. Mayr
Reagent-free mechanical patterning of gelatin surfaces by two-step electron irradiation treatment
Mater. Des. 153 (2018) 80-85

S. Riedel, S.G. Mayr
Reagent-free programming of shape-memory behavior in gelatin by electron beams: Experiments and modeling
Phys. Rev. Appl. 9 (2018) 024011

M. Schmidt, D. Breite, I. Thomas, M. Went, A. Prager, A. Schulze
Polymer membranes for active degradation of complex fouling mixtures
J. Membr. Sci. 563 (2018) 481-491

K.R. Siefermann, A. Neff
Time-resolved photoemission electron microscopy
Encyclopedia of Interfacial Chemistry - Surf. Sci. Electrochem. (2018) 557-566

F. Siewert, B. Löchel, J. Buchheim, F. Eggenstein, A. Firsov, G. Gwalt, O. Kutz, S. Lemke, B. Nelles, I. Rudolph, F. Schäfers, T. Seliger, F. Senf, A. Sokolov, C. Waberski, J. Wolf, T. Zeschke, I. Zizak, R. Follath, T. Arnold, F. Frost, F. Pietag, A. Erko
Gratings for synchrotron and FEL beamlines: A project for the manufacture of ultra-precise gratings at Helmholtz Zentrum Berlin
J. Synchrotron Rad. 25 (2018) 91-99

C. Stangel, F. Plass, A. Charisiadis, E. Giannoudis, G. Chararalambidis, K. Karikis, G. Rotas, G.-E. Zervaki, N.N. Lathiotakis, N. Tagmatarchis, A. Kahnt, A.-G. Coutsolelos
Interfacing tetrapyridyl-C_{60} with porphyrin dimers via π-conjugated bridges: Artificial photosynthetic systems with ultrafast charge separation
Phys. Chem. Chem. Phys. 20 (2018) 21269-21279

E.V. Stenson, U. Hergenhahn, M.R. Stoneking, T. Sunn Pedersen
Positron-induced luminescence
Phys. Rev. Lett. 120 (2018) 147401

S. Ullmann, R. Schorr, Ch. Laube, B. Abel, B. Kersting
Photoluminescence properties of tetrahedral zinc(II) complexes supported by calix(4)arene-based salicylaldiminato ligands
Dalton Trans. 47 (2018) 5801-5811

G. Wang, A. Lotnyk, C. Liac, X. Shen
Oxygen filling voids and direct element imaging of metastable ZnSb structures by aberration-corrected scanning transmission electron microscopy
Scr. Mater. 157 (2018) 115-119

G. Wang, A. Lotnyk, Q. Nie, R. Wang, X. Shen, Y. Lu
Shortening nucleation time to enable ultrafast phase transition in $Zn_1Sb_7Te_{12}$ pseudo-binary alloy
Langmuir 34 (2018) 15143-15149

G. Wang, H. Wan, A. Lotnyk, R. Wang, X. Shen
Unique interface-driven crystallization mechanism and element-resolved structure imaging of ZnO-$Ge_2Sb_2Te_5$ nanocomposites
Ceram. Int. 44 (2018) 22497-22503

S. Weyrauch, C. Wagner, C. Suckfuell, A. Lotnyk, W. Knolle, J.W. Gerlach, S.G. Mayr
Nanoporous gold synthesized by plasma-assisted inert gas condensation: Room temperature sintering, nanoscale mechanical properties and stability against high energy electron irradiation
J. Phys. D: Appl. Phys. 51 (2018) 065301

S. Zernia, R. Frank, R. Weiße, H.-G. Jahnke, K. Bellmann-Sickert, A. Prager, B. Abel, N. Sträter, A. Robitzki, A.G. Beck-Sickinger
Surface-binding peptide facilitates electricity-driven NADPH-free Cytochrome P450 catalysis
Chem. Cat. Chem. 10 (2018) 525

J. Zhou, C. Laube, W. Knolle, S. Naumov, A. Prager, F.-D. Kopinke, B. Abel
Efficient chlorine atom functionalization at nanodiamond surfaces by electron beam irradiation
Diam. Relat. Mater. 82 (2018) 150-159

S. Zöhrer, A. Anders, R. Franz
Time-resolved ion energy and charge state distributions in pulsed cathodic arc plasmas of Nb-Al cathodes in high vacuum
Plasma Sources Sci. Technol. 27 (2018) 055007

S. Zöhrer, A. Anders, R. Franz
Influence of Ar gas pressure on ion energy and charge state distributions in pulsed cathodic arc plasmas from NbAl cathodes studied with high time resolution
J. Phys. D: Appl. Phys. 52 (2018) 055201

2019

P. Ahrens, M. Zander, D. Hirsch, U. Hasse, H. Wulff, F. Frost, F. Scholz
Influence of argon ion beam etching and thermal treatment on polycrystalline and single crystal gold electrodes Au(100) and Au(111)
J. Electroanal. Chem. 832 (2019) 233-240

R.K. Al-Shewiki, M. Korb, A. Hildebrandt, S. Zahn, S. Naumov, R. Buschbeck, T. Rüffer, H. Lang
Diaqua-β-octaferrocenyltetraphenylporphyrin: a multiredox-active and air-stable 16π non-aromatic species
Dalton Trans. 48 (2019) 1578-1585

B.S. Basel, C. Hetzer, J. Zirzlmeier, D. Thiel, R. Guldi, F. Hampel, A. Kahnt, T. Clark, D.M. Guldi, R.R. Tykwinski
Davydov splitting and singlet fission in excitonically coupled pentacene dimers
Chem. Sci. 10 (2019) 3854-3863

F. Bauer, R. Meyer, S. Czihal, M. Bertmer, U. Decker, S. Naumov, H. Uhlig, M. Steinhart, D. Enke
Functionalization of mesoporous siliceous materials, Part 2: Surface characterization by inverse gas chromatography
J. Chrom. A 1603 (2019) 297-310

J. Bauer, F. Frost, A. Lehmann, M. Ulitschka, Y. Li, T. Arnold
Finishing of metal optics by ion beam technologies
Opt. Eng. 58 (2019) 092612

M. Behrens, A. Lotnyk, J.W. Gerlach, M. Ehrhardt, P. Lorenz, B. Rauschenbach
Direct measurement of crystal growth velocity in epitaxial phase-change material thin films
ACS Appl. Mater. Interfaces 11 (2019) 41544-41550

M. Berndt-Paetz, P. Schulze, P.C. Stenglein, A. Weimann, Q. Wang, L.-C. Horn, Y.M. Riad, J. Griebel, R. Hermann, A. Glasow, J.-U. Stolzenberg, J. Neuhaus
Reduction of muscle-invasive tumors by photodynamic therapy with tetrahydroporphyrin-tetratosylat in an orthotopic rat bladder cancer model
Mol. Cancer Ther. 18 (2019) 743-750

P. Bielytskyi, D. Gräsing, S. Zahn, K.D. Mote, A. Alia, P.K. Madhu, J. Matysik
Assignment of NMR resonances of protons covalently bound to photochemically active cofactors in photosynthetic reaction centers by ^{13}C-^{1}H photo-CIDNP MAS-J-HMQC experiment
J. Magn. Reson. 298 (2019) 64-76

P. Bielytskyi, D. Gräsing, S. Zahn, A. Alia, J. Matysik
^{15}N-^{1}H transfer of light-induced nuclear hyperpolarization in frozen photosynthetic reaction centers
Appl. Magn. Reson. 50 (2019) 695-708

L. Botsch, I. Lorite, Y. Kumar, P.D. Esquinazi, J. Zajadacz, K. Zimmer
All-semiconducting spin filter prepared by low-energy proton irradiation
ACS Appl. Electron. Mater. 1 (2019) 1832-1841

D. Breite, M. Went, A. Prager, M. Kühnert, A. Schulze
Charge separating microfiltration membrane with pH-dependent selectivity
Polymers 11 (2019) 3

C. Bundesmann, T. Amelal
Secondary particle properties for the ion beam sputtering of TiO_2 in a reactive oxygen atmosphere
Appl. Surf. Sci. 485 (2019) 391-401

F. Clauder, A.S. Czerniak, S. Friebe, S.G. Mayr, D. Scheinert, A.G. Beck-Sickinger
Endothelialization of titanium surfaces by bioinspired cell adhesion peptide coatings
Bioconjugate Chem. 30 (2019) 2664-2674

O. Daikos, K. Heymann, T. Scherzer
Development of a PLS approach for the determination of the conversion in UV-cured white-pigmented coatings by NIR chemical imaging and its transfer to other substrates
Prog. Org. Coat. 132 (2019) 116-124

R. Das, M. Kühnert, A.S. Kazemi, Y. Abdi, A. Schulze
Water softening using light responsive spiropyran modified nanofiltration membrane
Polymers 11 (2019) 344

A. Delavari, D. Breite, A. Schulze, R.E. Baltus
Latex particle rejections from virgin and mixed charged surface
J. Membr. Sci. 584 (2019) 110-119

M. Deppe, J.W. Gerlach, S. Shvarkov, D. Rogalla, H.-W. Becker, D. Reuter, D.J. As
Germanium doping of cubic GaN grown by molecular beam epitaxy
J. Appl. Phys. 125 (2019) 095703

M. Ehrhardt, B. Han, F. Frost, P. Lorenz, K. Zimmer
Generation of laser-induced periodic surface structures (LIPSS) in fused silica by single NIR nanosecond laser pulse irradiation in confinement
Appl. Surf. Sci. 470 (2019) 56-62

C. Eichhorn, F. Scholze, C. Bundesmann, D. Spemann, H. Neumann, H. Leiter
Two-photon laser-induced fluorescence in a radiofrequency ion thruster plume in Krypton
J. Propul. Power 35 (2019) 1175-1178

A. Finzel, F. Koch, G. Dornberg, D. Lehr, F. Frost, T. Glaser
Reactive ion beam etching of highly dispersive, high-efficiency transmission gratings for the VIS range
Opt. Eng. 58 (2019) 092614

S. Friebe, S.G. Mayr
Regeneration of TiO_2 nanotube arrays after long-term cell and tissue culture for multiple use - an environmental scanning electron microscopy (ESEM) survey of adult pig retina and beyond
Biol. Proced. Online 21 (2019) 2

S. Glaß, M. Kühnert, B. Abel, A. Schulze
Controlled electron-beam synthesis of transparent hydrogels for drug delivery applications
Polymers 11 (2019) 501

M. Glöß, R. Pütt, M. Moors, E. Kentzinger, W. Pyckhout-Hintzen, K.Y. Monakhov
Interplaying the amphipathic polyoxometalate interactions in solution and at solid-liquid interfaces: A toolbox for the technical application
Nanoscale 11 (2019) 4267-4277

D. Gräsing, K. M. Dziubińska-Kühn, S. Zahn, A. Alia, J. Matysik
Studying hydrogen bonding and dynamics of the acetylate groups of the Special Pair of Rhodobacter sphaeroides WT
Sci. Rep. 9 (2019) 10528

R. Haldar, K. Batra, S.M. Marschner, A.B. Kuc, S. Zahn, R.A. Fischer, S. Bräse, T. Heine, C. Wöll
Bridging the green gap: Metal-organic framework heteromultilayers assembled from porphyrinic linkers identified by using computational screening
Chem. Eur. J. 25 (2019) 7847-7851

R. Hesse, C. Bundesmann, R. Denecke
Automatic spike correction using UNIFIT 2020
Surf. Interface Anal. 51 (2019) 1342-1350

I. Hilmi, A. Lotnyk, J.W. Gerlach, P. Schumacher, B. Rauschenbach
Influence of substrate dimensionality on the growth mode of epitaxial 3D-bonded GeTe thin films: From 3D to 2D growth
Mater. Des. 168 (2019) 107657

A. Holm, S.G. Mayr
Thermal and structural properties of the martensitic transformations in Fe_7Pd_3 shape memory alloys: An ab initio-based molecular dynamics study
New J. Phys. 21 (2019) 063007

B. Holzer, M. Lunzer, A. Rosspeintner, G. Licari, M. Tromayer, S. Naumov, D. Lumpi, E. Horkel, C. Hametner, A. Ovsianikov, R.Liska, E. Vauthey, J. Fröhlich
Towards efficient initiators for two-photon induced polymerization: Fine tuning of the donor/acceptor properties
Mol. Syst. Des. Eng. 4 (2019) 437-448

L. Jablonowski, T. Kocher, A. Schindler, K. Müller, F. Dombrowski, T. von Woedtke, T. Arnold, A. Lehmann, S. Rupf, M. Evert, K. Evert
Side effects by oral application of atmospheric pressure plasma on the mucosa in mice
PLoS ONE 14 (2019) e0215099

T. John, G.W. Greene, N.A. Patil, T.J.A. Dealey, M.A. Hossain, B. Abel, L.L. Martin
Adsorption of amyloidogenic peptides to functionalized surfaces is biased by charge and hydrophilicity
Langmuir 35 (2019) 14522-14531

T. John, T.J.A. Dealey, N.P. Gray, N.A. Patil, M.A. Hossain, B. Abel, J.A. Carver, Y. Hong, L.L. Martin
The Kinetics of amyloid fibrillar aggregation of uperin 3.5 is directed by the peptide's secondary structure
Biochemistry 58 (2019) 3656-3668

D. Kalanov, A. Anders, C. Bundesmann
Ion beam sputtering of silicon: Energy distributions of sputtered and scattered ions
J. Vac. Sci. Technol. A 37 (2019) 051507

F. Kazemi, G. Böhm, T. Arnold
Development of a model for ultra-precise surface machining of N-BK7® using microwave-driven reactive plasma jet machining
Plasma Process Polym. 16 (2019) 1900119

K.S. Kisel, A.S. Melnikov, E.V. Grachova, A.J. Karttunen, A. Doménech-Carbó, K.Y. Monakhov, V.G. Semenov, S.P. Tunik, I.O. Koshevoy
Supramolecular construction of cyanide-bridged Re^{I} diimine multichromophores
Inorg. Chem. 58 (2019) 1988-2000

J. Klose, T. Severin, P. Hahn, A. Jeremies, J. Bergmann, D. Fuhrmann, J. Griebel, B. Abel, B. Kersting
Coordination chemistry and photoswitching of dinuclear macrocyclic cadmium-, nickel-, and zinc complexes containing azobenzene carboxylato co-ligands
Beilstein J. Org. Chem. 15 (2019) 840-851

J. Kolbeck, A. Anders, I. Beilis, M. Keidar
Micro-propulsion based on vacuum arcs
J. Appl. Phys. 125 (2019) 220902

I. Lacey, R.D. Geckler, A. Just, F. Siewert, Th. Arnold, H. Paetzelt, B.V. Smith, V.V. Yashchuk
Optimization of the size and shape of the scanning aperture in autocollimator-based deflectometric profilometers
Rev. Sci. Instrum. 90 (2019) 021717

S. Lai, P. Lorenz, M. Ehrhardt, B. Han, D. Hirsch, I. Zagoranskiy, J. Lu, K. Zimmer
Laser-induced frontside etching of silicon using 1550-nm nanosecond laser pulses
Opt. Lasers Eng. 122 (2019) 245-253

S. Lai, P. Lorenz, M. Ehrhardt, B. Han, J. Lu, K. Zimmer
Dot line pattern formation in photoresist films by mask-guided LIPSS formation due to Excimer laser irradiation
J. Laser Micro Nanoen. 14 (2019) 124-128

C. Laube, T. Oeckinghaus, J. Lehnert, J. Griebel, W. Knolle, A. Denisenko, A. Kahnt, J. Meijer, J. Wrachtrup, B. Abel
Controlling the fluorescence properties of nitrogen vacancy centers in nanodiamonds
Nanoscale 11 (2019) 1770-1783

S. Liedtke-Grüner, C. Grüner, A. Lotnyk, J.W. Gerlach, M. Mensing, P. Schumacher, B. Rauschenbach
Crystallinity and texture of molybdenum thin films obliquely deposited at room temperature
Thin Solid Films 685 (2019) 8-16

X. Liu, Z. Di, P.K. Chu, S. Mändl
14th International Conference on Plasma-Based Ion Implantation and Deposition
Surf. Coat. Technol. 365 (2019) 1

A. Lotnyk, M. Behrens, B. Rauschenbach
Phase change thin films for non-volatile memory applications
Nanoscale Adv. 1 (2019) 3836-3857

A. Lotnyk, T. Dankwort, I. Hilmi, L. Kienle, B. Rauschenbach
In situ observations of reversible vacancy ordering process in van der Waals-bonded Ge-Sb-Te thin films and GeTe-Sb_2Te_3 superlattices
Nanoscale 11 (2019) 10838-10845

A. Lotnyk, T. Dankwort, I. Hilmi, L. Kienle, B. Rauschenbach
Atomic-scale observation of defects motion in van der-Waals layered chalcogenide based materials
Scr. Mater. 166 (2019) 154-158

X. Luo, S. Chen, L. Liu, J. Lv, A. Qadir, K. Shehzad, X. Qiao, Y. Xu, L. Kienle, A. Lotnyk, X. Zhang, G. Qian, X. Fan
Micron-scale photodetectors based on one-dimensional single-crystalline $Sb_{2-x}Sn_xSe_3$ microrods: Simultaneously improving responsivity and extending spectral response region
J. Phys. Chem. C 123 (2019) 810-816

S. Mändl, D. Manova
Modification of metals by plasma immersion ion implantation
Surf. Coat. Technol. 365 (2019) 83-93

D. Manova, S. Mändl
Dynamic msurements of optical emission during plasma immersion ion implantation
Surf. Coat. Technol. 365 (2019) 94-101

D. Manova, S. Mändl
In situ XRD measurements to explore phase formation in the near surface region
J. Appl. Phys. 126 (2019) 200901

A. Mayer, W. Ai, J. Rond, J. Staabs, C. Steinberg, M. Papenheim, H.-C. Scheer, M. Tormen, A. Cian, J. Zajadacz, K. Zimmer
Electrically-assisted nanoimprint of block copolymers
J. Vac. Sci. Technol. B 37 (2019) 011601

A. Mayer, J. Rond, J. Staabs, M. Leifels, J. Zajadacz, M. Ehrhardt, P. Lorenz, H. Sunagawa, Y. Hirai, K. Zimmer, H.-C. Scheer
Multiple replication of hierarchical structures from polymer masters with anisotropy
J. Vac. Sci. Technol. B 37 (2019) 061601

M. Mensing, P. Schumacher, J.W. Gerlach, S. Herath, A. Lotnyk, B. Rauschenbach
Influence of nitrogen ion species on mass-selected low energy ion-assisted growth of epitaxial GaN thin films
Appl. Surf. Sci. 498 (2019) 143830

G. Mirschel, O. Daikos, T. Scherzer
In-line monitoring of the thickness distribution of adhesive layers in black textile laminates by hyperspectral imaging
Comput. Chem. Eng. 124 (2019) 317-325

F. Niefind, A. Neff, S.C.B. Mannsfeld, A. Kahnt, B. Abel
Computational analysis of the orientation persistence length of the polymer chain orientation
Phys. Chem. Chem. Phys. 21 (2019) 21464-21472

F. Niefind, S. Karande, F. Frost, B. Abel, A. Kahnt
Solvent influence on the surface morphology of P3HT thin films revealed by photoemission electron microscopy
Nanoscale Adv. 1 (2019) 3883-3886

R. Pütt, X. Qiu, P. Kozłowski, H. Gildenast, O. Linnenberg, S. Zahn, R.C. Chiechi, K.Y. Monakhov
Self-assembled monolayers of polyoxovanadates with phthalocyaninato lanthanide moieties on gold surfaces
Chem. Commun. 55 (2019) 13554-13557

P. Räcke, R. Staacke, J.W. Gerlach, J. Meijer, D. Spemann
Image charge detection statistics relevant for deterministic ion implantation
J. Phys. D: Appl. Phys. 52 (2019) 305103

E. Reisz, A. Tekle-Röttering, S. Naumov, W. Schmidt, T.C. Schmidt
Reaction of 1-propanol with ozone in aqueous media
Int. J. Mol. Sci. 20 (2019) 4165

S. Riedel, P. Hietschold, C. Krömmelbein, T. Kunschmann, R. Konieczny, W. Knolle, C.T. Mierke, M. Zink, S.G. Mayr
Design of biomimetic collagen matrices by reagent-free electron beam induced crosslinking: Structure-property relationships and cellular response
Mater. Des. 168 (2019) 107606

S. Schmitz, X. Qiu, M. Glöß, J. van Leusen, N.V. Izarova, M.A. Nadeem, J. Griebel, R.C. Chiechi, P. Kögerler, K.Y. Monakhov
Conductive self-assembled monolayers of paramagnetic $\{Co^{II}Co^{III}_4\}$ and $\{Co^{II}_4Co^{III}_2\}$ coordination clusters on Gold surfaces
Front. Chem. 7 (2019) 681

S. Schmitz, N.V. Izarova, C. Besson, J. van Leusen, P. Kögerler, K.Y. Monakhov
Ion-directed coordinative polymerization of copper(II) pyridyl-alcohol complexes through thiane functionalities
Z. Anorg. Allg. Chem. 645 (2019) 409-415

D.S. Seregin, S. Naumov, W.-Y. Chang, Y.-H. Wu, Y. Wang, N.M. Kotova, A.S. Vishnevskiy, S. Wei, J. Zhang, K.A. Vorotilov, M. Redzheb, J. Leu, M.R. Baklanov
Effect of the C-bridge on UV properties of organosilicate films
Thin Solid Films 685 (2019) 329-334

A. Solé-Daura, A. Notario-Estévez, J.J. Carbó, J.M. Poblet, C. de Graaf, K.Y. Monakhov, X. López
How does the redox state of polyoxovanadates influence the collective behavior in solution? A case study with $[I@V18O42]^{q-}$ (q = 3, 5, 7, 11 and 13)
Inorg. Chem. 58 (2019) 3881-3894

F. Strieth-Kalthoff, C. Henkel, M. Teders, A. Kahnt, W. Knolle, A. Gómez-Suárez, K. Dirian, W. Alex, K. Bergander, C. G. Daniliuc, B. Abel, D.M. Guldi, F. Glorius
Discovery of unforeseen energy-transfer-based transformations using a combined screening approach
Chem 5 (2019) 2183-2194

M. Stuckart, K.Y. Monakhov
Polyoxometalates as components of supramolecular assemblies
Chem. Sci. 10 (2019) 4364-4376

M. Tadsen, R.P. Friedrich, S. Riedel, C. Alexiou, S.G. Mayr
Contact guidance by microstructured gelatin hydrogels for prospective tissue engineering applications
ACS Appl. Mater. Interfaces 11 (2019) 7450-7458

S. Ullmann, P. Hahn, L. Blömer, A. Mehnert, C. Laube, B. Abel, B. Kersting
Dinuclear lanthanide complexes supported by a hybrid Salicylaldiminato/Calix[4]arene-Ligand: synthesis, structure, magnetic and luminescence properties of $(HNEt_3)[Ln^{III}_2(HL)(L)]$ (Ln = Sm, Eu, Gd, Tb)
Dalton Trans. 48 (2019) 3893-3905

G. Wang, Y. Zhang, C. Li, A. Lotnyk, Y. Lu, X. Shen
Self-limited growth of nanocrystals in structural heterogeneous phase-change materials during the heating process
Cryst. Growth Des. 19 (2019) 1356-1363

R. Wei, D. Breite, C. Song, D. Gräsing, T. Ploss, P. Hille, R. Schwerdtfeger, J. Matysik, A. Schulze, W. Zimmermann
Biocatalytic degradation efficiency of postconsumer polyethylene terephthalate packaging determined by their polymer microstructures
Adv. Sci. 6 (2019) 1900491

N. Wilharm, T. Fischer, F. Ott, R. Konieczny, M. Zink, A.G. Beck-Sickinger, S.G. Mayr
Energetic electron assisted synthesis of highly tunable temperature-responsive collagen/elastin gels for cyclic actuation: macroscopic switching and molecular origins
Sci. Rep. 9 (2019) 12363

P.C. With, J. Lehnert, L. Seifert, S. Dietrich, H. Krautscheid, S. Naumov, A. Prager, B. Abel, L. Prager, U. Helmstedt
Photochemical low-temperature synthesis of iron(III) oxide thin films
Appl. Surf. Sci. 493 (2019) 525-532

I. Zagoranskiy, P. Lorenz, M. Ehrhardt, K. Zimmer
Guided self-organization of nanodroplets induced by nanosecond IR laser radiation of molybdenum films on sapphire
Opt. Lasers Eng. 113 (2019) 55-61

X. Zhao, M. Ehrhardt, P. Lorenz, B. Han, K. Zimmer, L. Xu, X. Ni
Nanosecond Nd:YAG laser induced backside wet etching of NaCl with eutectic gallium-indium alloy as absorbing liquid
Surf. Int. 17 (2019) 100353

H. Zhu, M. Ehrhardt, P. Lorenz, J. Zajadacz, J. Lu, K. Zimmer
Combined effects of nanosecond laser-induced surface oxidation and nanostructure formation for selective colorization of nickel surfaces
Appl. Phys. A 125 (2019) 701

K. Zimmer, J. Zajadacz, F. Frost, A. Mayer, C. Steinberg, H.-F. Chang, J.-Y. Cheng, H.-C. Scheer
Towards fast nanopattern fabrication by local laser annealing of block copolymer (BCP) films
Appl. Surf. Sci. 470 (2019) 639-644

S. Zöhrer, A. Anders, R. Franz
Influence of Ar gas pressure on ion energy and charge state distributions in pulsed cathodic arc plasmas from Nb-Al cathodes studied with high time resolution
J. Phys. D.: Appl. Phys. 52 (2019) 055201

Conference Proceedings

2018

Th. Arnold, J.-B. Abadie, G. Böhm
Surface figure error correction by additive plasma jet machining and ion beam assisted mask transfer
Paper Nr. O1.02, Proc. EUSPEN 18th Int. Conf. & Exhibition, Venice, Italy, 04.-08.06. (2018) 47

T. Arnold, F. Frost, M. Nestler, A. Schindler, M. Zeuner
Ultra-precision ion beam and plasma jet processing for advanced optics manufacturing
Proc. Int. Symposium on Extreme Optical Manufacturing and Laser-Induced Damage in Optics, Chengdu, China, 26.-28.09. (2018)

J. Bauer, M. Ulitschka, F. Frost, T. Arnold, L. Alber, M. Sondermann, G. Leuchs
Ultra-precision surface figuring of optical aluminium devices
Paper Nr. NoM3D.3, Proc. OSA Advanced Photonics 2018, Novel Optical Materials and Applications, Zurich, Switzerland, 02.-05.07. (2018)

J. Bauer, M. Ulitschka, F. Pietag, T. Arnold
Improved ion beam tools for ultra-precision figure correction of curved aluminium mirror surfaces
Paper Nr. 10692-21, SPIE Optical Systems Design, Proc. Vol. 10692, Optical Fabrication, Testing, and Metrology VI, Frankfurt/Main, Germany, 14.-17.05. (2018) 106920M

D. Breite, A. Prager, A. Schulze
Charge selective polymer membranes with pH dependent selectivity
Paper Nr. 269, Euromembrane 2018, Valencia, Spain, 09.-13.07. (2018) 211-212

D. Breite, R. Schiewe, M. Went, A. Prager, A. Schulze
Surface hydrophilization of a microfiltration membrane using polyamide
Paper Nr. P1.10, 17th Aachener Membran Kolloquium, Aachen, Germany, 14.-15.11. (2018) 227-231

M.A. Cisternas, M. Jose Retamal, P. Saikia, N. Casanova, N. Moraga, A. Chandia, A. Alvarez, D.E. Diaz-Droguett, F. Guzman, S. Mändl, D. Manova, T.P. Corrales, U.G. Volkmann, M. Favre, H. Bhuyan
Study of phospholipid bilayers supported on Chitosan-Titanium Nitride coatings produced by plasma immersion ion implantation (PIII)
Biophys. J. 114 (2018) 105a

K. Fischer, A. Gawel, D. Rosen, M. Krause, A. Abdul Latif, J. Henke, I. Thomas, M. Kühnert, J. Griebel, A. Prager, A. Schulze
Easy dip-coating method to covalently immobilize highly photocatalytic active TiO_2 nanoparticles on a PES membrane
Paper Nr. 340, Euromembrane 2018, Valencia, Spain, 09.-13.07. (2018) 243

A. Lotnyk, M. Behrens, I. Hilmi, B. Rauschenbach
Epitaxial GeSbTe-based thin films and heterostructures: growth, microstructure and optical properties
European Phase Change and Ovonic Symposium, Catania, Italy, 23.-25.09. (2018) 54-59

M. Schmidt, D. Breite, M. Went, A. Prager, A. Schulze
Self-cleaning polymer membranes by chemical conjugation of digestive enzymes
Paper Nr. OC35, EUPOC 2018, Como, Italy, 20.-24.05. (2018) 47

M. Schmidt, D. Breite, A. Prager, A. Schulze
Self-cleaning studies on biocatalytic active polymer membranes
Paper Nr. P1.12, 17th Aachener Membran Kolloquium, Aachen, Germany, 14.-15.11. (2018) 241-248

A. Schulze, S. Glaß, M. Kühnert
Tailored synthesis of hydrogels and cryogels by the use of electron beam irradiation-mediated polymerization
Proc. 6th Belgian Symposium on Tissue Engineering, Gent, Belgium, 21.-23.11. (2018) 48

A. Schulze, I. Thomas, M. Went, D. Breite, K. Fischer, M. Schmidt, A. Prager
Directed surface engineering of polymer membranes by the use of electron beam irradiation
Paper Nr. 229, Euromembrane 2018, Valencia, Spain, 09.-13.07. (2018) 185-186

A. Schulze, L. Drößler, S. Weiß, M. Went, A. Abdul Latif, D. Breite, K. Fischer
Membrane functionalization in pilot scale: Roll-to-roll electron beam system with In-line contact angle determination
Paper Nr. P1.1, 17th Aachener Membran Kolloquium, Aachen, Germany, 14.-15.11. (2018) 183-186

C. Steier, A. Allézy, A. Anders, K. Baptiste, E. Buice, K. Chow, G. Cutler, R. Donahue, D. Filippetto, J. Harkins, T. Hellert, M. Johnson, J.-Y. Jung, S. Leemann, D. Leitner, M. Leitner, T. Luo, H. Nishimura, T. Oliver, O. Omolayo, J. Osborn, et al.
Status of the conceptual design of ALS-U
Paper Nr. THPMF06, 9th Int. Particle Accelerator Conf., Vancouver, Canada, 29.04.-04.05. (2018) 4134

N. Wolff, P. Jordt, A. Lotnyk, V. Duppel, S. Beirle, B.M. Murphy, L. Kienle
Nanostructure of multifunctional and ultra-thin FeCo/TiN (bilayer period Λ ≈ 2.3 nm) multilayer thin films
Paper Nr. 280, 19th Int. Microscopy Congress, Sydney, Australia, 09.-14.09. (2018)

S. Zöhrer, A. Anders, R. Franz
Time and energy-resolved average ion charge states in pulsed cathodic vacuum arc plasmas of Nb-Al cathodes as a function of Ar pressure
28th Int. Symposium on Discharges and Electrical Insulation in Vacuum 2 (2018) 357-360

2019

Th. Arnold, A. Maiwald, G. Böhm, M. Ehrhardt, K. Zimmer
Optical freeform generation by laser machining and plasma-assisted polishing
EPJ Web. Conf. EOS Optical Technologies 215, Munich, Germany, 24.-26.06. (2019) 03003

Th. Arnold, J. Bauer, F. Pietag
Advancements in ion beam figuring
Paper Nr. OM4A.6, Proc. OSA Optical Design and Fabrication 2019, Optical Fabrication and Testing, Washington D.C., USA, 10.-12.06. (2019)

J. Bauer, M. Ulitschka, F. Frost, T. Arnold
Figuring of optical Aluminium devices by reactive ion beam etching
EPJ Web. Conf. EOS Optical Technologies 215, Munich, Germany, 24.-26.06. (2019) 06002

M. Behrens, A. Lotnyk, J. W. Gerlach, M. Ehrhardt, P. Lorenz, B. Rauschenbach
Ultrafast epitaxial crystal growth in phase-change material thin films
Proc. European Phase-Change and Ovonic Symposium, Grenoble, France, 08.-10.09. (2019) 158-159

M. Behrens, A. Lotnyk, J.W. Gerlach, B. Rauschenbach
Vacancy distributions, optical properties and switching mechanisms in epitaxial $Ge_2Sb_2Te_5$ thin films
Z. Kristallogr. Suppl. 39 (2019) 33

M. Behrens, A. Lotnyk, J.W. Gerlach, B. Rauschenbach
Epitaxial recrystallization of 3D-bonded metastable Ge-Sb-Te based phase-change materials induced by single ns-laser pulse irradiation
Paper Nr. MS4.P007, Microscopy Conference 2019, Berlin, Germany, 01.-05.09. (2019) 164

C. Bundesmann
Schichtabscheidung mittels Ionenstrahlzerstäuben
Vakuum in Forschung und Praxis 31 (5) (2019) 25-31

C. Bundesmann, R. Feder, T. Lautenschläger, D. Spemann, H. Neumann
Das Ionenstrahlzerstäuben - Ein bewährtes Abscheideverfahren aus anderen (Streu)Winkeln betrachtet
Galvanotechnik 110 (2019) 1338-1344

C. Bundesmann
Schichten mit maßgeschneiderten Eigenschaften
J. Oberfl. Techn. 59 (2019) 46-49

C. Bundesmann, R. Feder, T. Amelal, L. Pietzonka, D. Spemann
Tailoring thin film properties by ion beam sputter deposition
14. ThGOT Thementage Grenz- und Oberflächentechnik und 6. Kolloquium Dünne Schichten in der Optik, Zeulenroda, 12.-14.03. (2019)

C. Eichhorn, F. Scholze, C. Bundesmann, D. Spemann, H. Neumann, H. Leiter
Two-photon laser-induced fluorescence diagnostics of a radiofrequency ion thruster: Measurements in Xenon and Krypton
Paper Nr. IEPC-2019-503, 36th Int. Electric Propulsion Conf., Vienna, Austria, 15.-20.09. (2019)

C. Eichhorn, F. Scholze, C. Bundesmann, D. Spemann, H. Neumann, H. Leiter
Laser-induced fluorescence in the plume of a radiofrequency ion thruster: Measurements and excitation schemes
Paper Nr. AIAA-2019-4168, AIAA Propulsion and Energy Forum and Exhibition, Indianapolis, IN, USA, 19.-22.08. (2019)

A. Finzel, G. Dornberg, S. Görsch, M. Mitzschke, J. Bauer, F. Frost
Realization of depth reference samples with surfaces amplitudes between 0.1 nm and 5 nm
EPJ Web. Conf. EOS Optical Technologies 215, Munich, Germany, 24.-26.06. (2019) 03004

S. Liedtke-Grüner, C. Grüner, A. Lotnyk, M. Mensing, J.W. Gerlach, P. Schumacher, B. Rauschenbach
Texture formation in obliquely deposited metal thin films
Z. Kristallogr. Suppl. 39 (2019) 69

P. Lorenz, I. Zagoranskiy, M. Ehrhardt, K. Zimmer
Laser-induced large area sub-µm and nanostructuring of dielectric surfaces and thin metal layer
Proc. SPIE 10906, Laser-based Micro- and Nanoprocessing XIII (2019) 109060T

A. Lotnyk, T. Dankwort, I. Hilmi, L. Kienle, B. Rauschenbach
In situ observations of the reversible vacancy ordering in layered chalcogenide-based thin films
Proc. European Phase-Change and Ovonic Symposium, Grenoble, France, 08.-10.09. (2019) 86-87

A. Lotnyk, U. Ross, T. Dankwort, L. Kienle, B. Rauschenbach
In situ observation of dynamic reconfiguration of van der Waals interfaces in 2D-bonded Ge-Sb-Te phase-change memory alloys
Paper Nr. MS4.P001, Microscopy Conference 2019, Berlin, Germany, 01.-05.09. (2019) 153-154

D. Manova, S. Mändl
In situ X-ray diffraction measurements during low energy ion beam nitriding & etching
Z. Kristallogr. Suppl. 39 (2019) 47

M. Mensing, P. Schumacher, C. Grüner, S. Herath, A. Lotnyk, J.W. Gerlach, B. Rauschenbach
Ion beam assisted thin film growth using mass separated low-energy nitrogen ions
Z. Kristallogr. Suppl. 39 (2019) 56

G. Mirschel, O. Daikos, C. Steckert, T. Scherzer
Monitoring of the application weight of laminating adhesives to PUR foam by NIR chemical imaging
Proc. 18th Int. Conf. on Near Infrared Spectrosc. (2019) 163-168
H. Mueller, G. Böhm, Th. Arnold
Next generation of a linear chirped slope profile fabricated by plasma jet machining
Proc. SPIE 11171, Sixth European Seminar on Precision Optics Manufacturing (2019) 111710A

M. Schmidt, D. Breite, A. Prager, A. Schulze
Bioactive self-cleaning PVDF membrane filters
Paper Nr. BIO-P126, European Polymer Congress 2019, Heraklion, Greece, 09.-14.06. (2019) 723

F. Scholze, D. Spemann, D. Feili
Design and performance test of a RF plasma bridge neutralizer
Paper Nr. IEPC-2019-475, 36th Int. Electric Propulsion Conf., Vienna, Austria, 15.-20.09. (2019)

F. Scholze, C. Bundesmann, C. Eichhorn, D. Spemann
Determination of the beam divergence of a gridded ion thruster using the AEPD platform
Paper Nr. IEPC-2019-738, 36th Int. Electric Propulsion Conf., Vienna, Austria, 15.-20.09. (2019)

M. Ulitschka, J. Bauer, F. Frost, T. Arnold
Reactive ion beam etching-based finishing of optical Aluminium surfaces
EPJ Web. Conf. EOS Optical Technologies 215, Munich, Germany, 24.-26.06. (2019) 04002

M. Ulitschka, J. Bauer, F. Frost, T. Arnold
Reactive ion beam etching-based planarization of optical aluminium surfaces
Proc. SPIE 11032, EUV and X-ray Optics: Synergy between Laboratory and Space VI (2019) 110320D

V.V. Yashchuk, I. Lacey, Th. Arnold, H. Paetzelt, S. Rochester, F. Siewert, P.Z. Takacs
Investigation on lateral resolution of surface slope profilers
Proc. SPIE 11109, Advances in Metrology for X-Ray and EUV Optics VIII (2019) 111090M

Talks

2018

*B. Abel**
Counter-ion stabilized carbenes and room-temperatur conversion of carbon dioxide in ionic liquids: Theory and experiment
Colloquium of Physikalische und Theoretische Chemie, Freie Universität Berlin, Berlin, Germany, 12.12.2018

*B. Abel**
Macromolecular organic compounds from the depths of Enceladus
Seminar, UC Berkeley, Berkeley, CA, USA, 11.09.2018

*B. Abel**
Macromolecular organic compounds from the depths of Enceladus
GDCh-Kolloquium, Universität Potsdam, Potsdam, Germany, 26.11.2018

*B. Abel**
Peptide/protein aggregation at surfaces: Blessing or curse?
Miller Lunch Lectures, UC Berkeley, Berkeley, CA, USA, 18.09.2018

*B. Abel**
Peptides at Surfaces
Seminar, Monash University, Melbourne, Australia, 20.11.2018

T. Albert, A.J. Dittrich, T. Arnold, A. Lehmann, P.G. Braun*
Atmosphärisches Plasma zur Desinfektion von Schneidmesseroberflächen
9. Leipziger Tierärztekongress, Leipzig, Germany, 18.-20.01. 2018

T. Albert, A.J. Dittrich, T. Arnold, A. Lehmann, P.G. Braun*
Antibakterielle Wirkung von kaltem atmosphärischem Plasma auf Slicermesseroberflächen
59. Arbeitstagung des Arbeitsgebietes Lebensmittelsicherheit und Verbraucherschutz der DVG, Garmisch-Partenkirchen, Germany, 25.-28.09.2018

*A. Anders**
Plasma-based and plasma-assisted deposition: A brief overview including cathodic arcs and magnetron sputtering
Kolloquium, Technische Universität Bergakademie Freiberg, Freiberg, Germany, 07.05.2018

*A. Anders**
Plasma and ion beam tools to engineer surfaces and coatings
2018 IEEE 8th Int. Conf. on Nanomaterials: Applications & Properties, Zatoka, Ukraine, 09.-14.09.2018

*A. Anders**
Plasma potential distribution and electron heating in sputtering magnetrons
Physikalisches Kolloquium, Christian Albrechts Universität zu Kiel, Kiel, Germany, 05.05.2018

*A. Anders**
Ionization and transport in magnetrons
XXV. Erfahrungsaustausch Oberflächentechnologien mit Plasma- und Ionenstrahlprozessen, Mühlleithen, Germany, 19.-23.03.2018

*A. Anders**
Plasma physics of sputtering magnetrons revisited
16th Int. Conf. on Plasma Surface Engineering, Garmisch-Partenkirchen, Germany, 16.-21.09.2018

*A. Anders**
Electron heating in sputtering magnetrons
2018 Annual Meeting and Exhibition, Northern California Chapter of the AVS, San Jose, CA, USA, 22.02.2018

*A. Anders**
Metal plasmas for thin film synthesis
3rd Conf. on Advanced Functional Materials, Norrköping, Sweden, 21.-23.08.2018

*A. Anders**
Advanced magnetron sputtering for thin film deposition
Colloquium, Argonne National Laboratory, Argonne, IL, USA, 18.02.2018

*A. Anders**
Current-voltage-time characteristics of HiPIMS discharges revisited
AVS 65th Int. Symposium & Exhibition 2018, Long Beach, CA, USA, 21.-26.10.2018

*A. Anders, Y. Yang**
Properties of spokes observed with a linear magnetron
9th Int. Conf. on Fundamentals and Industrial Applications of HIPIMS, Sheffield, UK, 25.-28.06.2018

Th. Arnold, M. Ulitschka, J. Bauer*
Ionenstrahlgestützte Formgebung und Planarisierung von Aluminiumoptiken
13. ThGOT Thementage Grenz- und Oberflächentechnik mit 11. Thüringer Biomaterial-Kolloquium, Zeulenroda, Germany, 13.-15.03.2018

Th. Arnold, G. Böhm*
Metrology systems for asphere and freeform production in IOM
CCUPOB 9th High Level Expert Meeting - Asphere Metrology on Joint Investigations, Braunschweig, Germany, 28.02.-01.03.2018

Th. Arnold, G. Böhm, H. Paetzelt*
Plasma-assisted, cost-effective optical freeform manufacturing
OPTONET Workshop Ultra Precision Manufacturing of Aspheres & Freeforms, Jena, Germany, 19.-20.09.2018

Th. Arnold, J.-B. Abadie, G. Böhm*
Surface figure error correction by additive plasma jet machining and ion beam assisted mask transfer
EUSPEN 18th Int. Conf. & Exhibition, Venice, Italy, 04.-08.06. 2018

Th. Arnold, G. Böhm, H. Paetzelt*
Plasma jet - based process chains for freeform optics manufacturing
European Optical Society Biennial Meeting 2018, Delft, Netherlands, 08.-12.10.2018

J. Bauer, M. Ulitschka, F. Pietag, F. Frost, T. Arnold*
Formfehlerkorrektur einer stark gekrümmten Al-Spiegeloptik mit reaktiven Sub-mm-Ionenstrahlwerkzeugen
XXV. Erfahrungsaustausch Oberflächentechnologie mit Plasma- und Ionenstrahlprozessen, Mühlleithen, Germany, 20.-23.03.2018

J. Bauer, M. Ulitschka, F. Pietag, T. Arnold*
Ultra-precision figure correction of a strongly curved aluminium mirror
SPIE Optical Systems Design, Optical Fabrication, Testing, and Metrology VI, Frankfurt/Main, Germany, 14.-17.05.2018

J. Bauer, M. Ulitschka, F. Pietag, F. Frost, T. Arnold*
Customized ion beam technologies for ultra-precision surface machining of optical devices
16th Int. Conf. on Plasma Surface Engineering, Garmisch-Partenkirchen, Germany, 17.-21.09.2018

J. Bauer, M. Ulitschka, F. Pietag, F. Frost, T. Arnold*
Figure error correction of aluminium mirrors
4th Int. Summer School on Trends in Ultra-Precision Surface Engineering, Leipzig, Germany, 03.-07.09.2018

J. Bauer, M. Ulitschka, F. Frost, T. Arnold, L. Alber, M. Sondermann, G. Leuchs*
Ultra-precision surface figuring of optical aluminium devices
OSA Advanced Photonics Congress, Zurich, Switzerland, 02.-05.07.2018

D. Breite, A. Prager, A. Schulze*
Charge selective polymer membranes with pH dependent selectivity
Euromembrane 2018, Valencia, Spain, 09.-13.07.2018

S.P. Brühl, S. Simison, L. Escalada, D. Manova, S, Mändl, L. Vaca, F. Soldera, M.A. Guitar*
Corrosion and wear properties of plasma nitrided 316L stainless steel
Materials Science Engineering - European Congress and Exhibition on Advanced Materials and Processes, Darmstadt, Germany, 26.-28.09.2018

C. Bundesmann, R. Feder, T. Lautenschläger, L. Pietzonka, D. Spemann, H. Neumann*
Unravelling the systematics in ion beam sputter deposition
Symposium OCLA 2018 - Optical Coatings for Laser Applications, Buchs SG, Switzerland, 12.04.2018

C. Bundesmann, F. Scholze, D. Spemann, F. Frost, H. Neumann*
Ion beam source developments at IOM
Kolloquium, Forschungsinstitut RhySearch, Buchs SG, Switzerland, 11.04.2018

*C. Bundesmann**
Mehr als 50 Jahre Ionenquellenentwicklung in Leipzig (am Wissenschaftsstandort Permoserstraße)
XXV. Erfahrungsaustausch Oberflächentechnologie mit Plasma- und Ionenstrahlprozessen, Mühlleithen, Germany, 20.-23.03.2018

*C. Bundesmann**
Mehr als 50 Jahre Entwicklung und Anwendung von Ionenstrahlquellen am Wissenschaftsstandort Permoserstraße (Ein Beitrag zur Geschichte des IOM)
Kolloquium, Leibniz Institute of Surface Engineering (IOM), Leipzig, Germany, 27.09.2018

*C. Bundesmann**
The systematics of ion beam sputter deposition
Summer School on the Physics of Plasma-Surface Interactions, National Research Nuclear University MEPhI, Moscow, Russia, 16.-20.07.2018

M. Burkhardt, F. Koch, A. Kalies, L. Erdmann, M. Helgert, A. Pesch, O. Schönbrodt, F. Frost, F. Finzel, D. Lehr, A. Gatto, S. Sinzinger*
Angepasste Interferenzgitter für spektroskopische und Laser-Anwendungen von EUV bis NIR
119. Jahrestagung der deutschen Gesellschaft für angewandte Optik, Aalen, Germany, 21.-26.05.2018

M. Demmler, M. Nestler, F. Frost*
Patterning and pattern transfer with ion beam etching
SPIE Advanced Lithography, San Jose, CA, USA, 25.02.-01.03.2018

M. Deppe, F. Tacken, J.W. Gerlach, D. Reuter, D.J. As*
Structural and optical characterisation of germanium doped cubic $Al_xGa_{1-x}N$ grown by molecular beam epitaxy
DPG-Frühjahrstagung der Sektion Kondensierte Materie, Berlin, Germany, 11.-16.03.2018

G. Dornberg, A. Finzel, F. Koch, D. Lehr, T. Glaser, F. Frost*
Entwicklung einer RIBE-Technologie zur Strukturierung von dielektrischen Schichtsystemen mit höchster Tiefengenauigkeit
XXV. Erfahrungsaustausch Oberflächentechnologie mit Plasma- und Ionenstrahlprozessen, Mühlleithen, Germany, 20.-23.03.2018

*M. Ehrhardt, B. Han, I. Zagoranskiy, F. Frost, P. Lorenz, K. Zimmer**
Generation of laser-induced periodic surface structures (LIPSS) in fused silica by single NIR nanosecond laser pulse irradiation in confinement
8th Int. Workshop on Laser Induced Periodic Surface Structures, Bochum, Germany, 27.-28.09.2018

C. Eichhorn, F. Scholze, C. Bundesmann, D. Spemann, H. Leiter, H. Neumann*
Laser induced fluorescence diagnostics of the radiofrequency ion thruster RIT-10: Current activities at IOM
7th Russian-German Conf. on Electric Propulsion and Their Application, Rauischholzhausen, Germany, 21.-26.10.2018

C. Eichhorn, F. Scholze, C. Bundesmann, D. Spemann, H. Neumann*
Non-intrusive plasmadiagnostic activities at IOM: Present developments
XXV. Erfahrungsaustausch Oberflächentechnologie mit Plasma- und Ionenstrahlprozessen, Mühlleithen, Germany, 20.-23.03.2018

K. Fischer, P. Schulz, I. Atanasov, A. Gawel, D. Rosen, M. Krause, A. Abdul Latif, J. Henke, I. Thomas, M. Kühnert, J. Griebel, A. Prager, A. Schulze*
Easy dip-Ccoating method to covalently immobilize highly photocatalytic active TiO_2 Nanoparticles on a PES Membrane
Euromembrane 2018, Valencia, Spain, 09.-13.07.2018

*F. Frost**
Ion beam assisted patterning and smoothing of optical surfaces with sub-nanometer precision
4th Int. Summer School on Trends in Ultra-Precision Surface Engineering, Leipzig, Germany, 03.-07.09.2018

*F. Frost**
Reactive ion beam etching (RIBE) for the manufacturing of highly precise optical elements
2nd NTG IBF Conf. on the occasion of the 50th company anniversary of NTG, Gelnhausen, Germany, 21.09.2018

*F. Frost**
Reactive ion beam etching (RIBE) for the manufacturing of ultraprecise optical elements
5th anniversary scia Systems GmbH, Chemnitz, Germany, 05.-06.06.2018

*F. Frost**
Reaktives Ionenstrahlätzen (RIBE) für die Herstellung ultrapräziser optischer Elemente
XXV. Erfahrungsaustausch Oberflächentechnologie mit Plasma- und Ionenstrahlprozessen, Mühlleithen, Germany, 20.-23.03.2018

J.W. Gerlach, P. Schumacher, M. Mensing, A. Lotnyk, S. Rauschenbach, B. Rauschenbach*
Generation of an energy and mass selected hyperthermal ion beam for investigation of ion-assisted thin film growth processes
15th European Vacuum Conf., Geneva, Switzerland, 17.-22.06.2018

J.W. Gerlach, P. Schumacher, M. Mensing, A. Lotnyk, S. Rauschenbach, B. Rauschenbach*
An energy and mass selected hyperthermal ion beam for ion-assisted thin film deposition purposes
Workshop on Ion and Particle Beams & MAT Science Week, Darmstadt, Germany, 24.-27.04.2018

S. Glaß, A. Schulze, B. Abel*
Poly(ethylene glycol) diacrylate hydrogels used as carriers for photodynamic therapy Photosensitizers
Polymers: Design, Function and Application, Barcelona, Spain, 21.-23.03.2018

S.Glaß, B. Trinklein, B. Abel, A. Schulze*
TiO_2 as photosensitizer and photoinitiator for the synthesis of photoactive TiO_2-PEGDA hydrogels
6th Belgian Symposium on Tissue Engineering, Ghent, Belgium, 22.-23.11.2018

*S. Glaß, T. Pelras, C. Elsner, A. Schulze, B. Abel, T. Scherzer**
Transparent hydrogels made from poly(ethylene glycol) diacrylate as drug delivery materials for photosensitizer systems
5th European Symposium of Photopolymer Science (ESPS 2018), Mulhouse, France, 03.-06.09.2018

S. Glaß, A. Schulze, B. Abel*
Poly(ethylene glycol) diacrylate hydrogels for application as antimicrobial wound patches
Int. Conf. on Biomaterials 2018, London, UK, 16.08.-18.08.2018

S. Görsch, A. Nickel, A. Finzel, G. Dornberg, F. Frost*
Generation of rotationally symmetric removal using (R)IBE on large surfaces: Mathematical introduction and practical realization
XXV. Erfahrungsaustausch Oberflächentechnologie mit Plasma- und Ionenstrahlprozessen, Mühlleithen, Germany, 20.-23.03.2018

C. Grüner, S. Liedtke-Grüner, S.G. Mayr, B. Rauschenbach*
Morphology of thin films formed by oblique physical vapor deposition
Materials Science Engineering - European Congress and Exhibition on Advanced Materials and Processes, Darmstadt, Germany, 26.-28.09.2018

C. Grüner, S. Liedtke, B. Rauschenbach*
Physical vapor deposition at oblique angles
DPG-Frühjahrstagung der Sektion Kondensierte Materie, Berlin, Germany, 11.-16.03.2018

C. Grüner, S. Liedtke, S.G. Mayr, B. Rauschenbach*
Anisotropies in on-lattice simulations of thin film growth
Leibniz MMS Days 2018, Leipzig, Germany, 28.02.-02.03.2018

P. Hietschold, M. Deuflhard, S. Riedel, M. Zink, S.G. Mayr*
Characteristics of modified hydrogels with and without incorporated magnetic nanoparticles
Untergruppentreffen des DFG-Schwerpunktsprogramm 1681, Jülich, Germany, 12.06.2018

P. Hietschold, S. Riedel, M. Deuflhard, M. Zink, S.G. Mayr*
Collagen hydrogels: Electron beam induced modification and nanoparticle composites
6. Kolloquium des DFG-Schwerpunktsprogramm 1681, Benediktbeuern, Germany, 28.09.2018

T. John, B. Abel, L.L. Martin*
Amyloid-like aggregation of the antimicrobial peptide uperin 3.5 and its selectivity towards membranes
7th EuCheMS Chemistry Congress, Liverpool, UK, 26.-30.08.2018

T. John, B. Abel, L.L. Martin*
Peptide aggregation near membranes
7th EuCheMS Chemistry Congress, European Young Chemist Award Competition Session, Liverpool, UK, 26.-30.08.2018

A. Kahnt, S. Eigler, R. Fluynt, S. Naumov, B. Abel*
Radiation chemical GO reduction kinetics and mechanisms
Bunsentagung 2018, Hannover, Germany, 10.-12.05.2018

F. Kazemi, T. Arnold*
Ultra-precise machining of surfaces using microwave-driven reactive plasma etching
XXVI. Erfahrungsaustausch Oberflächentechnologie mit Plasma- und Ionenstrahlprozessen, Mühlleithen, Germany, 20.-23.03.2018

T. Lautenschläger, D. Spemann, J.W. Gerlach, E. Thelander, M. Mensing, L. Pietzonka, E. Rohkamm, C. Bundesmann*
Reactive ion beam sputter deposition of TiO_2: Influence of target material and sputter gas
XXV. Erfahrungsaustausch Oberflächentechnologie mit Plasma- und Ionenstrahlprozessen, Mühlleithen, Germany, 20.-23.03.2018

J. Lehnert, D. Spemann, M.H. Hatahet, S. Mändl, P. With, M. Mensing, P. Schumacher, B. Rauschenbach*
Structured graphene films on silicon dioxide synthesized by carbon ion implantation
XXV. Erfahrungsaustausch Oberflächentechnologie mit Plasma- und Ionenstrahlprozessen, Mühlleithen, Germany, 20.-23.03.2018

S. Liedtke, Ch. Grüner, J.W. Gerlach, A. Lotnyk, B. Rauschenbach*
Texture, morphology and microstructure of nanostructured titanium thin films grown by oblique angle deposition
DPG-Frühjahrstagung der Sektion Kondensierte Materie, Berlin, Germany, 11.-16.03.2018

S. Liedtke-Grüner, C. Grüner, J.W. Gerlach, A. Lotnyk, B. Rauschenbach*
Growth of obliquely deposited Titanium thin films
15th European Vacuum Conf., Geneva, Switzerland, 17.-22.06.2018

S. Liedtke-Grüner, C. Grüner, J.W. Gerlach, M. Mensing, P. Schumacher, A. Lotnyk, B. Rauschenbach*
Crystallinity and texture of nanostructured Molybdenum thin films deposited obliquely at room temperature
Materials Science Engineering - European Congress and Exhibition on Advanced Materials and Processes, Darmstadt, Germany, 26.-28.09.2018

*P. Lorenz, M. Klöppel, I. Zagoranskiy, K. Zimmer**
From statistic to deterministic nanostructures in fused silica induced by nanosecond laser radiation
10th CIRP Conf. on Photonic Technologies, Fürth, Germany, 03.-06.09.2018

M. Lorenz, V. Lazenka, C. Patzig, S. Selle, D. Hirsch, T. Höche, K. Temst, M. Grundmann*
Origin of high magnetoelectric coupling in multiferroic $BiFeO_3$-$BaTiO_3$ superlattices
14th Int. Ceramics Congress, Perugia, Italy, 04.-08.06.2018

P. Lorenz, X. Zhao, M. Ehrhardt, J. Zajadacz, I. Zagoransky, K. Zimmer, B. Han*
Nanostructuring of dielectric surfaces by nanosecond laser irradiation
DPG-Frühjahrstagung der Sektion Kondensierte Materie, Berlin, Germany, 11.-16.03.2018

*P. Lorenz, L. Bayer, N. Kehagias, K. Zimmer**
Laser patterning of metal cylinders for roll to toll application
11th Int. Conf. on Photo-Excited Processes and Applications, Vilnius, Lithuania, 10.-14.09.2018

*P. Lorenz, L. Bayer, T. Tachtsidis, K. Zimmer**
Laser patterning of hierarchical structures on metal cylinders for UV-NIL replication
10th CIRP Conf. on Photonic Technologies, Fürth, Germany, 03.-06.09.2018

*A. Lotnyk**
Epitaxial GeSbTe-based thin films and heterostructures: Growth, microstructure and optical properties
European Phase Change and Ovonic Symposium, Catania, Italy, 23.-25.09.2018

*A. Lotnyk**
Nanoscale phenomena in GeSbTe-based thin films studied by advanced electron microscopy
Sino-German Symposium on Electronic and Memory Materials, Xian Jiaotong University, Xian, China, 05.-07.09.2018

*A. Lotnyk**
Interfacial phenomena in layered chalcogenide-based materials studied by advanced electron microscopy
3rd Sino-German Symposium: Advanced Electron Microscopy and Spectroscopy-Interface Structure and Property of Materials, Tsinghua University, Beijing, China, 24.-28.09.2018

A. Lotnyk
Epitaxial GeSbTe-based thin films and heterostructures: Growth, microstructure, optical properties and switching
Seminar, Ningbo University, Ningbo, China, 15.11.2018

A. Lotnyk, U. Ross, T. Dankwort, I. Hilmi, L. Kienle, B. Rauschenbach*
In situ observations on dynamic reconfiguration of bilayer defects in van der Waals bonded Ge-Sb-Te based alloys
DPG-Frühjahrstagung der Sektion Kondensierte Materie, Berlin, Germany, 11.-16.03.2018

S. Mändl, D. Manova*
Time resolved OES during high voltage pulses
XXV. Erfahrungsaustausch Oberflächentechnologie mit Plasma- und Ionenstrahlprozessen, Mühlleithen, Germany, 20.-23.03.2018

D. Manova, S. Mändl*
Development of in-situ x-ray diffraction measurements during low energy ion beam etching
Workshop on Ion and Particle Beams & MAT Science Week, Darmstadt, Germany, 24.-27.04.2018

D. Manova, S. Mändl*
In-situ XRD during ion implantation and ion etching of Austenitic stainless steel
Materials Science Engineering - European Congress and Exhibition on Advanced Materials and Processes, Darmstadt, Germany, 26.-28.09.2018

D. Manova, S. Mändl*
In-situ x-ray diffraction measurements during low energy ion beam etching
16th Int. Conf. on Plasma Surface Engineering, Garmisch-Partenkirchen, Germany, 17.-21.09.2018

D. Manova, D. Hirsch, S. Mändl*
In-situ XRD during ion implantation and ion etching
XXV. Erfahrungsaustausch Oberflächentechnologie mit Plasma- und Ionenstrahlprozessen, Mühlleithen, Germany, 20.-23.03.2018

A. Mayer, W. Ai, J. Rond, J. Stabs, C. Steinberg, M. Papenheim, H.-C. Scheer, M. Torman, A. Cian, J. Zajadacz, K. Zimmer*
Electrically-assisted nanoimprint of block-copolymers
62nd Int. Conf. on Electron, Ion and Photon Beam Technology and Nanofabrication, Rio Mar, Puerto Rico, 29.05.-01.06.2018

M. Mensing, P. Schumacher, J.W. Gerlach, S. Rauschenbach, S. Herath, A. Lotnyk, B. Rauschenbach*
Investigation of the influence of molecular and atomic nitrogen ion species during epitaxial nitride thin film growth
15th European Vacuum Conf., Geneva, Switzerland, 17.-22.06.2018

M. Mitzschke, F. Carstens, H. Ehlers, F. Frost*
Optisches in-situ Monitoring von reaktiven Ionenstrahlprozessen: Fortschrittsbericht
XXV. Erfahrungsaustausch Oberflächentechnologie mit Plasma- und Ionenstrahlprozessen, Mühlleithen, Germany, 20.-23.03.2018

M. Panjan, A. Anders*
The role of spokes on energy and transport of ions in magnetron sputtering
15th European Vacuum Conf., Geneva, Switzerland, 17.-22.06.2018

T. Pelras, S. Glaß, A. Schulze, C. Elsner, T. Scherzer, B. Abel*
UV-cured hydrogels based on low-molecular weight poly(ethylene glycol) diacrylate for use as transparent drug delivery system
Int. Symposium of Photopolymer Science, Wuxi, China, 23.-25.04.2018

P. Räcke, D. Spemann, N. Raatz, R. Staacke, J.W. Gerlach, B. Rauschenbach, J. Meijer*
A concept for deterministic ion implantation by image charge detection
14th Int. Conf. on Nuclear Microprobe Technology and Applications, Guildford, UK, 08.-13.07.2018

P. Räcke, D. Spemann, J.W. Gerlach, B. Rauschenbach, J. Meijer*
A concept for deterministic ion implantation by image charge detection
21st Int. Conf. on Ion Beam Modification of Materials, San Antonio, TX, USA, 24.-29.06.2018

S. Riedel, S.G. Mayr*
Electron-beam-induced crosslinking of hydrogels: Modifications and application
3rd Soft Matter Day 2018, Leipzig, Germany, 06.07.2018

S. Riedel, B. Heyart, K. Apel, E.I. Wisotzki, S.G. Mayr*
Smart gelatin hydrogels: Modification by electron irradiation towards stimuli-responsive elements
2018 MRS Spring Meeting & Exhibit, Phoenix, AZ, USA, 02.-06.04.2018

S. Riedel, K. Bela, M. Tadsen, C. Krömmelbein, C. Suckfüll, J. Zajadacz, T. Kunschmann, E.I. Wisotzki, S.G. Mayr*
Electron irradiation assisted crosslinking of hydrogels: Reagent-free modification towards functional scaffolds
2018 MRS Spring Meeting & Exhibit, Phoenix, AZ, USA, 02.-06.04.2018

M. Schmidt, D. Breite, M. Went, A. Prager, A. Schulze*
Self-cleaning polymer membranes by chemical conjugation of digestive enzymes
EUPOC 2018, Como, Italy, 20.-24.05.2018

F. Scholze, C. Bundesmann, C. Eichhorn, D. Spemann*
Determination of the beam divergence of a gridded ion thruster using the AEPD platform
7th Russian-German Conf. on Electric Propulsion and Their Application, Rauischholzhausen, Germany, 21.-26.10.2018

F. Scholze, D. Feili, D. Spemann*
RF plasma bridge neutralizer design and tests
7th Russian-German Conf. on Electric Propulsion and Their Application, Rauischholzhausen, Germany, 21.-26.10.2018

*A. Schulze**
Maßgeschneidertes Oberflächendesign von Polymermembranen für reale Anwendungen
GDCh Kolloquium Universität Leipzig, Leipzig, Germany, 25.10.2018

*A. Schulze**
Gezielte Oberflächenmodifizierung von Polymermembranen für die Wasseraufbereitung
VCI Landesverband Nordost, Gatersleben, Germany, 24.10.2018

A. Schulze, I. Thomas, M. Went, D. Breite, K. Fischer, M. Schmidt, A. Prager*
Directed surface engineering of polymer membranes by the use of electron beam irradiation
Euromembrane 2018, Valencia, Spain, 09.-13.07.2018

A. Schulze, S. Glaß, M. Kühnert*
Tailored synthesis of hydrogels and cryogels by the use of electron beam irradiation-mediated polymerization
6th Belgian Symposium on Tissue Engineering, Gent, Belgium, 21.-23.11.2018

*A. Schulze**
Directed surface engineering of porous polymer materials by the use of electron beam irradiation
Polymer Chemistry and Biomaterials Seminar, Gent University, Gent, Belgium, 25.09.2018

P. Schumacher, M. Mensing, J.W. Gerlach, S. Rauschenbach, B. Rauschenbach*
Energy and mass selective ion beam assisted epitaxy for deposition of thin nitride films
DPG-Frühjahrstagung der Sektion Kondensierte Materie, Berlin, Germany, 11.-16.03.2018

D. Spemann, P. Räcke, J. Meijer, J.W. Gerlach, B. Rauschenbach*
Current status of the deterministic ion implanter of the Leibniz Joint Lab at IOM
XXV. Erfahrungsaustausch Oberflächentechnologie mit Plasma- und Ionenstrahlprozessen, Mühlleithen, Germany, 20.-23.3.2018

M. Ulitschka, J. Bauer, F. Frost, T. Arnold*
Reactive ion beam planarization process of metal mirror surfaces
4th Int. Summer School on Trends in Ultra-Precision Surface Engineering, Leipzig, Germany, 03.-07.09.2018

M. Ulitschka, J. Bauer, F. Frost, T. Arnold*
Ultra-precision processing of optical aluminium surfaces with reactive sub-aperture ion beam techniques
Special Interest Group Meeting: Structured & Freeform Surfaces, École Normale Supérieure Paris-Saclay, Cachan, France, 27.-29.11.2018

M. Ulitschka, J. Bauer, Th. Arnold*
Study of reactive ion beam planarization process of a negative tone resist for smoothing aluminium mirrors
DPG-Frühjahrstagung der Sektion Kondensierte Materie, Berlin, Germany, 11.-16.03.2018

M. Ulitschka, J. Bauer, F. Frost, Th. Arnold*
Eigenschaftsoptimierung Novolak-basierter Photolacke für die Ionenstrahlplanarisierung von Al-Optiken
XXV. Erfahrungsaustausch Oberflächentechnologie mit Plasma- und Ionenstrahlprozessen, Mühlleithen, Germany, 20.-23.03.2018

G. Wang, Q. Nie, X. Shen, Y. Lu, A. Lotnyk*
Controllable crystallization and interface microstructure stability of new phase-change films
15th Int. Conf. on the Physics of Non-Crystalline Solids & 14th European Society of Glass Conf., Saint Malo, France, 09.-13.07.2018

A. Weidt, S.G. Mayr, M. Zink*
Organization of fibronectin and NIH/3T3 fibroblasts on bulk microgrooved TiO_2
DPG-Frühjahrstagung der Sektion Kondensierte Materie, Berlin, Germany, 11.-16.03.2018

*S. Zahn**
Deep eutectic solvents: Similia similibus solvuntur?
27th Conf. on Molten Salts and Ionic Liquids, Lisboa, Portugal, 07.-12.10.2018

*S. Zahn**
Modellierung chemischer Reaktionen am Computer
Tag der Technik, Landesschule Pforta, Naumburg, Germany, 25.10.2018

K. Zimmer, C. Petersen, J. Zajadacz, P. Lorenz*
Origami folding of laser-cut polymer foils
2nd Int. Workshop on Advanced 3D Patterning, Dresden, Germany, 04.-05.10.2018

K. Zimmer, J. Zajadacz, A. Mayer, C. Steinberg, H.-C. Scheer*
Towards fast nanopattern fabrication by local laser annealing of diblock copolymer (BiCBP) films
2018 E-MRS Spring Meeting, Strasbourg, France, 18.-22.06.2018

B. Zitouni, S. Mändl, D. Manova*
Ions and surface interactions: a new erosion modelling approach
7th Russian-German Conf. on Electric Propulsion and Their Application, Rauischholzhausen, Germany, 21.-26.10.2018

S. Zöhrer, A. Anders, R. Franz*
Time and energy-resolved average ion charge states in pulsed cathodic vacuum arc plasmas of Nb-Al cathodes as a function of Ar pressure
28th Int. Symposium on Discharges and Electrical Insulation in Vacuum, Greifswald, Germany, 23.-28.09.2018

*S. Zöhrer, A. Anders, D. Holec, R. Franz**
Time-resolved analysis of the cathodic arc plasma from Nb-Al cathodes
AVS 65th Int. Symposium & Exhibition 2018, Long Beach, CA, USA, 21.-26.10.2018

S. Zöhrer, A. Anders, R. Franz*
Time-resolved ion energy and charge state distributions in pulsed cathodic arc plasmas of Nb-Al cathodes in high vacuum
45th Int. Conf. on Metallurgical Coatings and Thin Films, San Diego, CA, USA, 23.-27.04.2018

2019

*A. Anders**
Metal plasmas for thin film synthesis
XXVI. Erfahrungsaustausch Oberflächentechnologie mit Plasma- und Ionenstrahlprozessen, Mühlleithen, Germany, 05.-07.03.2019

*A. Anders**
Electron heating in magnetron sputtering
19. Fachtagung für Plasmatechnologie, Cottbus, Germany, 17.-19.06.2019

*A. Anders**
Plasma-target interactions in magnetron sputtering
15th Int. Symposium on Sputtering & Plasma Processes, Kanazawa, Japan, 11.-14.06.2019

*A. Anders**
Magnetron sputtering: The special role of localized electron heating and supply of neutrals
Int. Surfaces, Coatings and Interfaces Conf. SurfCoat Korea 2019, Incheon, South Korea, 27.-29.03.2019

*A. Anders**
Plasmas in physical vapor deposition, including arcs and HiPIMS
46th Int. Conf. on Metallurgical Coatings und Thin Films, San Diego, CA, USA, 19.-24.05.2019

*A. Anders**
Plasma physics of sputtering magnetrons
21st Int. Conf. on Surface Modification of Materials by Ion Beams, Tomsk, Russia, 25.-30.08.2019

*A. Anders**
Metal plasmas for thin film synthesis
Kolloqium der Montanuniversität Leoben, Leoben, Austria, 24.04.2019

*A. Anders**
Magnetron sputtering extended: HiPIMS, plasma instabilities, and more news about on old theme
Colloqium at Applied Materials Inc., Santa Clara, CA, USA, 29.05.2019

*A. Anders**
Part 1: Localized electron heating and supply of neutrals in magnetron sputtering, Part 2: Plasma and ion beam technologies at the Leibniz Institute for Surface Engineering (IOM) Leipzig
Kolloqium, Evatec AG, Trübbach, Switzerland, 24.01.2019

*A. Anders**
Physical vapor deposition: Affecting film microstructure by plasma methods
Kolloqium des Fraunhofer-Instituts für Mikrostruktur von Werkstoffen und Systemen, Halle (Saale), Germany, 28.01.2019

Th. Arnold, J. Bauer, F. Pietag*
Advancements in ion beam figuring
OSA Optical Design and Fabrication Congress, Washington, DC, USA, 10.-12.06.2019

Th. Arnold, A. Maiwald, G. Böhm, M. Ehrhardt, K. Zimmer*
Optical freeform generation by laser machining and plasma-assisted polishing
EOS Optical Technologies: Optofluidics and Manufacturing, Tolerancing, and Testing of Optical Systems, München, Germany, 24.-27.06.2019

*T. Arnold**
Bearbeitung optischer Materialien mit Plasmajets und Ionenstrahlquellen
478. JENAer Optikkolloquium, Jena, Germany, 12.11.2019

J. Bauer, F. Frost*
Orientation-dependent nanostructuring of titanium surfaces by low-energy ion-beam treatment
18th European Conf. on Applications of Surface and Interface Analysis, Dresden, Germany, 15.-20.09.2019

J. Bauer, M. Ulitschka, F. Frost, T. Arnold*
Figuring of optical Aluminium devices by reactive ion beam etching
EOS Optical Technologies: Optofluidics and Manufacturing, Tolerancing, and Testing of Optical Systems, München, Germany, 24.-27.06.2019

M. Behrens, A. Lotnyk, J.W. Gerlach, B. Rauschenbach*
Switching behaviour of epitaxial $Ge_2Sb_2Te_5$ thin films
DPG-Frühjahrstagung der Sektion Kondensierte Materie, Regensburg, Germany, 31.03.-05.04.2019

M. Behrens, A. Lotnyk, J.W. Gerlach, B. Rauschenbach*
Vacancy distributions, optical properties and switching mechanisms in epitaxial $Ge_2Sb_2Te_5$ thin films
27th Annual Meeting of the German Crystallographic Society, Leipzig, Germany, 25.-28.03.2019

H. Bryja, C. Grüner, J.W. Gerlach, M. Behrens, B. Rauschenbach, A. Lotnyk*
Investigation of bipolar resistive switching mechanisms in $Ge_2Sb_2Te_5$ thin films using different electrode materials
Int. Conf. on Memristive Materials, Devices & Systems 2019, Dresden, Germany, 08.-11.07.2019

H. Bryja, C. Grüner, J. W. Gerlach, M. Behrens, B. Rauschenbach, A. Lotnyk*
Investigation of bipolar resistive switching mechanisms in $Ge_2Sb_2Te_5$ thin films using different electrode materials
15th Meeting of the Working Group: Materials for Nonvolatile Memories of the GMM - VDE/VDI, Darmstadt, Germany, 04.06.2019

*C. Bundesmann**
Tutorial: The systematics of ion beam sputtering for deposition of thin films with tailored properties
XXVI. Erfahrungsaustausch Oberflächentechnologie mit Plasma- und Ionenstrahlprozessen, Mühlleithen, Germany, 05.-07.03.2019

C. Bundesmann, T. Amelal, J. Bernstein, M. Mateev, L. Pietzonka, D. Spemann*
Reactive ion beam sputter deposition of SiO_2 and TiO_2 thin films
Int. Conf. on Reactive Sputter Deposition RSD, Braunschweig, Germany, 05.-06.12.2019

C. Bundesmann, T. Amelal, L. Pietzonka, D. Spemann, H. Neumann*
Tailoring optical and other properties of TiO_2 films by ion beam sputter deposition
8th Int. Conf. on Spectroscopic Ellipsometry, Barcelona, Spain, 26.-31.05.2019

C. Bundesmann, R. Feder, T. Amelal, L. Pietzonka, D. Spemann*
Tailoring thin film properties by ion beam sputter deposition
14. ThGOT Thementage Grenz- und Oberflächentechnik und 6. Kolloquium Dünne Schichten in der Optik, Zeulenroda, Germany, 12.-14.03.2019

C. Bundesmann, R. Feder, T. Lautenschläger, L. Pietzonka, D. Spemann*
Options to tailor thin film properties by ion beam sputter deposition (IBSD)
Int. Conf. on Sputter Technology, Braunschweig, Germany, 19.-20.06.2019

M. Ehrhardt, P. Lorenz, S. Lai, K. Zimmer*
Excimer laser generated LIPSS in micro-patterned and geometrical-restricted polymer thin films
9th Int. LIPSS Workshop 2019, Ljubljana, Slovenia, 26.-27.09.2019

*Ehrhardt, S. Lai, P. Lorenz, J. Zajadacz, B. Han, K. Zimmer**
Fabrication of hierarchical structures by LIPSS formation on pre-patterned polymer
2019 EMRS Spring Meeting, Nice, France, 27.-31.05.2019

C. Eichhorn, F. Scholze, C. Bundesmann, D. Spemann, H. Neumann, H. Leiter*
Laser-induced fluorescence in the plume of a radiofrequency ion thruster: Measurements and excitation schemes
AIAA Propulsion and Energy Forum and Exhibition, Indianapolis, IN, USA, 19.-22.08.2019

C. Eichhorn, F. Scholze, C. Bundesmann, D. Spemann, H. Leiter, H. Neumann*
Ion thruster plume diagnostics in krypton using TALIF
XXVI. Erfahrungsaustausch Oberflächentechnologie mit Plasma- und Ionenstrahlprozessen, Mühlleithen, Germany, 05.-07.03.2019

C. Eichhorn, F. Scholze, C. Bundesmann, D. Spemann, H. Neumann, H. Leiter*
Two-photon laser-induced fluorescence diagnostics of a radiofrequency ion thruster: Measurements in Xenon and Krypton
36th Int. Electric Propulsion Conf., Vienna, Austria, 15.-20.09.2019

*A. Finzel, G. Dornberg, S. Görsch, M. Mitzschke, J. Bauer, F. Frost**
Realization of depth reference samples with surfaces amplitudes between 0.1 nm and 5 nm
EOS Optical Technologies: Optofluidics and Manufacturing, Tolerancing, and Testing of Optical Systems, München, Germany, 24.-27.06.2019

K. Fischer, A. Gawel, D. Rosen, P. Schulz, I. Atanasov, A. Schulze*
Synthesis of highly photocatalytic active TiO_2 nanoparticles on a polymer membrane
14th Int. Conf. on Catalysis in Membrane Reactors, Eindhoven, Netherlands, 08.-11.07.2019

S. Friebe, J. Haunschild, C.D. Etz, S. G. Mayr*
Human aorta under tensile stress
5th Euro BioMAT 2019, Weimar, Germany, 08.-09.05.2019

S. Friebe, S. Weigel, M. Francke, M. Zink, S.G. Mayr*
TiO_2 nanotube arrays as platform for long-term organotypic culture and mechanical characterization of retina explants - from imaging to mechanical response
2019 MRS Spring Meeting & Exhibit, Phoenix, AZ, USA, 22.-26.04.2019

S. Friebe, S. Weigel, M. Francke, M. Zink, S.G. Mayr*
TiO_2 nanotube arrays as platform for long-term organotypic culture and mechanical characterization of retina explants - from imaging to mechanical response
5th Euro BioMAT 2019, Weimar, Germany, 08.-09.05.2019

S. Friebe, J. Haunschild, C.D. Etz, S. G. Mayr*
Human aorta under tensile stress
2019 MRS Spring Meeting & Exhibit, Phoenix, AZ, USA, 22.-26.04.2019

J.W. Gerlach, M. Mensing, P. Schumacher, S. Herath, A. Lotnyk, B. Rauschenbach*
Thin film epitaxy using mass selected hyperthermal ions
Seminar, Erich-Schmid-Institut für Materialwissenschaft der ÖAW, Leoben, Österreich, 11.09.2019

S. Glaß, M. Kühnert, B. Abel, A. Schulze*
Hydrogel wound patches for the photodynamic inactivation of bacteria
7. Institutskolloquium Biozide - Materialien, Anwendungen und Trends, Weißandt-Gölzau, Germany, 24.09.2019

*S. Glaß, T. Pelras, B. Trinklein, T. Rüdiger, B. Abel, C. Elsner, A. Schulze, T. Scherzer**
UV-cured acrylic hydrogels as delivery materials for photosensitizers for use in photodynamic therapy
257th American Chemical Society National Meeting & Exposition: Chemistry for New Frontiers, Orlando, FL, USA, 31.03.-04.04.2019

A. Kahnt, F. Plass, A. Cadranel, V. Strauss, D. Guldi, W. Knolle, B. Abel*
Radiation chemical modification of carbon-nanodots
14th Tihany Symposium on Radiation Chemistry, Siófok, Hungary, 25.-30.05.2019

A. Kahnt, E. Hofmeister, T. Ullrich, K. Hanus, M. von Delius*
Reduction of cobaloxime-based complexes: Mechanisms, products and implication
31st Miller Conf. on Radiation Chemistry, Workington, UK, 09.-14.09.2019

D. Kalanov, A. Anders, C. Bundesmann*
Energy distributions of secondary particles in ion beam sputtering of Si
XXVI. Erfahrungsaustausch Oberflächentechnologie mit Plasma- und Ionenstrahlprozessen, Mühlleithen, Germany, 05.-07.03.2019

F. Kazemi, T. Arnold*
Ultra-precise machining of surfaces using microwave-driven reactive plasma etching
XXVI. Erfahrungsaustausch Oberflächentechnologie mit Plasma- und Ionenstrahlprozessen, Mühlleithen, Germany, 20.-23.03.2019

F. Kazemi, T. Arnold*
Development of a model for ultra-precise surface machining of N-BK7® using reactive plasma etching
6th European Seminar on Precision Optics Manufacturing, Deggendorf Institute of Technology, Teisnach, Germany, 09.-10.04.2019

S. Liedtke-Grüner, C. Grüner, A. Lotnyk, M. Mensing, J.W. Gerlach, P. Schumacher, B. Rauschenbach*
Texture formation in obliquely deposited metal thin films
27th Annual Meeting of the German Crystallographic Society, Leipzig, Germany, 25.-28.03.2019

O. Lorenz, M. Wagner, B. Abel*
Activation of Platinum thin film electrodes of solid acid fuel cells via cyclic voltammetry
11th Central European Meeting on Molecular Electrochemistry 2019, Chemnitz, Germany, 17.-19.11.2019

P. Lorenz, M. Kloeppel, J. Zajadazc, I. Zagoranskiy, M. Ehrhardt, K. Zimmer, B. Hopp, H. Bing*
Self-assembly laser-induced nanostructuring of dielectric surfaces - a review
DPG-Frühjahrstagung der Sektion Materie und Kosmos, München, Germany, 17.-23.03.2019

P. Lorenz, K. Zimmer, I. Zagoranskiy, M. Ehrhardt*
Large area sub-µm and nanostructuring of dielectric surfaces and thin metal layers by ns laser radiation
SPIE LASE, San Francisco, CA, USA, 05.-07.02.2019

A. Lotnyk, M. Behrens, I. Hilmi, B. Rauschenbach*
Epitaxial chalcogenide-based thin films and heterostructures
15th Meeting of the Working Group: Materials for Nonvolatile Memories of the GMM - VDE/VDI, Darmstadt, Germany, 04.06.2019

*A. Lotnyk**
Nanoscale characterization of phase change materials for memory applications
Seminar, Fakultät für Maschinenbau, Technische Universität, Chemnitz, Germany, 22.08.2019

A. Lotnyk, T. Dankwort, L. Kienle, B. Rauschenbach*
In situ observations of the reversible vacancy ordering in layered chalcogenide-based thin films
European Phase-Change and Ovonic Symposium, Grenoble, France, 08.-10.09.2019

S. Mändl, D. Manova*
Dynamic OES during high voltage pulses
XXVI. Erfahrungsaustausch Oberflächentechnologie mit Plasma- und Ionenstrahlprozessen, Mühlleithen, Germany, 05.-07.03.2019

*D. Manova, S. Mändl**
In situ X-ray diffraction measurements during low energy ion beam nitriding & etching
27th Annual Meeting of the German Crystallographic Society, Leipzig, Germany, 25.-28.03.2019

A. Mayer, J. Rond, J. Staabs, M. Leifels, H.-C. Scheer, J. Zajadacz, M. Ehrhardt, P. Lorenz, K. Zimmer*
Multiple replication of hierarchical structures from polymer masters with anisotropy
The 63rd Int. Conf. on Electron, Ion and Photon Beam Technology & Nanofabrication, Minneapolis, MN, USA, 28.-31.05.2019

M. Mensing, P. Schumacher, J.W. Gerlach, S. Herath, A. Lotnyk, B. Rauschenbach*
Mass selected low energy ion-assisted growth of epitaxial GaN thin films: Impact of the nitrogen ion species
Ion beam physics workshop 2019, Dresden, Germany, 24.-26.06.2019

M. Mensing, P. Schumacher, C. Grüner, S. Herath, A. Lotnyk, J.W. Gerlach, B. Rauschenbach*
Mass separated low-energy nitrogen ion assisted film growth
DPG-Frühjahrstagung der Sektion Kondensierte Materie, Regensburg, Germany, 31.03.-05.04.2019

M. Mensing, P. Schumacher, C. Grüner, S. Herath, A. Lotnyk, J.W. Gerlach, B. Rauschenbach*
Ion beam assisted thin film growth using mass separated low-energy nitrogen ions
27th Annual Meeting of the German Crystallographic Society, Leipzig, Germany, 25.-28.03.2019

*K. Monakhov**
Development of polyoxometalate compounds for the 'more than moore' technology
Kolloquium der Fakultät für Chemie & Mineralogie, Universität Leipzig, Leipzig, Germany, 05.06.20192019

*K. Monakhov**
Paving the way for neuromorphic computing with redox-based switching of metal-oxo clusters
15th Nanotech Congress Int. Topical Meeting on Nanostructured Materials and Nanotechnology, Puerto Vallarta, Mexico, 21.-25.10.2019

*K. Monakhov**
Development of metal-oxo clusters for redox-based resistive switching memory cells
Collaborative Conf. on Advanced Materials, St. Julian, Malta, 26.-30.08.2019

H. Müller, Th. Arnold*
Next generation of an instrument calibration element fabricated by plasma jet machining
6th European Seminar on Precision Optics Manufacturing, Deggendorf Institute of Technology, Teisnach, Germany, 09.-10.04.2019

F. Niefind, S. Karande, A. Kahnt, B. Abel*
New insights into solvent effects on the P3HT thin film morphology via PEEM
Bunsentagung 2019, Jena, Germany, 30.05.-01.06.2019

F. Niefind, A. Neff, K. Siefermann, A. Kahnt, S. Mannsfeld, B. Abel*
Laser-PEEM - A new tool for deciphering the morphology of semi-crystalline polymer films
2019 MRS Spring Meeting & Exhibit, Phoenix, AZ, USA, 22.-26.04.2019

*F. Niefind**
Investigating the P3HT thin film morphology with PEEM
Department of Chemistry, University of Chicago, Chicago, IL, USA, 18.04.2019

*K. Ohndorf, T. Liebeskind, J. Bauer, F. Frost**
Auf dem Weg zur Realisierung von Nanometer- und sub-Nanometer-Tiefenstandards mittels RIBE
XXVI. Erfahrungsaustausch Oberflächentechnologie mit Plasma- und Ionenstrahlprozessen, Mühlleithen, Germany, 05.-07.03.2019

P. Räcke, R. Staacke, J.W. Gerlach, J. Meijer, D. Spemann*
Image charge detection statistics relevant for deterministic ion implantation
Ion Beams for Future Technologies 2019, Dubrovnik, Croatia, 01.-03.04.2019

P. Räcke, J. Meijer, J.W. Gerlach, D. Spemann*
Image charge detection for deterministic ion implantation
XXVI. Erfahrungsaustausch Oberflächentechnologie mit Plasma- und Ionenstrahlprozessen, Mühlleithen, Germany, 05.-07.03.2019

A. Schindler, Th. Arnold, F. Frost, M. Nestler, M. Zeuner*
Ultra-precision ion beam processing for advanced optics manufacturing
Colloquium at ASML, Veldhoven, Netherlands, 20.05.2019

M. Schmidt, D. Breite, A. Prager, A. Schulze*
Self-cleaning polymer membranes for wastewater treatment
14th Int. Conf. on Catalysis in Membrane Reactors, Eindhoven, Netherlands, 08.-11.07.2019

F. Scholze, C. Bundesmann, C. Eichhorn, D. Spemann*
Determination of the beam divergence of a gridded ion thruster using the AEPD platform
36th Int. Electric Propulsion Conf., Vienna, Austria, 15.-20.09.2019

F. Scholze, D. Spemann, D. Feili*
Design and performance test of an RF plasma bridge neutralizer
36th Int. Electric Propulsion Conf., Vienna, Austria, 15.-20.09.2019

F. Scholze, D. Spemann*
Development and test of a plasma bridge neutralizer based on radio-frequency ionization for electric propulsion applications
Space Engineering and Technology Final Presentation Days, ESTEC, Noordwijk, Netherlands, 02.07.2019

*A. Schulze**
Bioactive polymer surfaces for medical application
Integrierter Graduiertenkolleg Matrixengineering - Materials in Medicine, Transregio 67, Leipzig, Germany, 28.11.2019

A. Schulze, S. Nieß, P. Langowski, S. Glaß*
Photoactive polymer membranes for degradation of pharmaceuticals from water
14th Int. Conf. on Catalysis in Membrane Reactors, Eindhoven, Netherlands, 08.-11.07.2019

*D. Spemann**
Deterministic ion implantation: Approaches and challenges
XXVI. Erfahrungsaustausch Oberflächentechnologie mit Plasma- und Ionenstrahlprozessen, Mühlleithen, Germany, 05.-07.03.2019

M. Ulitschka, J. Bauer, F. Frost, T. Arnold*
Reactive ion beam etching-based planarization of optical aluminium surfaces
SPIE Optics + Optoelectronics, EUV and X-ray Optics: Synergy between Laboratory and Space, Prague, Czech Republic, 01.-04.04.2019

M. Ulitschka, J. Bauer, F. Frost, T. Arnold*
Reactive ion beam etching - based finishing of optical Aluminium surfaces
EOS Optical Technologies: Optofluidics and Manufacturing, Tolerancing, and Testing of Optical Systems, München, Germany, 24.-27.06.2019

N. Wilharm, T. Fischer, W. Knolle, F. Ott, A. Beck-Sickinger, M. Zink, S. Mayr*
A biocompatible reversible thermal actuator with tunable transition temperature
5th Euro BioMAT 2019, Weimar, Germany, 08.-09.05.2019

*S. Zahn**
Deep eutectic solvents: Like dissolve like?
1st Int. Meeting on Deep Eutectic Systems, Lisboa, Portugal, 24.-27.06.2019

*S. Zahn**
Deep eutectic solvents: Like dissolves like
11th Central European Meeting on Molecular Electrochemistry 2019, Chemnitz, Germany, 17.-19.11.2019

*S. Zahn**
Deep eutectic solvents: Like dissolves like?
5. Int. Conf. on Ionic Liquid-Based Materials, Jussieu, Paris, France, 04.-08.11.2019

Posters

2018

A. Abdul Latif, K. Fischer, M. Längrich, R. Zoerner, E. Hertwig, C. Cornejo Rivera, J. Arb, T. Lange, A. Schulze*
Reduction of pharmaceutical residues by engineering a TiO_2/ membrane reactor
17. Aachener Membran Kolloquium, Aachen, Germany, 14.-15.11.2018

Th. Arnold, G. Böhm, H. Paetzelt*
High-precision freeform generation by plasma based manufacturing technology
EUSPEN Special Interest Group Meeting: Structured & Freeform Surfaces, Paris-Saclay, France, 27.-29.11.2018

P.A. Atanasov, N.N. Nedyalkov, Ru. Nikov, N. Fukata, D. Hirsch, B. Rauschenbach*
SERS of fungicides Dithane DG (mancozeb) assisted by Au and Ag nanostructures produced by laser techniques
2018 E-MRS Spring Meeting, Strasbourg, France, 18.-22.06.2018

J. Bauer, M. Ulitschka, F. Frost, T. Arnold*
Roughening prevention in reactive ion beam figuring of aluminium mirror surfaces
DPG-Frühjahrstagung der Sektion Kondensierte Materie, Berlin, Germany, 11.-16.03.2018

J. Bauer, M. Ulitschka, F. Pietag, F. Frost, T. Arnold*
Ultra-precision surface figuring of aluminium mirror devices
DPG-Frühjahrstagung der Sektion Kondensierte Materie, Berlin, Germany, 11.-16.03.2018

J. Bauer, M. Ulitschka, F. Frost, T. Arnold*
Sub-aperture ion beam finishing of optical mirror devices
16th Int. Conf. on Plasma Surface Engineering, Garmisch-Partenkirchen, Germany, 17.-21.09.2018

M. Behrens, A. Lotnyk, J. Griebel, J.W. Gerlach, B. Rauschenbach*
Control of structural order and its impact on optical reflectivity contrast of epitaxial $Ge_2Sb_2Te_5$ thin films
Non-Volatile Memory Technology Symposium 2018, Sendai, Japan, 22.-24.10.2018

M. Behrens, A. Lotnyk, T. Abel, J.W. Gerlach, B. Rauschenbach*
Structural changes in epitaxial $Ge_2SbN_2Te_5$ thin films with highly ordered vacancy layers upon ns-laser irradiation
DPG-Frühjahrstagung der Sektion Kondensierte Materie, Berlin, Germany, 11.-16.03.2018

D. Breite, R. Schiewe, M. Went, A. Prager, A. Schulze*
Surface hydrophilization of a microfiltration membrane using polyamide
17th Aachener Membran Kolloquium, Aachen, Germany, 14.-15.11.2018

C. Bundesmann, T. Lautenschläger, R. Feder, L. Pietzonka, D. Spemann*
Options to tailor thin film properties by ion beam sputter deposition
16th Int. Conf. on Plasma Surface Engineering, Garmisch-Partenkirchen, Germany, 17.-21.09.2018

M.A. Cisternas, M. Jose Retamal, P. Saikia, N. Casanova, N. Moraga, A. Chandia, A. Alvarez, D.E. Diaz-Droguett, F. Guzman, S. Mändl, D. Manova, T.P. Corrales, U.G. Volkmann, M. Favre, H. Bhuyan*
Study of phospholipid bilayers supported on Chitosan-Titanium Nitride coatings produced by plasma immersion ion implantation (PIII)
62nd Annual Meeting Biophysical Society, San Francisco, CA, USA, 17.-21.02.2018

A. Dalke, D. Manova, S. Mändl, H. Biermann*
In-situ XRD analysis during Ar ion etching of compound layers generated on AISI 4140 steel by plasma nitrocarburizing using a solid carbon source
Materials Science Engineering - European Congress and Exhibition on Advanced Materials and Processes, Darmstadt, Germany, 26.-28.09.2018

A.J. Dittrich, T. Albert, A. Lehmann, T. Arnold, P.G. Braun*
Einfluss verschiedener Träger- und Reaktivgase auf die antimikrobielle Wirkung von kaltem atmosphärischem Plasma auf Slicermesseroberflächen
59. Arbeitstagung des Arbeitsgebietes Lebensmittelsicherheit und Verbraucherschutz der DVG, Garmisch-Partenkirchen, Germany, 25.-28.09.2018

A.J. Dittrich, T. Albert, A. Lehmann, T. Arnold, P.G. Braun*
Antimicrobial effect of cold atmospheric plasma jet treatment on cutting blade surfaces
26th Int. ICFMH Conf. FoodMicro 2018, Berlin, Germany, 03.-06.09.2018

J. Edelmann, E. Gärtner, U. Eckert, J. Griebel*
Tool System for UV induced micro moulding of biomedical disposables
EUSPEN, 18th Int. Conf. & Exhibition, Venice, Italy, 04.-08.06.2018

R. Flyunt, W. Knolle, A. Kahnt, A. Lotnyk, S. Eigler, B. Abel*
Optimized reduction of graphene oxide by electron-beam irradiation
PULS-2018 - Pulse Investigations in Chemistry, Physics, and Biology with RKCM-2018 Reaction Kinetics in Condensed Matter, Lodz, Poland, 02.09.-07.09.2018

S. Friebe, J. Haunschild, C.D. Etz, S.G. Mayr*
Human aorta under tensile stress
9th Annual Symposium Physics of Cancer, Leipzig, Germany, 24.09.-26.09.2018

S. Friebe, J. Haunschild, C.D. Etz, S.G. Mayr*
Human aorta under tensile stress
3rd Soft Matter Day 2018, Leipzig, Germany, 06.07.2018

S. Friebe, S. Weigel, M. Francke, M. Zink, S.G. Mayr*
TiO_2 nanotube arrays as platform for environmental scanning electron microscopy studies - from imaging to mechanical response
14. Research Festival, Leipzig, Germany, 19.01.2018

S. Glaß, B. Trinklein, B. Abel, A. Schulze*
TiO_2 as photosensitizer and photoinitiator for the synthesis of photoactive TiO_2-PEGDA hydrogels
6th Belgian Symposium on Tissue Engineering, Ghent, Belgium, 22.-23.11.2018

C. Hackl, J. Griebel, C. Elsner, J. Edelmann, B. Abel*
Microstructured multifunctional polymer chips by UV-photopolymerization injection molding
EUSPEN, 18th Int. Conf. & Exhibition, Venice, Italy, 04.-08.06.2018

P. Hietschold, S. Riedel, M. Deuflhard, M. Zink, S.G. Mayr*
Collagen hydrogels: Electron beam induced modification and nanoparticle composites
6. Kolloquium des DFG-Schwerpunktsprogramm 1681, Benediktbeuern, Germany, 26.-28.09.2018

P. Hietschold, S. Riedel, S.G. Mayr, M. Zink*
Collagen hydrogels: Electron beam induced modification and nanoparticle composites
3rd Soft Matter Day, Leipzig, Germany, 06.07.2018

I. Hilmi, A. Lotnyk, J.W. Gerlach, P. Schumacher, B. Rauschenbach*
Two-dimensional growth of three-dimensionally bonded GeTe
DPG-Frühjahrstagung der Sektion Kondensierte Materie, Berlin, Germany, 11.-16.03.2018

Q. Ji, Z. Yang, H. Wang, X. Wang, A. Anders*
Cathodic arc deposition of V_2O_3 films and their application in quench protection of high-temperature superconducting magnets
Gordon Research Conference (GRC) Plasma Processing Science - Fundamental Insights in Plasma Processes, Smithfield, RI, USA, 05.-10.08.2018

F. Kazemi, T. Arnold*
Surface machining of N-BK7® using microwave-driven plasma etching
16th Int. Conf. on Plasma Surface Engineering, Garmisch-Partenkirchen, Germany, 17.-21.09.2018

F. Kazemi, T. Arnold*
Ultra-precise machining of surfaces using microwave-driven Cl-based plasma etching
82. Jahrestagung der DPG und DPG-Frühjahrstagung der Sektion Atome, Moleküle, Quantenoptik und Plasmen, Erlangen, Germany, 04.-09.03.2018

A. Lehmann, T. Arnold, T. Albert, A.J. Dittrich, P.G. Braun*
Antimikrobielle Wirksamkeit eines atmosphärischen Plasmajets auf Schneidmesseroberflächen unter dem Einfluss verschiedener Trägergase
13. ThGOT Thementage Grenz- und Oberflächentechnik, Zeulenroda, Germany, 13.-14.03. 2018

A. Lehmann, T. Arnold, T. Albert, A.J. Dittrich, P.G. Braun*
Investigation on the antimicrobial effect and the surface modifications on cutting blades by atmospheric plasma jet treatment
16th Int. Conf. on Plasma Surface Engineering, Germany, 17.-21.09.2018

J. Lehnert, D. Spemann, M.H. Hatahet, S. Mändl, P. Schumacher, M. Mensing, A. Finzel, C. Grüner, D. Hirsch, B. Rauschenbach*
Preparation and characterisation of carbon-free Cu(111) films on sapphire for graphene synthesis
DPG-Frühjahrstagung der Sektion Kondensierte Materie, Berlin, Germany, 11.-16.03.2018

J. Lehnert, D. Spemann, H. Hatahet, M. Mensing, C. Grüner, P. With, P. Schumacher, A. Finzel, D. Hirsch, B. Rauschenbach*
Preparation and characterisation of carbon-free Cu(111) films on sapphire for graphene synthesis
Flatlands beyond Graphene 2018, Leipzig, Germany, 03.-07.09.2018

*P. Lorenz, L. Bayer, T. Tachtsidis, M. Ehrhardt, K. Zimmer**
Laser structuring of metal cylinders for industrial UV-NIL application
17th Int. Conf. on Nanoimprint and Nanoprint Technologies, Braga, Portugal, 18.-20.09.2018

*P. Lorenz, M. Klöppe, I. Zagoranskiy, F. Frost, K. Zimmer**
Laser forming of photolithographic produced square metal pattern
2018 E-MRS Spring Meeting, Strasbourg, France, 17.-22.06.2018

A. Lotnyk, S. Herath, P. Schumacher, M. Mensing, J.W. Gerlach, B. Rauschenbach*
Structural study of GaN nanostructures and thin films prepared by energy and mass selective ion-beam assisted MBE
DPG-Frühjahrstagung der Sektion Kondensierte Materie, Berlin, Germany, 11.-16.03.2018

S. Mändl, D. Manova*
Time resolved optical emission spectroscopy measurements during PIII high voltage pulses
16th Int. Conf. on Plasma Surface Engineering, Garmisch-Partenkirchen, Germany, 17.-21.09.2018

*D. Manova, F. Haase, H. Kersten, S. Mändl**
Dynamic measurements of secondary electron emission during plasma immersion ion implantation
Workshop on Ion and Particle Beams & MAT Science Week, Darmstadt, Germany, 24.-27.04.2018

D. Manova, F. Haase, H. Kersten, S. Mändl*
Dynamic measurements of secondary electron emission coefficient during PIII processing
16th Int. Conf. on Plasma Surface Engineering, Garmisch-Partenkirchen, Germany, 17.-21.09.2018

M. Mensing, P. Schumacher, J.W. Gerlach, B. Rauschenbach*
Investigation of the influence of molecular and atomic nitrogen ion species during thin film growth
DPG-Frühjahrstagung der Sektion Kondensierte Materie, Berlin, Germany, 11.-16.03.2018

*R. Meyer, F. Bauer, S. Naumov, B. Abel, D. Enke**
Characterisation of porous materials by Inverse Gas Chromatography (IGC)
Quantachrome-Workshop Neue Strategien bei der Charakterisierung von Oberflächen und Porenstrukturen, Leipzig, Germany, 18.04.2018

F. Niefind, A. Neff, K. Siefermann, R. Shivhare, S. Mannsfeld, A. Kahnt, B. Abel*
Imaging the nanoscale morphology of semiconducting polymer blends with photoemission electron microscopy
Bunsentagung 2018, Hannover, Germany, 10.-12.05.2018

S. Riedel, C. Krömmelbein, K. Bela, C. Suckfüll, J. Zajadacz, S.G. Mayr*
Electron-irradiated hydrogels: Reagent-free modification towards biomedical applications
4th Euro Bio-inspired Materials, Potsdam, Germany, 19.-22.03.2018

S. Riedel, C. Krömmelbein, T. Kunschmann, S.G. Mayr*
Electron irradiation of collagen: Reagent-free crosslinking towards tailored matrices
14. Research Festival, Leipzig, Germany, 19.01.2018

S. Riedel, C. Krömmelbein, K. Bela, C. Suckfüll, J. Zajadacz, S.G. Mayr*
Electron-irradiated hydrogels: Reagent-free modification towards biomedical applications
DPG-Frühjahrstagung der Sektion Kondensierte Materie, Berlin, Germany, 11.-16.03.2018

S. Riedel, C. Krömmelbein, K. Bela, C. Suckfüll, J. Zajadacz, S.G. Mayr*
Electron-irradiated hydrogels: Reagent-free modification towards biomedical applications
9th Annual Symposium Physics of Cancer, Leipzig, Germany, 24.-26.09.2018

M. Schmidt, D. Breite, A. Prager, A. Schulze*
Self-cleaning studies on biocatalytic active polymer membranes
17. Aachener Membran Kolloquium, Aachen, Germany, 14.-15.11.2018

A. Schulze, L. Drößler, S. Weiß, M. Went, A. Abdul Latif, D. Breite, K. Fischer*
Functionalization in pilot scale: Roll-to-roll electron beam system with in-line contact angle determination
17th Aachener Membran Kolloquium, Aachen, Germany, 14.-15.11.2018

C. Steier, A. Allézy, A. Anders, K. Baptiste, E. Buice, K. Chow, G. Cutler, R. Donahue, D. Filippetto, J. Harkins, T. Hellert, M. Johnson, J.-Y. Jung, S. Leemann, D. Leitner, M. Leitner, T. Luo, H. Nishimura, T. Oliver, O. Omolayo, J. Osborn, et al.*
Status of the conceptual design of ALS-U
9th Int. Particle Accelerator Conf., Vancouver, Canada, 29.04.-04.05.2018

M. Ulitschka, J. Bauer, F. Frost, U. Decker, I. Reinhardt, Th. Arnold*
Optimization of novolak-based photoresists for ion beam planarization of aluminium mirrors
16th Int. Conf. on Plasma Surface Engineering, Garmisch-Partenkirchen, Germany, 17.-21.09.2018

A. Weidt, M. Mensing, J. Lehnert, S. Mändl, M. Zink, S.G. Mayr*
Carbon implantation of TiO_2 nanotubes for biomedical applications
9th Annual Symposium Physics of Cancer, Leipzig, Germany, 25.09.2018

A. Weidt, M. Mensing, J. Lehnert, S. Mändl, M. Zink, S.G. Mayr*
Carbon implantation of TiO_2 nanotubes for biomedical applications
3rd Soft Matter Day, Leipzig, Germany, 06.07.2018

A. Weidt, S.G. Mayr, M. Zink*
Organization of fibronectin and NIH/3T3 fibroblasts on bulk microgrooved TiO_2
14. Research Festival, Leipzig, Germany, 19.01.2018

A. Weidt, M. Mensing, J. Lehnert, S. Mändl, M. Zink, S.G. Mayr*
Carbon implantation of TiO_2 nanotubes
Annual BuildMoNa Conf., Leipzig, Germany, 19.03.2018

N. Wilharm, S. Riedel, W. Knolle, F. Ott, A. Beck-Sickinger, M. Zink, S.G. Mayr*
Electron irradiated elastin/collagen hydrogels
9th Annual Symposium Physics of Cancer, Leipzig, Germany, 24.-26.09.2018

N. Wilharm, S. Riedel, W. Knolle, F. Ott, A. Beck-Sickinger, M. Zink, S.G. Mayr*
Electron irradiated elastin/collagen hydrogels
3. Soft Matter Day 2018, Leipzig, Germany, 06.07.2018

N. Wilharm, S. Riedel, W. Knolle, M. Zink, S.G Mayr*
A tissue model with tunable properties by electron irradiation of elastin-collagen hydrogels
14. Research Festival, Leipzig, Germany, 19.01.2018

*S. Zahn**
Deep eutectic solvents: Similia similibus solvuntur?
54th Symposium on Theoretical Chemistry, Halle (Saale), Germany, 17.-20.09.2018

J. Zajadacz, K. Zimmer, A. Mayer, C. Steinberg, H.-C. Scheer*
Short time high temperature annealing of diblock copolymers (DiBCP)
2018 E-MRS Spring Meeting, Strasbourg, France, 18.-22.06.2018

K. Zimmer, J. Zajadacz, A. Mayer, C. Steinberg, H.-F. Chang, J.-Y. Cheng, H.-C. Scheer*
Nanopattern formation by local laser annealing of diblock copolymer (BCB) films
11th Int. Conf. on Photo-Excited Processes and Applications, Vilnius, Lithuania, 10.-14.09.2018

V. Zviagin, P. Huth, C. Sturm, D. Spemann, J. Lenzner, A. Setzer, J. Meijer, R. Denecke, P. Esquinazi, M. Grundmann, R. Schmidt-Grund
Optical and magnetic properties of spinel type ferrites in relation to their crystallographic order
DPG-Frühjahrstagung der Sektion Kondensierte Materie, Berlin, Germany, 11.-16.03.2018

2019

M. Behrens, A. Lotnyk, J. W. Gerlach, M. Ehrhardt, P. Lorenz, B. Rauschenbach*
Epitaxial recrystallization of 3D-bonded metastable Ge-Sb-Te based phase-change materials induced by single ns-laser pulse irradiation
Microscopy Conference 2019, Berlin, Germany, 01.-05.09.2019

M. Behrens, A. Lotnyk, J. W. Gerlach, M. Ehrhardt, P. Lorenz, B. Rauschenbach*
Ultrafast epitaxial crystal growth in phase-change material thin films
European Phase-Change and Ovonic Symposium, Grenoble, France, 08.-10.09.2019

H. Bryja, M. Behrens, J.W. Gerlach, B. Rauschenbach, A. Lotnyk*
Investigation of bipolar resistive switching mechanisms in amorphous and crystalline $Ge_2Sb_2Te_5$ thin films
DPG-Frühjahrstagung der Sektion Kondensierte Materie, Regensburg, Germany, 31.03.-05.04.2019

G. Dornberg, A. Finzel, F. Koch, S. Görsch, T. Glaser, F. Frost*
Reaktives Ionenstrahlätzen von hochdispersiven Transmissionsgittern mit höchster Beugungseffizienz
120. Jahrestagung der deutsche Gesellschaft für angewandte Optik, Darmstadt, Germany, 11.-15.06.2019

M. Ehrhardt, B. Han, S. Lai, P. Lorenz, K. Zimmer*
Confinement-assisted indirect laser patterning of transparent dielectric material using single NIR nanosecond laser pulses
SPIE LASE, San Francisco, CA, USA, 05.-07.02.2019

S. Glaß, M. Kühnert, B. Abel, A. Schulze*
Tailor-made hydrogels by electron beam irradiation for drug release systems
European Polymer Congress 2019, Heraklion, Greece, 09.-14.06.2019

T. John, L.L. Martin, H.J. Risselada, B. Abel*
Impact of gold nanoparticles on amyloid peptide aggregation
21st JCF-Frühjahrssymposium and 2nd European Young Chemists' Meeting, Bremen, Germany, 20.-23.03.2019

T. John, H.J. Risselada, L.L. Martin, B. Abel*
Amyloid peptide aggregation near nanoparticle and membrane interfaces
47th IUPAC World Chemistry Congress, Paris, France, 07.-12.07.2019

S. Lai, M. Ehrhardt, P. Lorenz, B. Han, K. Zimmer*
Void formation in glasses by single ultra-short laser pulses
DPG-Frühjahrstagung der Sektion Materie und Kosmos, München, Germany, 17.-23.03.2019

S. Liedtke-Grüner, C. Grüner, A. Lotnyk, M. Mensing, J.W. Gerlach, P. Schumacher, B. Rauschenbach*
Texture formation in obliquely deposited metal thin films
27th Annual Meeting of the German Crystallographic Society, Leipzig, Germany, 25.-28.03.2019

P. Lorenz, M. Kloeppel-Gersdorf, I. Zagoranskiy, M. Ehrhardt, F. Frost, K. Zimmer*
Laser-induced melting and reshaping of µm- and sub-µm pre-structured chromium layers: experiment and theory
2019 EMRS Spring Meeting, Nice, France, 27.-31.05.2019

P. Lorenz, M. Himmerlich, M. Ehrhardt, M. Taborell, B. Hopp, K. Zimmer*
Laser fabrication of black copper surfaces to reduce the optical reflectivity and secondary electron yield
2019 EMRS Spring Meeting, Nice, France, 27.-31.05.2019

A. Lotnyk, I. Hilmi, U. Ross, B. Rauschenbach*
Nanoscale characterization of chalcogenide-based heterostructures by advanced electron microscopy
6th Nano Today Conf., Lisboa, Portugal, 16.-20.06.2019

A. Lotnyk, U. Ross, T. Dankwort, L. Kienle, B. Rauschenbach*
In situ observation of dynamic reconfiguration of van der Waals interfaces in 2D-bonded Ge-Sb-Te phase-change memory alloys
Microscopy Conference 2019, Berlin, Germany, 01.-05.09.2019

M. Mensing, P. Schumacher, C. Grüner, S. Herath, A. Lotnyk, J.W. Gerlach, B. Rauschenbach*
Ion beam assisted thin film growth using mass separated low-energy nitrogen ions
27th Annual Meeting of the German Crystallographic Society, Leipzig, Germany, 25.-28.03.2019

M. Schmidt, D. Breite, A. Prager, A. Schulze*
Bioactive self-cleaning PVDF membrane filters
European Polymer Congress 2019, Heraklion, Greece, 09.-14.06.2019

S. Zahn, S. Kühne, S. Frenzel*
Datenmanagement im Rahmen eines Transregios an der Universität Leipzig, der TU Chemnitz und dem Leibniz Institut für Oberflächenmodifizierung e.V. (IOM)
1. sächsische FDM-Tagung, Dresden, Germany, 19.09.2019

J. Zajadacz, K. Zimmer, P. Lorenz, A. Mayer, M. Papenheim, H.-C. Scheer*
Shear force measurement of actuated, gecko-inspired adhesion elements with hierarchical PDMS pattern
45th Int. Conf. on Micro & Nano Engineering, Rhodes, Greece, 23.-26.09.2019

Patents

2018

F. Frost, A. Nickel, S. Görsch, C. Alvermann
Verfahren und Vorrichtung zur Erzeugung eines gewünschten Oberflächenprofils
PCT/EP2018/084638

M. Erhrhardt, K. Zimmer, Bing Han, Rihong Zhu
Verfahren zum Induzieren der periodischen Struktur eines transparenten dielektrischen Werkstoffs durch einen einzelpuls-Nanosekundenlaser
CN 201810861914.5

M. Erhrhardt, K. Zimmer, Bing Han, Rihong Zhu
Lasernassätzverfahren für jeden gebogenen und transparenten dielektrischen Werkstoff
CN 201810861897.5

2019

J. Bauer, M. Ulitschka, F. Frost, T. Arnold
Verfahren zum Glätten von Oberflächen
DE 102019111681.3

M. Ehrhardt, K. Zimmer, P. Lorenz, J. Zajadacz, A. Anders
Verfahren zur Behandlung einer Festkörperoberfläche
DE 102019006322.8

A. Schulze, M. Hinkefuß, L. Drößler
Vorrichtung zum Spülen oder Imprägnieren einer Filtermembranbahn
DE 112019126317.4

A. Schulze, M. Hinkefuß, L. Drößler
Vorrichtung zum Spülen oder Imprägnieren einer Membranfaser
DE 122019126315.8

U. Helmstedt, H. Herrnberger, A. Freyer, O. Fechner, C. Gschossmann
Druckform und polymeres Beschichtungsmaterial dafür
DE 102019124814.0

IMPRINT

Leibniz-Institut für Oberflächenmodifizierung e.V.
Leibniz Institute of Surface Engineering (IOM)

Permoserstr. 15
04318 Leipzig, Germany

Director and CEO
Prof. Dr. André Anders
Phone: +49 (0)341 235 - 2308
Fax: +49 (0)341 235 - 2313
andre.anders@iom-leipzig.de

Public Relations
Yvonne Bohne
Phone: +49 (0)341 235 - 3175
Fax: +49 (0)341 235 - 2313
yvonne.bohne@iom-leipzig.de

www.iom-leipzig.de

Image directory

Cover: Center: Interior view of a system for ion-beam assisted thin film deposition (© IOM/ Photo: J.W. Gerlach);
Down left: View into a Kaufman-type broad-beam ion source (© IOM/ Photo: S. Görsch); Down center: “Inspired by Gecko foot”: SEM image of laser induced periodic surface structures generated on micrometer size columns (© IOM/ Photo: I. Mauersberger);
Down right: SEM image of anodic ZnO crystallized in water vapor (© IOM/ Photo: A. Prager)
S. 6: IOM-Building 16.2 (© IOM/ Photo: Y. Bohne)
S. 16: Image of an ion extraction grid system of a broad beam ion source (Kaufman-type) after a very long process time with intensive redeposition by etched material (© IOM/ Photo: A. Finzel)
S. 58: Entry grid of a quadrupole mass filter system for a hyperthermal ion beam (© IOM/ Photo: M. Mensing)
S. 74: SEM image of various morphologies of ZnO (© IOM/ Photo: A. Prager)
S. 82: Peron on the IOM-building 18.0 (© IOM/ Photo: Y. Bohne)
S. 90: Quadrupole mass filter system as seen by a low-energy ion right before entering (© IOM/ Photo: M. Mensing)

Print
FISCHER druck&medien OHG | Sestewitzer Straße 18 | 04463 Großpösna

Climate neutral
Print product
ClimatePartner.com/11836-1902-1002

Research & Development

- Ultra-precision machining with ions and plasma
- Structuring and thin film analysis
- Thin film deposition and nanostructures
- Electron beam and photonic technologies
- Functional layers
- Functional nano- and microstructured systems

Leibniz Institute of Surface Engineering (IOM)
Leibniz-Institut für Oberflächenmodifizierung e. V.
Permoserstraße 15 / 04318 Leipzig / Germany

Phone: +49 (0) 341 235-2308
Fax: +49 (0) 341 235-2313

www.iom-leipzig.de

Leibniz Association

Zertifikat seit 2011
audit berufundfamilie